Oleksandr Kotenko

Potential Analysis of Alternative Absorption Heat Pumping Processes with Special Emphasis on Sodium Hydroxide as Additive

DOCTORAL THESIS

For obtaining the academic degree of

Doctor of Technical Sciences

Doctoral Programme of the Doctoral School of Mechanical Engineering

Graz University of Technology

Supervisor (1st reader):

Ao. Univ.-Prof. Dipl.-Ing. Dr.techn. René Rieberer, Institute of Thermal Engineering, TU Graz

2nd reader:

Prof. Dr.-Ing. Felix Ziegler, Institute of Energy Engineering, TU Berlin

Graz, June 2012

ABSTRACT

The purpose of this work is to analyze both theoretically and experimentally innovative absorption heat pumping (AHP) processes found in related literature in order to find an alternative to a conventional ammonia / water (NH_3 / H_2O) absorption heat pump that is capable of performing at a higher COP (coefficient of performance) and is potentially competitive with it in cost, operating life and reliability.

A detailed survey of related literature on the following groups of innovative AHP-processes is presented within this work. These processes are analyzed by means of thermodynamic simulations using ASPEN Plus:

1. NH_3 / H_2O absorption heat pumping process using strong bases as additives;
2. Absorption heat transformer process using partially miscible working mixtures;
3. Absorption heat pumping processes using a condensable auxiliary fluid (Rojey cycle and Einstein-Szilard cycle);
4. Ammonia / ionic liquid absorption heat pumping processes.

From the simulation results, it was inferred that the preferred cycle for further experimental investigation is the NH_3 / H_2O absorption heat pumping process using sodium hydroxide (*NaOH*) as additive. There is an increase in the COP_C and at the same time a decrease in the generator temperature when *NaOH* is added.

To investigate experimentally the influence of *NaOH* on the NH_3 / H_2O AHP-process, the AHP test rig was designed and built within this work. The technical feasibility of this process with 5 wt.-% *NaOH* was shown. However, the predicted increase in COP_C was not proven by test results. The reason for this is an insufficient mass transfer area of the absorber, when operating with *NaOH*. Its efficiency decreases when *NaOH* is added, due to an increase in the solution viscosity and surface tension. Another crucial hurdle for its operating life and reliability is the crystallization issue in the evaporator.

It was also found that the UA-value of the generator increases when *NaOH* is added. It results in a closer temperature approach between the hot water side and solution side.

From the experimental and simulation results, it can be concluded that, in order to best a conventional NH_3 / H_2O absorption heat pump, further research and development of the test rig is needed. The absorber design is challenging and has to be improved, to ensure higher absorber efficiency when operating with *NaOH.* Furthermore, the construction of the test rig has to be modified to prevent *NaOH* from entering the refrigerant circuit during the operation and stand-by mode.

KURZFASSUNG

Das Ziel dieser Arbeit ist die innovativen Absorptions-Wärmpumpen (AWP) Prozesse theoretisch und experimentell zu analysieren, um eine Alternative zu einer konventionellen Ammoniak/Wasser (NH_3 / H_2O) Absorptions-Wärmpumpe zu finden, die einen höheren COP (coefficient of performance) hat und in Bezug auf Kosten, Lebensdauer und Betriebssicherheit konkurrenzfähig ist.

Eine detaillierte Literaturrecherche über die folgenden innovativen AWP-Prozesse wurde in dieser Arbeit durchgeführt. Diese Prozesse wurden mittels thermodynamischer Simulationen in ASPEN Plus analysiert:

1. NH_3 / H_2O AWP-Prozess mit starken Basen als Zusatz;
2. Absorptions-Wärmetransformator-Prozess mit teilweise mischbaren Arbeitsgemischen;
3. AWP-Prozess mit kondensierendem Hilfsmittel (Prozess von Rojey und Prozess von Einstein-Szilard);
4. Ammoniak / ionische Flüssigkeiten AWP-Prozess.

Die Simulationsergebnisse des NH_3 / H_2O AWP-Prozess mit Natrium Hydroxide (*NaOH*) als Zusatz haben gezeigt, dass die Zugabe von *NaOH* zu einer Erhöhung des COP_C und gleichzeitig zu einer Senkung der Austreibertemperatur führt.

Um den Einfluss von *NaOH* auf der NH_3 / H_2O Absorptions-Wärmepumpen-Prozess zu untersuchen, wurde ein entsprechender AWP-Prüfstand im Rahmen dieser Arbeit ausgelegt und aufgebaut. In den experimentellen Untersuchungen konnte die technische Machbarkeit dieses Prozesses bis 5% *NaOH*-Zugabe gezeigt werden. Die erwartete Verbesserung bezüglich der Prozess-Effizienz konnte bisher nicht nachgewiesen werden. Dies lag vor allem an einer nicht ausreichenden Stoffaustauschfläche für den Betrieb mit *NaOH*. Die Absorber-Effizienz sank durch die Zugabe von *NaOH* aufgrund der Erhöhung der Viskosität und Oberflächenspannung der Lösung. Weiters führten Ablagerungen von *NaOH* im Kältekreis zu Betriebsstörungen.

Die Verwendung von *NaOH* als Zusatz zum Gemisch NH_3 / H_2O führte bei den Messungen zur Verbesserung des Wärmeüberganges im Austreiber.

Die experimentellen sowie auch die Simulationsergebnisse haben gezeigt, dass noch erheblicher Forschungs- und Entwicklungsbedarf besteht. Der Absorber muss verbessert werden, um eine höhere Absorber-Effizienz im Betrieb mit *NaOH* zu gewährleisten. Die Konstruktion des AWP-Prüfstandes muss modifiziert werden, um die Kristallisationserscheinungen im Verdampfer zu verhindern.

STATUTORY DECLARATION

I declare that I have authored this dissertation independently, that I have not used other than the declared sources / resources, and that I have explicitly marked all material which has been quoted either literally or by content from the used sources.

_____

date (Signature)

БЛАГОДАРНОСТЬ

Во время моей работы над диссертацией я получил поддержку от многих людей, которые меня окружали, и хотел бы их всех поблагодарить: мою семью, друзей и сотрудников.

В первую очередь я бы хотел сказать спасибо моему руководителю Рене Риберу и Харальду Мозеру за их интеллектуальную и моральную помощь. Также хотелось бы поблагодарить всех сотрудников и студентов, помогавших мне в лаборатории при проектировании и создании экспериментальной установки.

Посвятить же эту работу я бы хотел самому ценному, что у меня есть, – моей семье. Спасибо моим родителям, бабушке с дедушкой, Свете с Аней и конечно же Эухении за то, что были рядом. Наконец-то наша общая мечта сбылась.

ACKNOWLEDGEMENTS

During my work on the doctoral thesis I have received support from a lot of people, who were around me, and would like to thank them all: my family, friends and colleagues.

First of all I would like to thank my supervisor Prof. René Rieberer and Dr. techn. Harald Moser for their intellectual and moral support. Also I would like to thank all my colleagues and students, who were helping me in the laboratory during my experimental work.

I devote this work to the most valuable that I have – my family. I would like to thank my parents, grandparents, Sveta and Anya and of course Eugenia for being always with me. Finally our common dream came true.

CONTENTS

NOMENCLATURE

Components:

ABS	Absorber
AHP	Absorption heat pump
AHT	Absorption heat transformer
CON	Condenser
CPUMP	Condensate pump
DEP	Dephlegmator
EVA	Evaporator
GEN	Generator
HE	Heating element
IHX	Internal heat exchanger
MEMB	Semipermeable membrane
PRC	Pre-cooler
PT	Pressure transmitter
PUMP	Solution pump
RAC	Refrigerant accumulator
REC	Rectification column
RSAC	Rich solution accumulator
RTH	Refrigerant throttle valve
SAC	Solution accumulator
SEP	Separator
SHX	Solution heat exchanger
STH	Solution throttle valve

Chemical substances:

[bmim][BF_4]	1-butyl-3-methylimidazolium tetrafluoroborate
[bmim][PF_6]	1-butyl-3-methylimidazolium hexafluorophosphate
[emim][$EtSO_4$]	1-ethyl-3-methylimidazolium ethylsulfate
[emim][SCN]	1-ethyl-3-methylimidazolium thiocyanate
[emim][Tf_2N]	1-ethyl-3-methylimidazolium bis(trifluoromethylsulfonyl)imide
[hmim][Cl]	1-hexyl-3-methylimidazolium chloride
[DMEA][Ac]	N,N-dimethyl-ethanol-ammonium acetate
C_4H_{10}	Butane
H_2O	Water
DMF	dimethylformamide
DMSO	dimethylsulfoxide
IL	Ionic liquid
KOH	potassium hydroxide
LiBr	Lithium bromide
LiCl	Lithium chloride
LiOH	Lithium hydroxide
NH_3	Ammonia
NaOH	Sodium hydroxide
PTFE	Polytetrafluorethylene

Formula symbols:

A	Area	m^2
c	Molar concentration	$mol \cdot mol^{-1}$
c_P	Specific heat capacity	$kJ \cdot (kg \cdot K)^{-1}$
COP	Coefficient of performance	–
G	Gibbs free energy	J
H	Height of the falling film	m
j	Empty tube velocity	$m \cdot s^{-1}$
m	Mass	kg
$\dot{m}$	Mass flow rate	$kg \cdot h^{-1}$
K	Coefficient of roughness	–
K_B	Base dissociation constant	$mol \cdot l^{-1}$
Nu	Nusselt number	
P	Power	W
p	Pressure	bar
Pr	Prandtl number	–
Re	Reynolds number	–
T	Absolute temperature	K
t	Temperature	℃
UCST	Upper critical solution temperature	℃
$\dot{V}$	Volume flow rate	$l \cdot h^{-1}$
$\dot{Q}$	Heating (cooling) capacity	W
U	Heat transfer coefficient	$W \cdot (m^2 \cdot K)^{-1}$
UA	Product of heat transfer coefficient and heat transfer area	$W \cdot K^{-1}$
$u\ (y)$	Experimental uncertainty	%
x	Vapor fraction	$kg \cdot kg^{-1}$
ø	Diameter	mm
α	Heat transfer coefficient	$W \cdot (m^2 \cdot K)^{-1}$
λ	Thermal conductivity coefficient	$W \cdot (m \cdot K)^{-1}$
ΔT	Temperature difference	K
η_{ABS}	Absorber Efficiency	–
ξ	Mass concentration	$kg \cdot kg^{-1}$

Indexes:

BRN	brine
C	Cooling mode
IN	Inlet
COP	Coefficient of performance
GMELCC,GMELCD	Electrolyte pair parameters of the thermodynamic model “ENRTL”
LLE	Liquid-liquid-equilibrium
LP	Low pressure level
MAX	Maximum
MIN	Minimum
OUT	Outlet
PSO	Poor solution
REF	Refrigerant
RSO	Rich solution
RSO_THEOR	Theoretical value (temperature or concentration) of the rich solution
SAT	Saturation
SNK	Cooling water (sink)
SRC	Hot water (source)
VLE	Vapor-liquid-equilibrium
VLLE	Vapor-liquid-liquid-equilibrium

1 INTRODUCTION

Over the past decades there has been an increasing demand on electrical energy for the needs of air conditioning and refrigeration. Absorption heat pumping (AHP) systems stand out as a good alternative to the widely used compression heat pumps. They allow the use of renewable energy sources, such as biomass or solar energy, and increase energy efficiency by means of heat recovery, e.g. using waste heat. Furthermore, conventional absorption heat pumps operate with natural refrigerants as opposed to compression heat pumps which use synthetic refrigerants that can contribute negatively to global warming.

The final energy balance (balance of the energy which is used by end consumers) in Austria in 2009 was about 1353 PJ (Statistik Austria, 2011). The largest contributors to this were oil (40.0%) followed by electricity (20%), natural gas (17%) and biomass (13%) (Figure 1-1). When combining all renewable energy sources into one group (biomass, combustible wastes, photovoltaic, wind energy and environmental energy) this share entails 16%.

In 2009, the thermal energy consumption in Austria was about 554.8 PJ, which is ca. 52 % of the final energy consumption. Here, the main sources of energy were natural gas (30%), renewable energy (26%), oil (15%), electricity (14%) and district heating (11%) (Figure 1-1) (Statistik Austria, 2009).

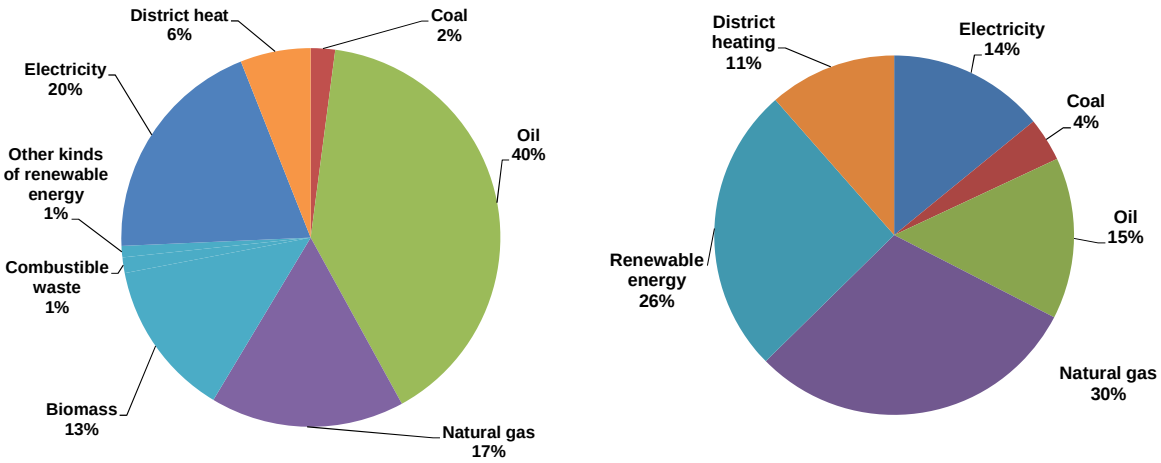

Figure 1-1: Final energy balance (left) and thermal energy production in Austria 2009 (Data according to Statistik Austria, 2011)

When analysing the use of thermal energy in Austria one can distinguish two groups:

- thermal energy used for space heating, air conditioning and hot water production;
- process heat.

The energy consumed by the first group is low-temperature energy (under 100℃). Its amount in 2009 was about 305.1 PJ and mainly produced from renewable energy (27%), natural gas (22%), oil (22%) and district heating (18%) (Figure 1-2a) (Statistik Austria, 2009).

The amount of energy consumed by the process heat production in Austria in 2009 was 249.7 PJ. It was mainly produced from natural gas (40%), renewable energy (25%) and electricity (19%) (Figure 1-2b) (Statistik Austria, 2009).

Obviously, the use of renewable energy plays an important role in thermal energy production in Austria. Its share increases each year. For instance, in 2006 it amounted to 23% of total thermal energy production and in 2008 to 26% (Statistik Austria, 2009). The majority of which is produced from biomass (92%) and the rest by means of solar heat (4%) and heat pumps (4%) (Biermayr et al., 2011).

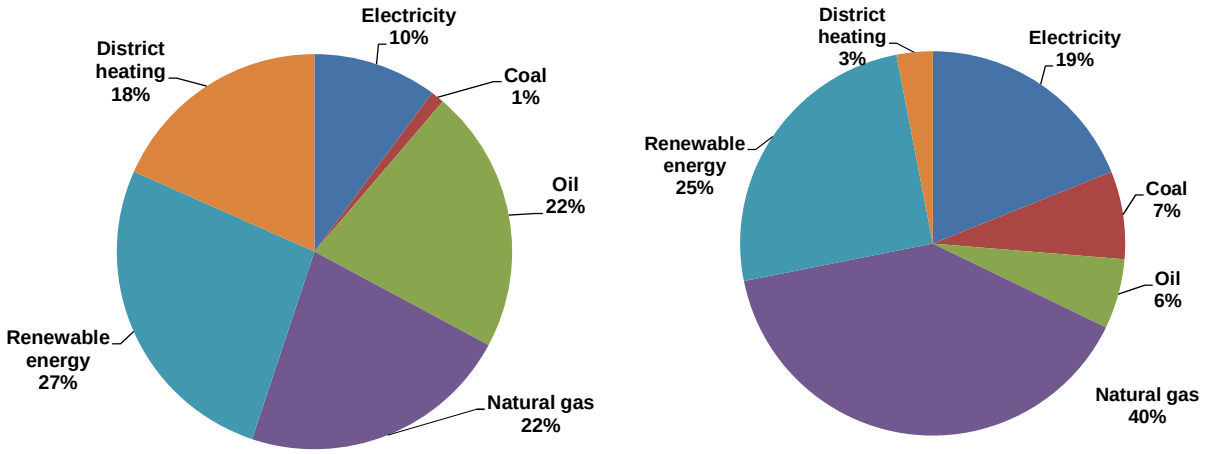

Figure 1-2: Energy consumption for space heating, air conditioning and hot-water supply (left) and energy consumption for process heat (right) in Austria 2009 (Data according to Statistik Austria, 2011)

Thus a continuous growth in the market of renewable energies can be expected. Apart from the conventional applications new markets, i.e. solar cooling or the use of gas-driven AHP for heating and cooling, will be developed. These will make the use of absorption technologies in combination with other renewable and fossil energy sources attractive, i.e. systems based on AHP and biomass boilers or solar panels or use of AHP for waste heat utilization.

In the past, various working mixtures were investigated for absorption heat pumps, however, only two of them ammonia / water (NH_3 / H_2O) and water / lithium bromide (H_2O / $LiBr$) are used in practice. Basically ammonia / water absorption is used for application at evaporator temperatures below 0℃ (refrigeration) and water / lithium bromide absorption for applications above 0℃ (water chillers). The main d rawback of ammonia / water as a working

mixture is the ensuing need for rectification while that of water / lithium bromide is its restricted temperature lift due to the crystallization issue and additional costs of corrosion inhibitors. On the one hand, the use of ammonia as a refrigerant enables more compact components; on the other hand, it addresses requirements with respect to material used in absorption heat pumps which has to be resistant to corrosion and leak proof.

In the past, to overcome the above mentioned drawbacks of conventional absorption heat pumping processes, several alternative cycles were suggested and investigated by different authors:

1. Absorption heat transformer (AHT)-process using partially miscible working mixtures;
2. AHP-processes using a condensable auxiliary fluid (Rojey cycle and Einstein-Szilard cycle);
3. NH_3 / H_2O AHP-process using strong bases as additives;
4. AHP-processes using ionic liquids as absorbents.

The absorption heat transformer using partially miscible working mixtures was suggested and analyzed by Niang et al., (1997, 1998) and Alonso et al. (2002, 2003). Its principle of operation is based on the separation of the working mixture without evaporation. Thus, no generator is necessary and the cycle seems to be competitive in terms of cost with a conventional AHT.

In the work of Einstein and Szilard (1930) as well as Rojey (1975) an auxiliary fluid, which condenses and evaporates within the process, was considered. The Einstein-Szilard cycle is a single pressure cycle, which does not require a solution pump, refrigerant, solution throttle valves or condenser. Instead, for the working fluid circulation, the thermal energy of electricity is used.

The Rojey cycle is similar to a conventional NH_3 / H_2O absorption heat pump, the difference being that an additional loop between the absorber and evaporator is necessary for the circulation of an auxiliary fluid. The use of an auxiliary fluid ensures an increase in the evaporator capacity compared to those of the single effect ammonia / water absorption system.

Several authors (Balamuru et al., 2000; Bruno et al., 2005; and Steiu et al., 2009) have reported that the use of strong bases such as sodium (*NaOH*) or potassium (*KOH*) hydroxides as additives to the ammonia / water working mixture in an absorption heat pumping process can increase its efficiency and at the same time decrease the required generator temperature. This process seems to be promising for application at low driving temperatures, e.g. by using solar energy, district heating or waste heat.

Recently, the use of ionic liquids as absorbents with ammonia and water as refrigerants is being investigated worldwide in order to overcome the above mentioned drawbacks of conventional working pairs.

1.1 Objectives

In order to investigate the above discussed alternative absorption heat pumping processes, the objectives of this work are defined as follows:

1. Analysis of the alternative absorption heat pumping processes in regard to their possible application areas and comparison with a conventional NH_3 / H_2O AHP by means of thermodynamic simulations using the software program ASPEN Plus.
2. Selection of the most promising process among them, that is capable of performing higher efficiency and is potentially competitive with conventional absorption heat pumping processes in cost, operating life and reliability.
3. Design and construction of a test rig to provide the validation of the simulation results for the absorption heat pumping process selected.
4. Analysis of the test results concerning the test rig efficiency and operation of its components at different boundary conditions by means of thermodynamic simulations using ASPEN Plus.

1.2 Thesis structure

Chapter 2 provides an overview of the state of the art in absorption heat pumping technologies.

Chapter 3 presents a detailed survey of related literature on alternative absorption heat pumping processes and analyzes them by means of thermodynamic simulations using ASPEN Plus.

Chapter 4 describes the design and construction of a test rig for investigation of the influence of natrium hydroxide as additive to the working mixture ammonia / water in an absorption heat pump.

Chapter 5 discusses the test results and analyzes them in regard to the influence of natrium hydroxide on the efficiency of the test rig and on the operation of its components.

Chapter 6 summarizes the main conclusions and contributions of this work and gives an overview of the further work required.

1.3 Publications on the topic of dissertation

This work was carried out within the following projects:

- “Feasibility Study: Innovative Absorption Heat Pumping processes” (“InnovAP”), which was carried out under the framework of „Energy Systems of Tomorrow“, an initiative by the Austrian Federal Ministry for Transport, Innovation and Technology (BMVIT), managed by the Austrian Research Promotion Agency (FFG);
- “The Potential and Limits of Use of Natrium Hydroxide as Additive to the Working Mixture Ammonia / Water in Absorption Heat Pumps” (“Hydroxide-AHP”), which has been financed by Klima- and Energiefonds within the program “NEUE ENERGIEN 2020”;
- “Feasibility of Absorption Heat Pumps using Ionic Liquids” (“IonA”), which has been financed by Klima- and Energiefonds within the program “NEUE ENERGIEN 2020”;
- IEE HPP Annex 34 “Thermally Driven Heat Pumps”, which has been financed within the framework of the IEA on behalf of the “Austrian Federal Ministry for Transport, Innovation and Technology”.

Within the project “InnovAP” two diploma theses were concluded. The diploma thesis of Ganster (2009) deals with thermodynamic simulation of the ammonia / water absorption heat pump using sodium hydroxide as additive. The design and construction of the test rig for the investigation of the ternary mixture ammonia / water / sodium hydroxide are described by Kalkgruber (2010).

The optimization and test results on the test rig were done within the project “Hydroxide-AHP” and are reported by Fenzl (2011).

Furthermore, the main achievements of this dissertation are also reported in 12 publications (see REFERENCES).

2 STATE OF THE ART IN ABSORPTION HEAT PUMPING TECHNOLOGIES

This chapter aims to give an overview of the state of the art of absorption heat pumps (AHP) and to analyze its market potential in Austria. Following a discussion of the operating principle of conventional absorption heat pumping processes, the main manufactures of absorption heat pumps and the most common application areas will be discussed. Finally, the working mixture selection and main requirements of the working mixtures will be analyzed.

2.1 Conventional absorption heat pumping processes

There are two types of conventional AHP-processes: absorption heat pumps (absorption heat pump Type I) and absorption heat transformers (absorption heat pump Type II). Both of them operate with either NH_3 / H_2O or H_2O / $LiBr$ as working mixture. In the past, various working mixtures have been investigated; however, just those mentioned above are state of the art. In this subchapter an operating principle of both types of AHP-processes will be discussed and a short overview of the working mixtures investigated for these processes and requirements of them will be given.

2.1.1 Cycles

The most common diagram, which is used for graphical representation of a conventional AHP-process, is a Duhring plot, *log (p) - 1/T* diagram. In the past, for heat engineering calculations an *h*, *ξ* – diagram was also used extensively. Recently, due to the development of various software programs, these calculations are made by means of thermodynamic simulations using software programs ASPEN Plus, EES, etc.

Absorption heat pump (absorption heat pump Type I)

The principle of operation of a single-stage NH_3 / H_2O AHP (see Figure 2-1) is shown by means of Duhring plot, *log (p) vs. 1/T* diagram, in Figure 2-2. The rich solution (1) at the low pressure level (3 bar) and with an NH_3 mass concentration (ξ_{RSO}) of 40% leaves the absorber (ABS) and is pumped by the solution pump (PUMP) to the high pressure level (15.4 bar) and enters the generator (GEN) (1-2). In the generator, heat ($\dot{Q}_{GEN}$) from a high temperature heat source is supplied to the rich solution. As a result, a poor solution (2-3) with an NH_3 mass concentration (ξ_{PSO}) of 22% and temperature of 140℃ is generated. The generated vapor enters the rectification column (REC), where the required NH_3 concentration (99,9%) is

provided by rejecting heat in the temperature range from 47 / 100℃ to an external heat sink. The condensed water flows back to the generator. The pressure of the poor solution is reduced again to the low pressure level (3 bar) in the solution throttle valve (STH) and it enters the absorber (3-4). The NH_3 vapor enters the condenser (CON) and condenses there by rejecting heat ($\dot{Q}_{CON}$) in the temperature range between 40 / 47℃ to an external heat sink (5-6). The condensed NH_3 is throttled then (RTH) to the low pressure level and partially evaporates. The partially evaporated NH_3 enters the evaporator (EVA) and evaporates in the temperature range between -10 / -5℃ by absorbing h eat ($\dot{Q}_{EVA}$) from a low temperature heat source (7-8). The NH_3 vapor enters the absorber and is absorbed by the poor solution coming from the generator (4-1). The absorption occurs in the temperature range between 40 / 78℃. The absorption heat ($\dot{Q}_{ABS}$) at the middle temperature level is rejected to an external heat sink.

To evaluate the efficiency of absorption heat pumping processes the Coefficient of Performance (COP) is used. Depending on their operating mode (heating or cooling) the heating COP (COP_H) or cooling COP (COP_C) are used. The heating COP is the ratio of the sum of the absorber, condenser and dephlegmator capacities to the sum of the generator and solution pump capacities (Eq. 2-1). The cooling COP is the ratio of the evaporator capacity to the sum of the generator and solution pump capacities (Eq. 2-2).

$$COP_H = \frac{\dot{Q}_{ABS} + \dot{Q}_{CON} + \dot{Q}_{DEP}}{\dot{Q}_{GEN} + P_{PUMP}} \qquad 2\text{-}1$$

$$COP_C = \frac{\dot{Q}_{EVA}}{\dot{Q}_{GEN} + P_{PUMP}} \qquad 2\text{-}2$$

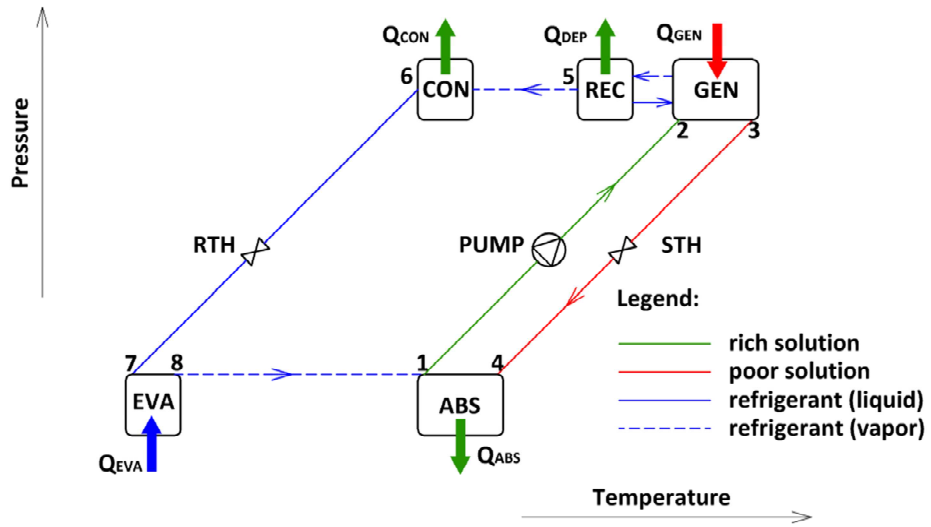

Figure 2-1: Schematic of a single-stage NH_3 / H_2O AHP (absorption heat pump Type I)

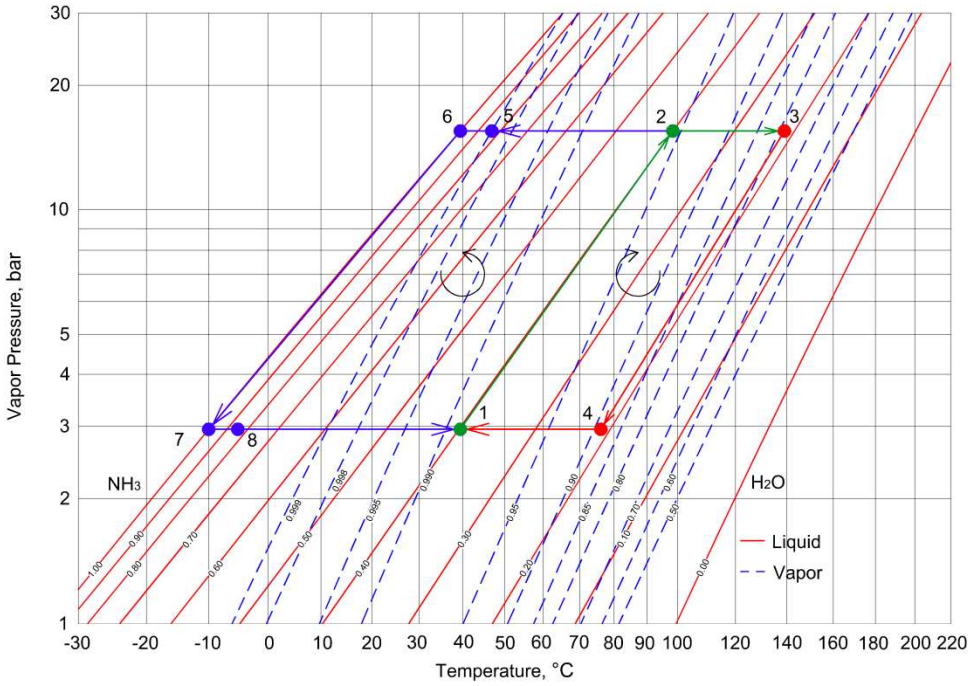

Figure 2-2: Principle of operation of a single-stage NH_3 / H_2O AHP in Duhring plot

Absorption heat transformer (absorption heat pump Type II)

In opposition to the above discussed absorption heat pump, a conventional absorption heat transformer is driven by heat at the middle temperature level. A certain part of this heat is rejected at high temperature and another at low temperature.

A schematic of an *H_2O / LiBr* AHT is shown in Figure 2-3. The poor solution leaves the generator (GEN) and is pumped by the solution pump (PUMP) to the high pressure level. It enters the absorber (ABS) and absorbs the *H_2O* vapor coming from the evaporator by rejecting heat ($\dot{Q}_{ABS}$) at high temperature. The rich solution leaves the absorber and is reduced again to the low pressure level in the solution throttle valve (STH) and returns to the generator. In the generator, the *H_2O* vapor is generated from the rich solution by supplying heat ($\dot{Q}_{GEN}$) at middle temperature. This vapor flows to the condenser (CON) and condenses there by rejecting heat ($\dot{Q}_{CON}$) at low temperature. Afterwards it is pumped by the condensate pump (CPUMP) to the high pressure level and enters the evaporator (EVA). In the evaporator the liquid *H_2O* is evaporated by supplying heat at middle temperature level ($\dot{Q}_{EVA}$). The generated vapor flows then to the absorber.

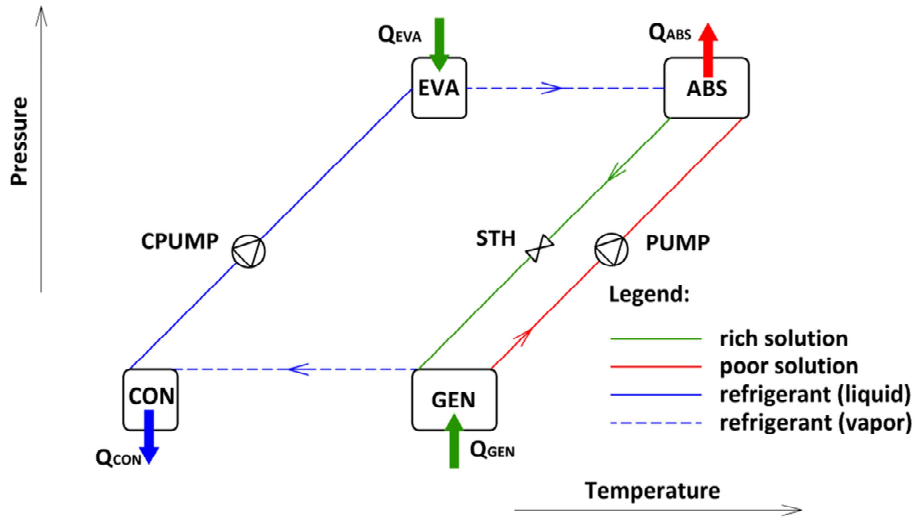

Figure 2-3: Schematic of an H_2O / LiBr AHT (absorption heat pump Type II)

Most of the conventional absorption heat transformers (absorption heat pumps Type II) use the working pair *H_2O / LiBr* and are utilized in industrial heat recovery. They are driven e.g. by waste heat at temperatures of approximately 80 - 90℃ in order to lift one portion of the driving energy to a useful temperature level of approximately 120 - 140℃ and reject the rest to a heat sink with a temperature level of approximately 20 - 40℃. According to Mostofizadeh and Kulick (1998) the typical COP of such a heat transformer is about 0.5 - 0.6.

The COP for the absorption heat transformer is defined as a ratio of the absorber capacity to the sum of the generator, evaporator and pumps capacities (Eq. 2-3).

$$COP = \frac{\dot{Q}_{ABS}}{\dot{Q}_{GEN} + \dot{Q}_{EVA} + P_{PUMP} + P_{CPUMP}} \qquad 2\text{-}3$$

2.1.1 Manufacturers of absorption heat pumping systems

The list of AHP manufactures according to Gluesenkamp et al. (2011) and Jakob and Kohlenbach (2010) is presented in Table 2-1. Nowadays, AHP with cooling capacities in the range between 10 - 500 kW are available on the market. The share of AHP with cooling capacities lower than 50 kW for use in small office buildings or multi-family houses is also ion the rise. The majority of companies use *H_2O / LiBr*, few *NH_3/ H_2O* AHP and only one uses *H_2O / LiCl* as a working mixture. In regard to multi-stage absorption cycles there are 7 manufactures producing double-effect absorption chillers and only one producing triple-absorption chillers.

Table 2-1: List of AHP manufactures (according to Gluesenkamp et al. (2011) and Jakob and Kohlenbach (2010))

Company	Country	Available absorption unit types	Available nominal cooling capacities [kW]
AGO	Germany	*NH_3 / H_2O*	30 - 1000
Broad	China	Various	175 - 23260
Carrier	USA	*H_2O / LiBr*, single- and double-effect	352 - 15977
ClimateWell	Spain	*H_2O / LiCl* with thermal storage	10 - 20
EAW	Germany	*H_2O / LiBr*	15 - 200
Ebara	Japan	Various	158 - 2462
Entropie	France	*H_2O / LiBr*	300 - 6000
Hitachi	Japan	*H_2O / LiBr*, parallel flow double-effect	106 - 19690
Kawasaki	Japan	*H_2O / LiBr*, double- and triple-effect	141 - 2462
LG	Korea	*H_2O / LiBr*	100 - 1750
Pink	Austria	*NH_3 / H_2O*	12
Rotarctica*	Spain	*H_2O / LiBr*, single-effect, rotary, air-cooled	4.5
Sanyo	Japan	*H_2O / LiBr*, single- and double-effect	105 - 5274
Shuangliang	China	*H_2O / LiBr*, single- and double-effect	930 - 5230
Solarice	Germany	*NH_3 / H_2O*	25 - 40
SolarNext	Germany	*NH_3 / H_2O* and *H_2O / LiBr*	18 - 50
Sonnenklima	Germany	*H_2O / LiBr*	10
Thermax	India	*H_2O / LiBr*	35 - 12000
Trane	USA	*H_2O / LiBr*, single- and double-effect	390 - 7136
Yazaki	Japan	*H_2O / LiBr*, air- and water-cooled	28 - 105
York	USA	*H_2O / LiBr*, single- and double-effect	422 - 4853

*no longer in production

2.1.1 Application areas of absorption heat pumping systems

The use of absorption heat pumps for cooling and heating purposes can be found in different types of buildings and using various sources of driving energy. Within this subchapter, different application areas of absorption heat pumps are performed and some realized systems are discussed.

Solar cooling

One of the most promising application areas for AHP systems is solar cooling. An overview of the situation on the solar cooling market was presented by Jakob and Kohlenbach (2010). In spite of the fact that the solar cooling market is very young it has developed rapidly over the last years. According to Jakob and Kohlenbach (2010) in 2004 approximately 50 solar

cooling systems had been installed worldwide. The number of installations had increased to 450 - 500 in 2008. The majority of these systems (400) are in Europe. The use of AHP for solar cooling systems plays an important role, 60% of all systems are based on absorption chillers, 11% on adsorption chillers and 29% on open systems, i.e. DEC and liquid sorption systems.

Concerning the total costs for solar cooling kits in Europe in 2009 (without installation costs and cold distribution) they varied between 3000 - 4500 EUR per kW with solar collector and between1500 - 2000 EUR per kW without solar collector (Jakob and Kohlenbach, 2010). An example of the solar cooling kit without solar collector is shown in Figure 2-4.

In Austria, solar cooling systems can be found in single family houses, multi-family houses and small commercial buildings. An example for solar cooling system in small commercial buildings is the office building (air-conditioned area 700 m^2) of Bachler Austria GmbH in Gröbming ("Solair" project, 2009). The cold water for the space cooling (16 / 19°C) is supplied by an NH_3 / H_2O AHP made by the company "Pink" with a cooling capacity of 9 kW and a COP_C of 0.64. As driving energy solar heat and heat produced by a biomass boiler at a temperature of 80°C are used. In winter the system is also used for space heating.

Figure 2-4: Photo of the solar cooling kit ISC11 of the company "SolarNext" (Solarnext, 2012)

District cooling

Another application for absorption chillers is district cooling. One such system has been created in Vienna by the company "Fernwärme Wien" in 2007 for the cooling of the commercial building complex "TownTown". At present, the system consists of 2 H_2O / *LiBr* absorption chillers (made by "York") with a cooling capacity of 2.2 MW each and 3 compression chillers with a cooling capacity of 0.9 MW each. Both absorption chillers are driven by the district heating system (110°C). In the future it has been planned to extend the system to a cooling capacity of 8 MW and to use it for the cooling of new buildings.

Waste heat utilization

H_2O / LiBr AHP. To accomplish the overview on AHP applications operating at low generator temperatures, the use of waste heat has to be discussed. In Austria such applications can be found both in small and large capacity application areas. The *H_2O / LiBr* AHP with a cooling capacity of approximately 35 kW utilizing the heat energy of exhaust gases of a micro-gas turbine installed in the boiler house of the company “Energie AG” in Steyr is an example of a small capacity application. The cold water has an outlet / inlet temperature of 9 / 14°C and is used for space cooling of an office building. The heat rejection outlet / inlet temperatures are 25 / 35°C and the driving heat temperature ranges from 75°C to 100°C. The COP_C of the absorption process is 0.70.

A large capacity *H_2O / LiBr* AHP using heat energy of flue gas condensation is installed in the biomass boiler house of the company “Inven” in Hallein (Rechberger, 2010). The AHP has a cooling capacity of 3 MW and a COP_C of 0.70.

H_2O / LiBr AHT. Most of the conventional absorption heat transformers (absorption heat pumps Type II) use the working pair *H_2O / LiBr* and are utilized for industrial heat recovery. They are driven e.g. by waste heat at temperatures of ca. 80 - 90°C in order to lift one portion of the driving energy to a useful temperature level of ca. 120 - 140°C and reject the rest to a heat sink with a temperature level of ca. 20 - 40°C. The typical COP of such an absorption heat transformer (AHT) is about 0.5 - 0.6 (Mostofizadeh and Kulick, 1998).

Attention to AHTs began to be paid in the 1980’s, when according to the Final report from Annex 21 of the IEA Heat Pump Program 15 heat transformers were in operation. Most of them (9) had been installed in Japan, 3 in Germany, 1 in South Korea, 1 in the Netherlands and 1 in Yugoslavia. The installed AHTs had a heating capacity between 0.5 - 7.0 MW and mostly used steam at temperatures between 80 - 100°C as a driving heat. Temperature of the useful heat were between 115 - 150°C and COP between 0.47 - 0.49. According to Ziegler (2002) all installed AHTs operated properly but a return on the investment was difficult to achieve.

NH_3 / H_2O Hybrid heat pump. Compression-absorption hybrid cycle is a modification of a compression cycle, which consists of a sorption cycle and a compressor. In the absorption cycle the *NH_3 / H_2O* solution circulates between a desorber (low pressure level) and an absorber (high pressure level). The compressor aims to increase the vapor pressure leaving the desorber and supplying it in turn to the absorber. The main advantage of this cycle in comparison to a conventional compression cycle is that it can operate at lower pressures than a compression cycles when external temperatures are fixed.

On the market this cycle is found in Norway for large capacity applications using waste heat as heat source. For instance, “Hybrid Energy” installed a hybrid heat pump at Nortura Rudshoega (Norway) with a heating capacity of 650 kW. It raises the hot water temperature from 49℃ to 87℃. The cycle COP is 5.3 and amount of time required for the investment to pay itself off is 2 years (Hybrid Energy, 2011).

Gas-fired AHP systems for heating and cooling

GAX-process. Gas-fired NH_3 / H_2O AHPs are commonly used for both heating and cooling applications. Nowadays, gas-fired AHP are being treated as the next step in terms of efficiency after condensing gas boilers and, thus, in the near future may play an important role in the modernization of old heating systems in single and multi-family houses. Gas-fired AHPs are based on the GAX-process, which is similar to a single-stage AHP-process but having higher efficiency than a conventional NH_3 / H_2O AHP, because of an additional heat exchanger that transfers heat between generator and absorber using temperature overlap.

Moser and Rieberer (2011) have performed an analysis of a gas-driven NH_3 / H_2O AHP-system used for heating and domestic hot water preparation in a storehouse in Graz. The system consists of 2 AHP units of the company “Helioplus Energy Systems GmbH” with a heating capacity of 37 kW each. The heating water supply temperature varies between 30 - 40℃ and the domestic hot water supply temperature is 55℃. The heat to the evaporator is supplied from ground probes, its temperature ranges from 0℃ to 5℃. The system had been measured during 2010 (winter operation – heating and domestic hot water; summer operation – domestic hot water only). The overall COP_H calculated using monitoring data is 1.54 / 1.40, based on lower / upper heating value respectively.

Figure 2-5: Photo of the installed gas-fired AHP units in Graz (Rieberer and Moser, 2011)

It is necessary to mention that the main barrier for using gas-fired AHPs is high investment costs in comparison to conventional technologies. Thus, government subsidies for their installation are necessary. For instance, in Germany an initiative for gas-driven heat pumps has been started. Within this initiative, ca. 100 gas-driven AHP-systems are being monitored and analyzed (http://igwp.de/; last accessed on 03.05.2012).

Double- and triple effect H_2O / LiBr AHP-processes. Since the first double-effect *H_2O / LiBr* absorption chiller had been commercialized by "Kawasaki" (Japan) in 1968 its installations can be found in different application areas. Nowadays this type of absorption chiller is mostly used for gas cooling in large capacity applications. According to Ziegler (2002) the underlying idea is the use of the gas grid instead of electricity for cooling purposes, thus, reducing mid-afternoon peak in electricity supply. The common COP_C varies from 1.0 to 1.1.

Up to now, the only commercialized gas-fired triple-effect *H_2O / LiBr* absorption chiller is being produced by "Kawasaki". Makita (2006) has reported field testing results of such a chiller with a cooling capacity of 1055 kW and chiller water temperatures of 15 / 7°C operating for 14000 hours (6000 hours per year). The field testing results have shown that the chiller COP_C equals approximately 1.6 when operating at the maximal cooling load and approximately 1.7 at 60% of the maximal cooling load.

Nowadays, the product line of triple-effect absorption chillers consists of 4 models: 2 types of direct-fired (cooling capacity of 651 kW and 1196 kW) and 2 types of waste hot water applied (cooling capacity of 580 kW and 1090 kW). Concerning the market implementation 12 installations using triple-effect absorption chillers are known. All of them are installed in Japan and are used in hospitals, factories, general buildings, etc. Unfortunately, no data concerning the operation experience was found.

Camping refrigerators (Diffusion-absorption absorption cycle)

The diffusion-absorption heat pumping process was proposed by Platen and Munters (1925) and represents a single-pressure *NH_3 / H_2O* absorption cycle with a non-condensable auxiliary gas (usually *He* or *H*). The main advantage of this cycle in comparison to a conventional absorption cycle is that there is no solution pump and the solution circulation occurs by means of a bubble pump using heat energy instead of electricity. The principle of operation is based on the use of an auxiliary non-condensable gas in order to achieve the partial pressure difference of ammonia. Nowadays, it is widely used in camping refrigerators with a cooling capacity of 200 W. Recently, several prototypes of a diffusion-absorption heat pump with a cooling capacity of 3 kW have been developed at the Stuttgart University of Applied Sciences (Jakob et al., 2008).

2.1.2 Working fluids

As is mentioned above, conventional AHP-processes use either NH_3 / H_2O or H_2O / *LiBr* as a working mixture. Essentially, NH_3 / H_2O AHP are used at evaporator temperatures below 0 (refrigeration) and H_2O / *LiBr* AHP above 0 (water chillers). The NH_3 / H_2O AHP operate at higher pressures than H_2O / *LiBr* AHP and therefore are more compact. The main drawbacks of NH_3 / H_2O AHP are the need for rectification, high working pressures and the toxicity of NH_3. Those of H_2O / *LiBr* AHP are restricted in their temperature lift due to the crystallization issue, toxicity and additional costs of corrosion inhibitors.

Apart from conventional working mixtures, few applicable examples with alternative working mixtures are known. One of them is a mixture of alcohols (refrigerant) and salts (absorbent). The idea behind using alcohols as refrigerants is to enable the operation of the AHP-process at lower working pressures. According to Löwer et al. (1987) methanol is the most recommended alcohol for such an undertaking. It has a high heat of evaporation (1170 $kJ \cdot kg^{-1}$ at 1 bar), a normal boiling temperature of 65°C, is less toxic than ammonia and is used with lithium-bromide as an absorbent. However, the application area is limited due to the crystallization issue. It can be overcome by means of using zinc-bromide as an additive; however the generator temperature cannot be higher than 130°C due to the decomposition of methanol.

Another alternative to ammonia as refrigerant is amines. From the literature (Lower et al., 1987) the use of methylamine and ethylamine together with water or different salts as absorbents is well known; the enthalpy of vaporization at 1 bar is 815 $kJ \cdot kg^{-1}$ and 590 $kJ \cdot kg^{-1}$, respectively. Methylamine has a condensation temperature of 50°C at 7.7 bar and ethylamine at 3.3 bar. The main drawback of both refrigerants is the need for rectification due to the small difference between their normal boiling temperatures and that of water.

According to Lower et al. (1987) the use of lithium-thiocyanate and natrium-thiocyanate as absorbent suggested in the literature is problematic due to high viscosity and the afore-mentioned crystallization issue.

The properties of conventional working pairs can be greatly improved either by use of new additives for NH_3 / H_2O (Salavera et al. 2005) and H_2O / *LiBr* (Gluesenkamp et al. 2011) or via new absorbents in place of H_2O and *LiBr*.

Requirements on refrigerant and absorbent

When choosing refrigerant and absorbent for use in an absorption process the following properties are essential for the process performance (Löwer et al., 1987):

- thermal stability, chemical compatibility, full miscibility and absence of crystallization;
- melting temperature of the refrigerant has to be lower than the lowest evaporator temperature;
- melting temperature of the absorbent has to be lower than the lowest absorber temperature;
- normal boiling temperature of the refrigerant should lie between the evaporator and absorber temperatures;
- critical temperature of the refrigerant has to be higher than the highest temperature within an AHP-process;
- heat of evaporation of the refrigerant should be higher than 800 $kJ \cdot kg^{-1}$, in order to decrease the mass flows, heat losses and the system size. However, too high values of heat of evaporation can cause low mass flows and, therefore, regulation problems;
- specific heat capacity of the refrigerant and of absorbent has to be low to minimize heat losses within an solution circuit of the absorption process (generator, solution heat exchanger) and losses in the refrigerant throttle valve;
- vapor pressure curve have to be as flat as possible, in order to have low difference between the high and low pressure levels;
- viscosity and surface tension of the refrigerant and absorbent have to be as low as possible;
- thermal conductivity of the refrigerant and absorbent have to be as high as possible.

Refrigerant pre-selection

At the present time, various refrigerants continue to be proposed for a use in AHP-processes. In order to evaluate and to pre-select from amongst them an analytical method introduced by Alefeld and Radermacher (1994) and further developed by Gluesenkamp et al. (2011) can be used. According to this method, a pre-selection of refrigerant can be completed knowing the specific heat capacity of refrigerant in the liquid phase ($c_{p,l}$), heat of evaporation of the refrigerant (h_{fg}), and density of refrigerant in the vapor phase (ρ_{vap}) (see Eq. 2-4 – 2-6). Using these properties 3 parameters for refrigerant selection can be obtained.

Losses in the refrigerant throttle valve. The first parameter describes losses in the refrigerant throttle valve (see Eq. 2-4) and is the ratio of the specific heat capacity of liquid refrigerant to its heat of evaporation as a function of the temperature lift. This ratio approximates the refrigerant vapor quality entering the evaporator. High values of the refrigerant vapor quality entering the evaporator hinder system efficiency. Therefore, the heat capacity of refrigerant in the vapor phase must be as low as possible and its heat of evaporation as high as possible.

$$x_{eva,in} \approx \frac{c_{p,l} \cdot \Delta T_{cond-evap}}{h_{fg}} \qquad 2\text{-}4$$

Losses in the solution circuit. The second parameter (see Eq. 2-5) describes amount of heat, which has to be supplied to the solution circuit and is the ratio of the mass flow of refrigerant to the evaporator capacity. This ratio is more or less inversely proportional to the liquid mass fraction entering the evaporator and therefore must be as low as possible to minimize the efficiency penalty.

$$\frac{\dot{m}_{ref}}{\dot{Q}_{eva}} \approx \frac{1}{(1 - x_{eva,in}) \cdot h_{fg}} \qquad 2\text{-}5$$

System size. To minimize the system size of the absorption cycle, low volumetric flow rate is necessary (see Eq. 2-6). The ratio of the volumetric flow rate to the evaporator capacity can be obtained by introducing to Eq. 2-5 the density of refrigerant vapor leaving the evaporator:

$$\frac{\dot{V}_{ref}}{\dot{Q}_{eva}} \approx \frac{1}{\rho_{vap}(1 - x_{eva,in}) \cdot h_{fg}} \qquad 2\text{-}6$$

A comparison of these parameters for various refrigerants is shown in Table 2-2. The main conclusion which can be drawn is that the use of organic refrigerants in AHP, apart from methanol, is disadvantageous, owing of their high specific heat capacity, low heat of evaporation, high mass flow rate and thus the size of absorber and generator in comparison to conventional refrigerants. It can be seen that ammonia is the most advantageous out of the listed refrigerants.

Table 2-2: Comparison of refrigerant properties at t_{CON} / t_{EVA} = 45 / 5℃ (literature review: Gluesenkamp et al. (2011))

Refrigerant	$\approx x_{eva,in}$	$\approx \frac{\dot{m}_{ref}}{\dot{Q}_{eva}}$	$\approx \frac{\dot{V}_{ref}}{\dot{Q}_{eva}}$
	[$kg_{VAP} \cdot kg_{TOT}^{-1}$]	[$g \cdot s^{-1}$ per kW]	[$L \cdot s^{-1}$ per kW]
Water	0.07	0.43	63.4
Methanol	0.08	0.91	11.9
Ammonia	0.15	0.95	0.2
R22	0.24	6.57	0.3
Isobutane	0.27	3.89	0.8
R134a	0.28	7.11	0.4
Propane	0.28	3.77	0.3
R410A	0.29	6.47	0.2
CO_2	0.51	9.42	0.1

Requirements on working mixtures

As is well-known, the theoretical cooling COP of a single-stage AHP, assuming that condenser and absorber temperatures are equal, is described by Eq. 2-7, where T_{EVA} is the temperature level in the evaporator, T_{CON} in the condenser and T_{GEN} in the generator.

$$COP_C = \frac{\frac{1}{T_{CON}} - \frac{1}{T_{GEN}}}{\frac{1}{T_{EVA}} - \frac{1}{T_{CON}}} \qquad 2\text{-}7$$

Graphic analysis of Eq. 2-7 can be done, when comparing the Duhring plot (*log (p) vs. 1/T* diagram) for different working mixtures. Generally, one can distinguish three variations within the Duhring plot for working mixtures (see Figure 2-6), assuming that the solution flow rate approaches infinity:

- the working mixture with a convergence between vapor pressure curves (Figure 2-6a);
- the working mixture with parallel vapor pressure curves (Figure 2-6b);
- the working mixture with a divergence between vapor pressure curves. (Figure 2-6c)

It can be seen that the theoretical cooling COP of a single-stage AHP (see Eq. 2-7) can be obtained graphically as a ratio of the horizontal line, joining the condenser temperature with the generator temperature, to the one, joining the condenser temperature with the evaporator temperatures. Apparently, the highest value of the COP_C has the working mixture with a divergence between the vapor pressure curves. In this case, the difference between the low and high temperature levels is maximal.

According to Alefeld and Radermacher (1994), the single-stage cooling COP (see Eq. 2-7) can be also obtained, if the heat of evaporation (h_{fg}) and heat of mixing (Δh_{mix}) are known. The slope of the vapor pressure line of the pure refrigerant in the Duhring plot (see Figure 2-6) is proportional to the heat of evaporation while the slope of the vapor pressure line of the working mixture is proportional to the sum of the heats of evaporation and mixture:

$$COP_C = \frac{h_{fg}}{h_{fg} + \Delta h_{mix}} \qquad 2\text{-}8$$

The expected single-effect cooling COP (Eq. 2-8) is about 0.9 for *H_2O / LiBr* and about 0.8 for *NH_3 / H_2O* (Gluesenkamp et al., 2011).

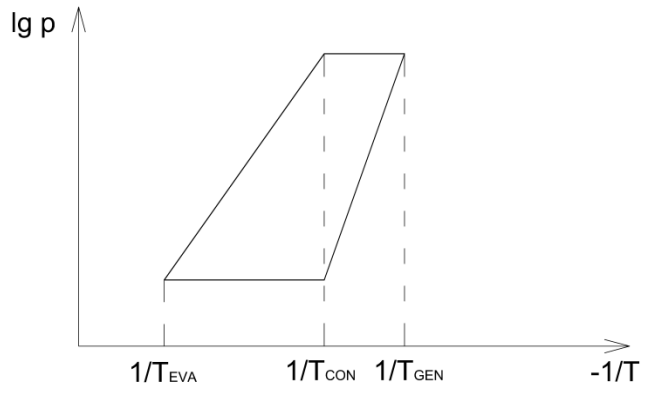

a

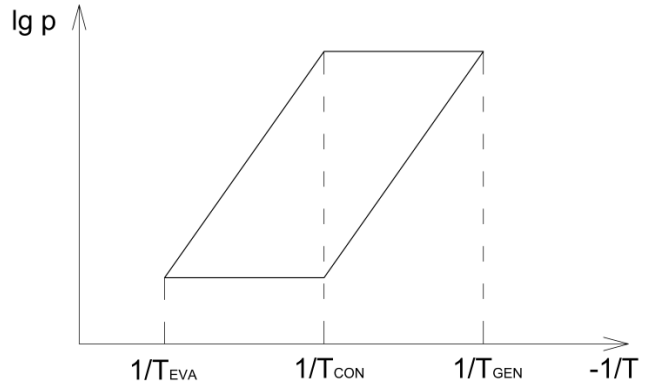

b

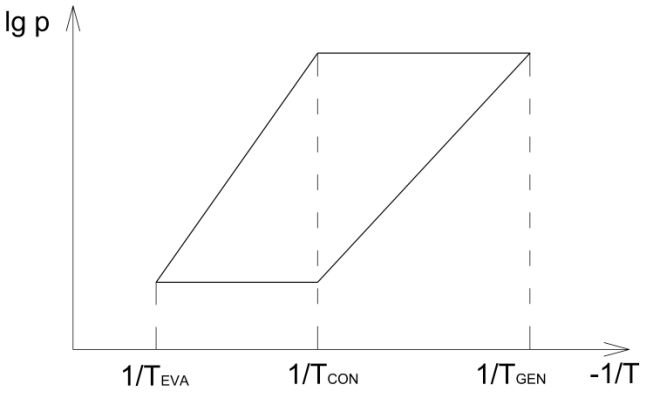

c

Figure 2-6: Duhring plot for a conventional AHP-process with: a – a convergence between the vapor pressure curves; b – parallel vapor pressure curves; c – a divergence between the vapor pressure curves

In an above discussed example, it was assumed, that the solution flow rate approaches infinity. However, in a real situation, excessively high values of the solution flow rate penalize the COP. The solution flow rate can be calculated knowing refrigerant mass concentration in the rich (ξ_{RSO}) and poor (ξ_{PSO}) solutions as well in the generated vapor (ξ_{REF}) (see Eq. 2-9).

$$f = \frac{\xi_{REF} - \xi_{PSO}}{\xi_{RSO} - \xi_{PSO}} \qquad 2\text{-}9$$

In regard to the Duhring plot, it is possible to conclude that the vapor pressure curves at constant refrigerant concentrations must be distributed uniformly between the vapor curves of the pure refrigerant and pure absorbent. Figure 2-7 shows a working mixture with a uniform (a) and with a non-uniform (b) distribution of the vapor pressure curves. Apparently, the first working mixture allows for higher refrigerant concentrations in the rich solution and therefore lower solution flow rates than the second one.

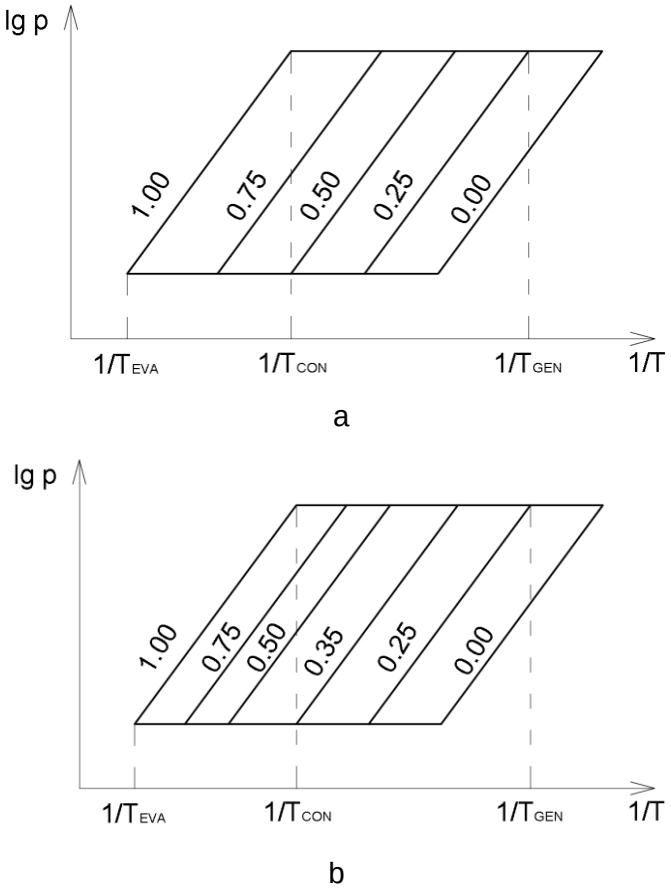

Figure 2-7: Duhring plot for a conventional AHP-process with: a – uniformly distributed vapor pressure curves; b – non-uniformly distributed vapor pressure curves

3 ALTERNATIVE ABSORPTION HEAT PUMPING PROCESSES

Within this chapter a detailed survey of related literature concerning the following groups of innovative AHP-processes will be presented:

1. ammonia / water (NH_3 / H_2O) absorption heat pumping (AHP) process using strong bases as additives;
2. absorption heat transformer (AHT) using partially miscible working mixtures;
3. absorption heat pumping (AHP) processes using a condensable auxiliary fluid: Rojey cycle and Einstein-Szilard cycle;
4. ammonia / ionic liquid absorption heat pumping (AHP) process.

The analysis of the AHP-processes discussed within this chapter will be done by means of thermodynamic simulation using the software program ASPEN Plus. This program has a library of typical components of an AHP-process, such as an absorber, rectification column, heat exchangers, etc. The program also allows for simulation of the AHP-processes with different working mixtures. Refrigerant and absorbent and their binary parameters can be chosen from the built-in library of ASPEN Plus. If binary parameters are not available, they can be regressed using experimental vapor-liquid-equilibrium (VLE) or liquid-liquid-equilibrium (LLE) data.

3.1 NH_3 / H_2O absorption heat pumping process using strong bases as additives

One of the most promising application areas for AHP is the cooling application at low driving temperatures, e.g. by using solar energy, district heating or waste heat. Several authors (Balamuru et al., 2000, Bruno et al., 2005, and Steiu et al., 2009) have reported that the use of strong bases such as *NaOH*, *KOH* and *LiOH* as additives to the working mixture NH_3 / H_2O in an AHP can increase its efficiency and at the same time decrease the required generator temperature.

3.1.1 Influence of strong bases on the absorption and desorption of ammonia

Before discussing the principle of operation of the NH_3 / H_2O AHP-process using *NaOH* as additive, it is necessary to analyze the influence of *NaOH* on the absorption / desorption of NH_3 by / from NH_3 / H_2O solution.

NH_3 / H_2O solution without additives

Figure 3-1 shows structural formulas of *NH_3* and *H_2O* molecules. Both of them are dipole molecules and are highly soluble in each other due to the dipole-dipole and hydrogen bonds.

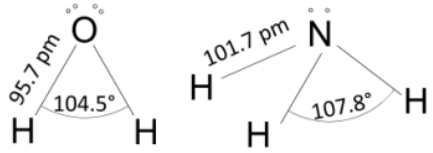

Figure 3-1: Structural formula of H_2O (left) and NH_3 (right) (according to Mortimer and Mueller, 2007)

Generally, the chemical processes in *NH_3* / *H_2O* solution can be described via of two equations:

- chemical equilibrium between the gaseous and dissolved in the *NH_3* / *H_2O* solution ammonia;
- chemical equilibrium between the dissolved and dissociated in the *NH_3* / *H_2O* solution ammonia.

The first chemical process can be described by Eq. 3-1, where on the left side, ammonia in the gaseous (g) phase and water in the liquid phase are in equilibrium with dissolved ammonia (sol) in *NH_3* / *H_2O* solution on the right.

$$NH_{3(g)} + H_2O_{(l)} \leftrightarrow NH_{3(sol)} + H_2O_{(sol)} \qquad 3\text{-}1$$

The *NH_3* dissociation process is described by Eq. 3-2. This reaction is an acid-base reaction, where *NH_3* is a base and *H_2O* is an acid. Being a weak base, *NH_3* does not dissociate completely.

$$NH_{3(sol)} + H_2O_{(sol)} \leftrightarrow NH_{4(aq)}^{+} + OH_{(aq)}^{-} \qquad 3\text{-}2$$

The chemical equilibrium depends on the *NH_3* concentration in the solution and its temperature and can be calculated using the base dissociation constant (*K_B*):

$$K_B = \frac{c(OH^-) \cdot c(NH_4^+)}{c(NH_3)} \qquad 3\text{-}3$$

NH_3 / H_2O solution with strong bases as additives

Strong bases, such as *NaOH*, *KOH* or *LiOH*, consist of ions and are soluble in *H_2O* due to ion-dipole bonds (Figure 3-2). The cations are in contact with the negative side of *H_2O* molecules (oxygen atoms), and the anions with the positive side of *H_2O* molecules (hydrogen atoms).

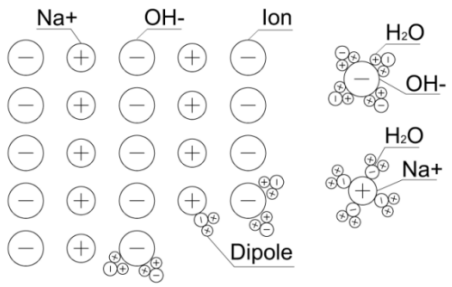

Figure 3-2: Hydration of an ionic crystal (according to Mortimer and Mueller, 2007)

The ion-dipole bonds are stronger than the dipole-dipole bonds between NH_3 and H_2O and, therefore, when a strong base is added into the NH_3 / H_2O solution, the equilibrium described by Eq. 3-2 is shifted to the left side. As a result, less NH_3 can be dissolved by H_2O.

In order to evaluate the influence of *NaOH* on the desorption of NH_3, the NH_3 dissociation depending on the pH value has been calculated. The calculation procedure is described in detail in the work of Wohlthan (2011). For the calculation of the base dissociation constant (K_B) the required properties of NH_3 / H_2O were obtained from the software program Factsage. The results for a temperature of 100℃ are presente d in Figure 3-3. The solid line represents the NH_3 fraction while the dashed line shows the NH_4^+ fraction depending on the pH value. It can be seen, that the NH_4^+ fraction decreases and the NH_3 fraction increases with the increasing pH value.

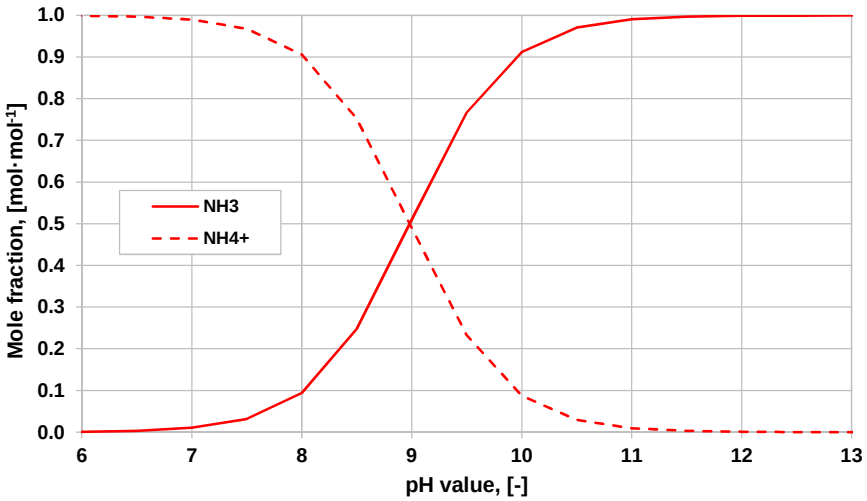

Figure 3-3: NH_3 vs. NH_4^+ fraction depending on the pH value at 100℃ (prope rties calculated in Factsage)

In order to evaluate the NH_3 dissociation pH, the value of the solution has to be known. Figure 3-4 shows the pH value of the NH_3 / H_2O / *NaOH* solution (ξ_{NH3} = 0.2) depending on the *NaOH* mass concentration at 100℃. It can be seen, that the NH_3 / H_2O solution without NaOH has a pH value of about 10.2. The pH value increases with the increasing *NaOH*

concentration. For instance, when 5% of *NaOH* are added the pH value is about 12.0. This means, the NH_3 fraction increases from 0.9 to 1.0 (see Figure 3-3) and can be easier separated from the NH_3 / H_2O / *NaOH* solution, which is advantageous for NH_3 desorption.

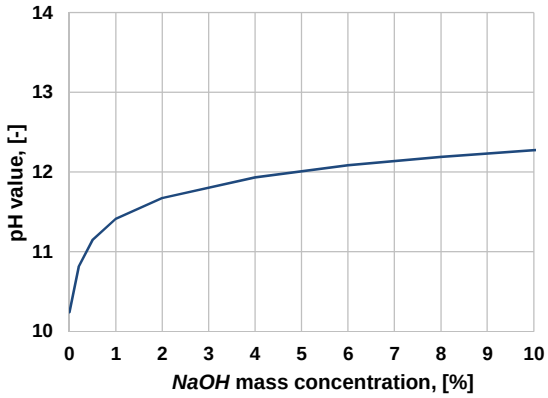

Figure 3-4: pH value of the NH_3 / H_2O / NaOH solution (ξ_{NH3} = 0.2) depending on the NaOH mass concentration at 100℃ (properties calculated in Fa ctsage)

Another advantage when using strong bases as additives to the working mixture NH_3 / H_2O in the AHP-process is a decrease in the boiling temperature of the NH_3 / H_2O solution. Figure 3-5 shows a comparison of boiling curves of the NH_3 / H_2O solution with *NaOH* mass concentrations of 0, 5 and 10 wt.-%. The properties of NH_3 / H_2O / *NaOH* solution have been calculated using the regressed experimental data of Salavera et al. (2005) in ASPEN Plus (see Chapter 3.1.3). Apparently, the solution boiling temperature decreases when *NaOH* is added. For instance, the boiling temperature of the NH_3 / H_2O solution without *NaOH* at NH_3 has a mass concentration of 0.3 kg·kg^{-1} is 102℃. It decreases to 93℃ when adding 5 wt.-% *NaOH* and to 85℃ when adding 10 wt.-% NaOH.

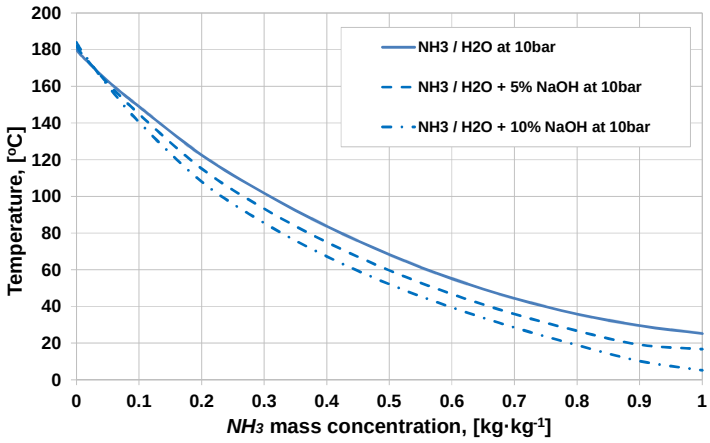

Figure 3-5: Comparison of boiling curves of the NH_3 / H_2O mixture and with 0, 5 and 10 wt.-% NaOH (properties calculated in ASPEN Plus)

3.1.2 Process description

The operating principle of the NH_3 / H_2O AHP-process using strong bases as additives is similar to a conventional NH_3 / H_2O AHP-process. The NH_3 / H_2O AHP-process using *NaOH* as an additive is shown in a pressure / temperature diagram in Figure 3-6.

The rich solution of NH_3 / H_2O / *NaOH* leaves the absorber (ABS),is pumped to the high pressure level by means of the solution pump (PUMP) and enters the generator (GEN). In the generator the NH_3-vapor and the poor solution of NH_3 / H_2O / *NaOH* are generated by supplying heat at high temperature ($\dot{Q}_{GEN}$) from an external heat source. The poor solution is throttled (STH) to the low pressure level and returns to the absorber. The generated NH_3-vapor enters the condenser (CON) and condenses there by rejecting heat at the middle temperature level ($\dot{Q}_{CON}$) to an external heat sink. The liquid NH_3 is throttled (RTH) back to the low pressure level, enters the evaporator (EVA) and evaporates there by supplying heat at low temperature ($\dot{Q}_{EVA}$) from an external heat source. Finally, the evaporated NH_3 enters the absorber and is absorbed there by the poor solution. The absorption heat ($\dot{Q}_{ABS}$) is relegated to an external heat sink at the middle temperature level. As can be seen, *NaOH* is present only in the sorption part (between the absorber and generator). The reason for that is the negligible vapor pressure of *NaOH* which thus does not evaporate in the generator.

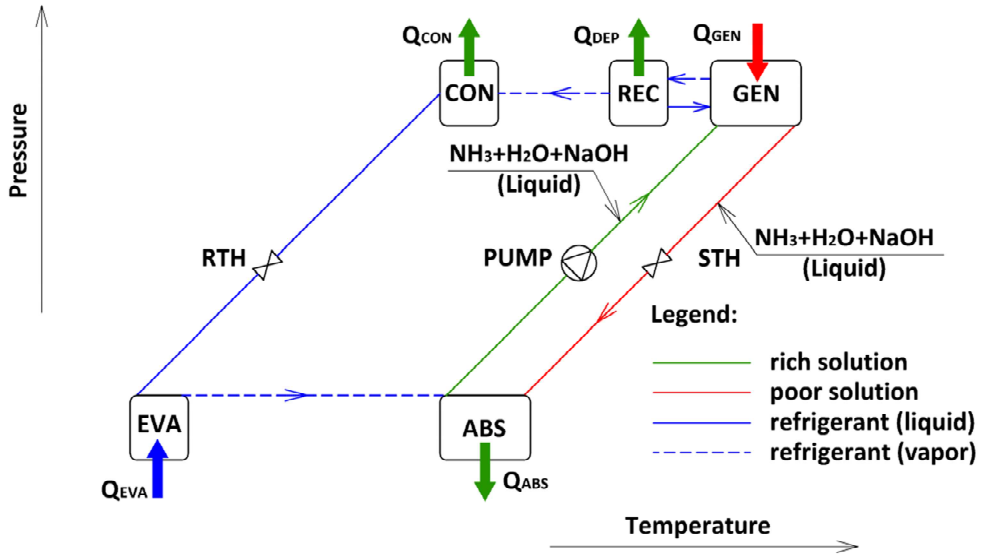

Figure 3-6: AHP-process using the working mixture NH_3 / H_2O / NaOH

The *NaOH* concentration in the strong or weak solution can be calculated on the base-free (Eq. 3-4) or base-containing basis (Eq. 3-5):

$$\xi_{NaOH\ base-free} = \frac{m_{NaOH}}{m_{NH_3} + m_{H_2O}} \qquad 3\text{-}4$$

$$\xi_{NaOH\ base-containing} = \frac{m_{NaOH}}{m_{NH_3} + m_{H_2O} + m_{NaOH}} \qquad 3\text{-}5$$

Where,

$\xi_{NaOH\ base-free}$ – *NaOH*-concentration based on base-free basis, kg·kg^{-1};

$\xi_{NaOH\ base-containing}$ – *NaOH*-concentration based on base-containing basis, kg·kg^{-1};

$m_{NH_3}; m_{H_2O}; m_{NaOH}$ – masses of NH_3; H_2O and *NaOH* in the rich solution, kg.

In the following, the *NaOH* concentration in the NH_3 / H_2O / *NaOH* solution will be calculated in line with a base-containing basis.

The use of *NaOH* as an additive to the working mixture NH_3 / H_2O in an AHP-process was investigated by Balamuru et al. (2000), Bruno et al. (2005), and Steiu et al. (2009). They investigated the process by means of thermodynamic simulations using the software program ASPEN Plus. The AHP-process has been analyzed at different *NaOH* concentrations. The simulation results showed that there is a upper-limit in the COP_C at a *NaOH* concentration in the rich solution of 8%.

Figure 3-7 shows the comparison between the COP_C calculated by Steiu et al. (2009) (red lines) and by Bruno et al. (2005) (blue lines). The comparison was done at the following boundary conditions: t_{CON_OUT} / t_{EVA_OUT} = 28 / -3℃, p_H = 12 bar, ξ_{RSO} / ξ_{PSO} = 0.40 / 0.31 kg/kg and $\xi_{NaOH\ base\text{-}free}$ = 0 - 8%. From Figure 3-7, it can be concluded that the COP_C increases (see Figure 3-7a) and the required generator temperature decreases (see Figure 3-7b) with the increasing *NaOH* concentration. For instance, the AHP-process operating with a *NaOH* concentration of 8% has a 12% higher COP_C than the process without *NaOH* (0%). At the same time, the driving heat can be supplied at a temperature of 93℃ instead of 107℃.

It is necessary to mention that the NH_3 concentration in the rich and poor solution was kept constant. This means that when keeping the temperature level in an absorber constant, while at the same time increasing the *NaOH* concentrations in the rich solution, both the low pressure level and the evaporator inlet temperature increase.

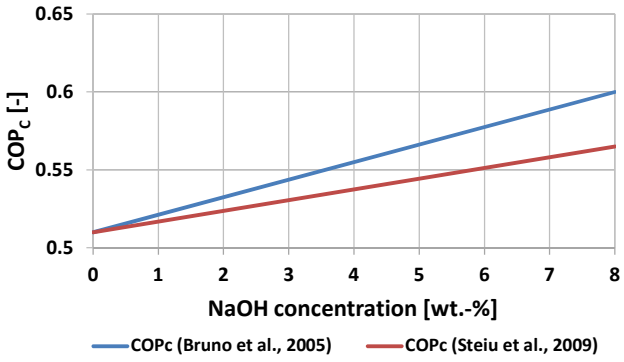

a

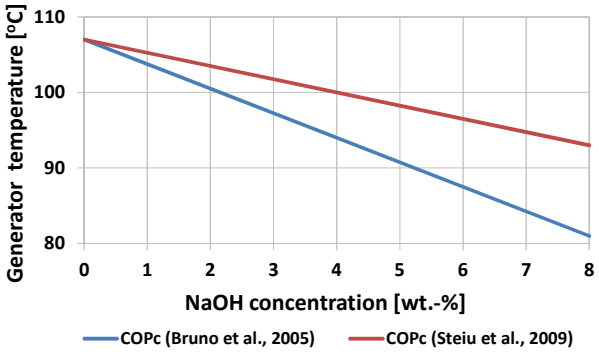

B

Figure 3-7: Simulation results of Steiu et al. (2009) in relation to those of Bruno et al. (2005): a – COP_C of an NH_3/H_2O/ NaOH AHP-process depending on NaOH-mass concentration; b – generator temperature of an NH_3/H_2O/ NaOH AHP-process depending on NaOH-mass concentration

As mentioned above, the use of *NaOH* is advantageous for the NH_3 generation and disadvantageous for its absorption by the poor solution. In order to overcome this drawback, the use of a semi-permeable membrane has been suggested and investigated by Bruno et al. (2005) and Steiu et al. (2009). According to Bruno et al. (2005) the COP_C can be increased if the semi-permeable membrane (MEMB) for the *OH*-ions separation is installed at the outlet from the generator as is shown in Figure 3-8. The principle of operation of the semi-permeable membrane is based on that of reversed osmosis. It separates the *OH*-ions and returns them back to the generator.

The calculated COP_C of this AHP-process relating on the membrane efficiency is shown in Figure 3-9 (Bruno et al., 2005). This diagram shows that the required membrane efficiency increases with the increasing *NaOH* concentration. The membrane efficiency is defined as the ratio of the mass flow of separated *OH*-ions to the mass flow of *OH*-ions in the poor solution entering the membrane. For instance, the COP_C at a *NaOH*-concentration of 10% requires a minimal membrane efficiency of 30%. When the *NaOH*-concentration is increased to 15%, the minimal membrane efficiency has to be higher than 80%. However, the use of such semi-permeable membranes in a conventional NH_3 / H_2O AHP is certainly not expected

anytime in the near future. Bruno et al. (2005) reported that these membranes are suitable for operation at temperatures below 70°C. Furthermore, to ensure the separation of *OH*-ions from the poor solution a pressure difference of approximately 39 bar is necessary. This means that an additional pump within the process is required and its power consumption must be taken into account when calculating the total cycle performance.

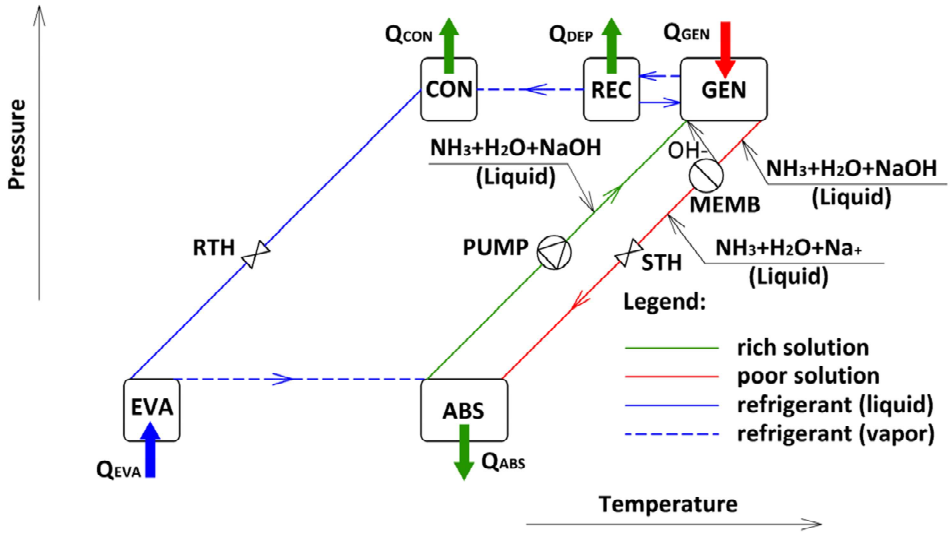

Figure 3-8: NH_3 / H_2O / NaOH AHP-process with semi-permeable membrane

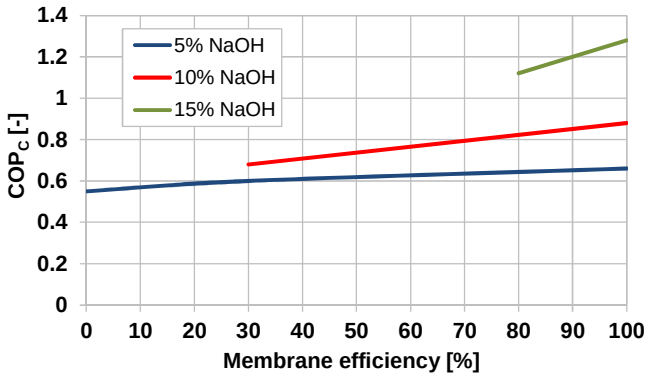

Figure 3-9: COP_C of the NH_3 / H_2O / NaOH AHP-process with semi-permeable membrane depending on the NaOH-concentration and the membrane efficiency (according to Bruno et al., 2005)

3.1.3 Calculation of properties of the working mixture NH_3 / H_2O / NaOH

For the thermodynamic simulation of the *NH_3* / *H_2O* AHP using NaOH as an additive, the data package “Ammonia” was used. This data package is based on the thermodynamic model ENRTL and uses “built-in” binary parameters for the mixture *NH_3* / *H_2O*. Additionally, the electrolyte pair parameters (GMELCC and GMELCD, as they called in ASPEN Plus) for the binary mixtures of *NH_3* / *NaOH* and *H_2O* / *NaOH* were regressed using the experimental VLE-data measured by Salavera et al. (2005) (see Table 3-1). These experimental VLE-data is valid for a temperature range of 20 - 80℃ and *NaOH* mass concentrations of 4 - 20%.

Table 3-1: Regressed electrolyte pair parameters for the working mixture NH_3 / H_2O / NaOH

Electrolyte pair parameter	*Molecule / ion pair*	*Value*
GMELCC	*NH_3 / Na^+ OH^-*	*22.800*
	Na^+ OH^- / NH_3	*-0.172*
	H_2O / Na^+ OH^-	*-1.065*
	Na^+ OH^- / H_2O	*3.754*
GMELCD	*NH_3 / Na^+ OH^-*	*0.166*
	Na^+ OH^- / NH_3	*-30.666*
	H_2O / Na^+ OH^-	*1.016*
	Na^+ OH^- / H_2O	*-2355.757*

The data regression results are shown in Figure 3-10 and Figure 3-11. The relative errors of the data regression vary from -6.3% to +8.4 %. They are higher at low temperatures and low *NaOH* mass concentrations, and decrease at high temperatures and high *NaOH* mass concentrations. For instance, relative errors at temperature of 20℃ and a *NaOH* mass concentration of 4 wt.-% are between ca. +4 and +8 % and at 50℃ and a *NaOH* mass concentration of 20 wt.-% between 0 and -3 %.

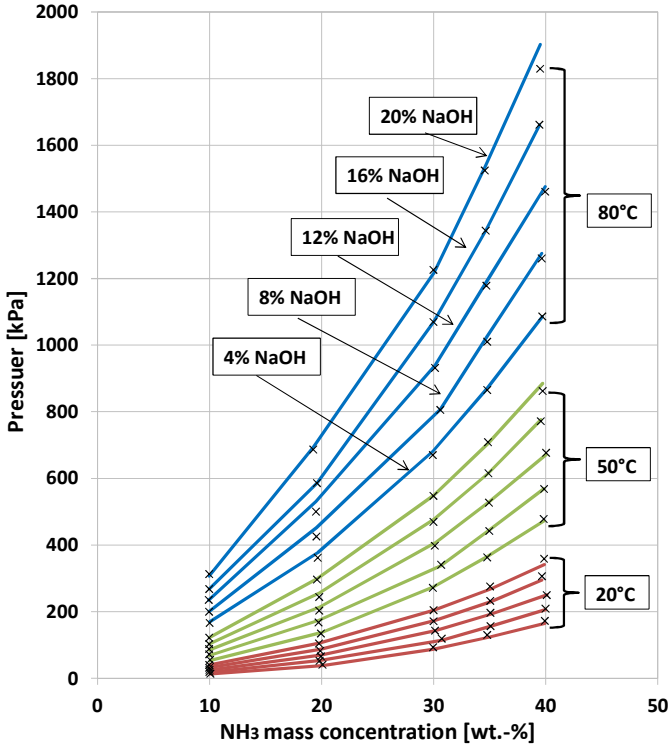

Figure 3-10: Comparison of calculated vapor pressures with those measured by Salavera et al. (2005)

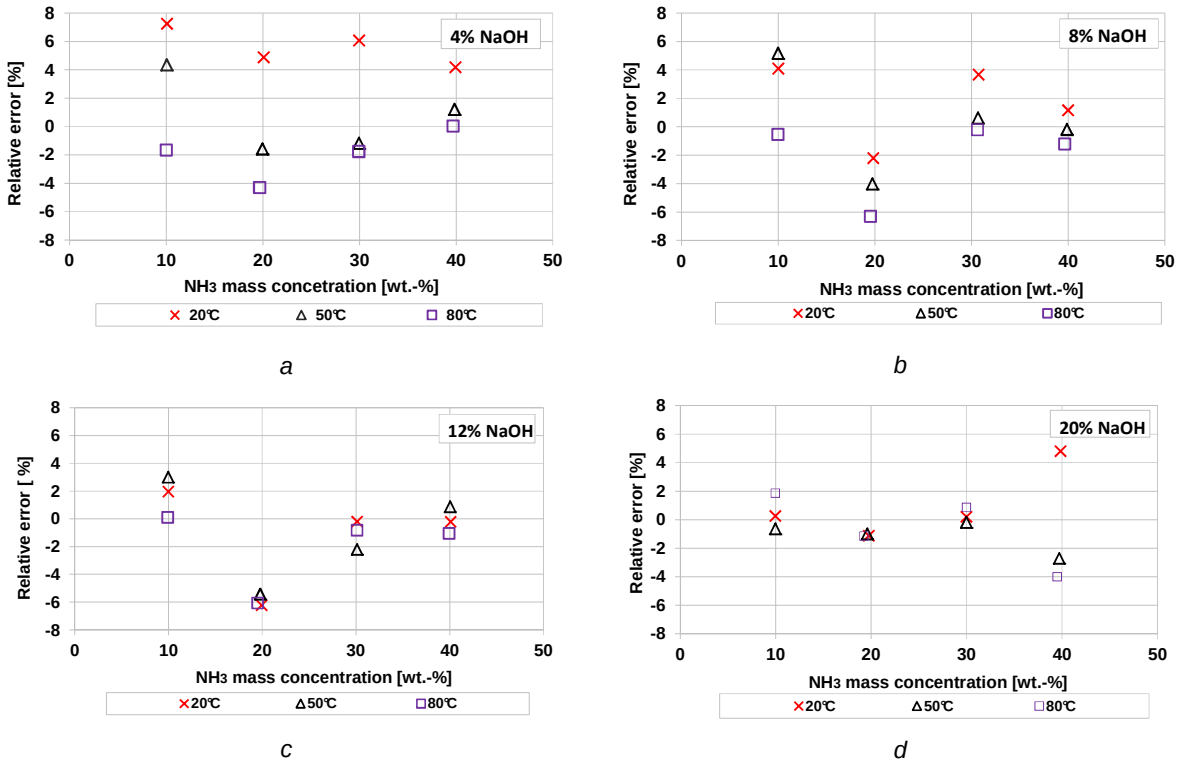

Figure 3-11: Calculation errors of vapor pressures for NH_3 mass concentrations of 10-40 wt.-%; temperatures 20, 50 and 80℃ and NaOH mass concentr ation of 4 wt.-% (a); 8 wt.-% (b); 12 wt.-% (c); 20 wt.-% (d)

3.1.4 Thermodynamic model and simulation results

The cycle was simulated at various generator outlet temperatures (t_{GEN_OUT}) with *NaOH* mass concentrations in the rich solution of 0, 5 and 10 wt.-% and at absorber / evaporator outlet temperatures (t_{ABS_OUT} / t_{EVA_OUT}) of 25 / 5℃; 35 / 5℃ and 45 / 5℃.

The schematic of the investigated NH_3 / H_2O AHP using *NaOH* as additives in ASPEN Plus is shown in Figure 3-12.

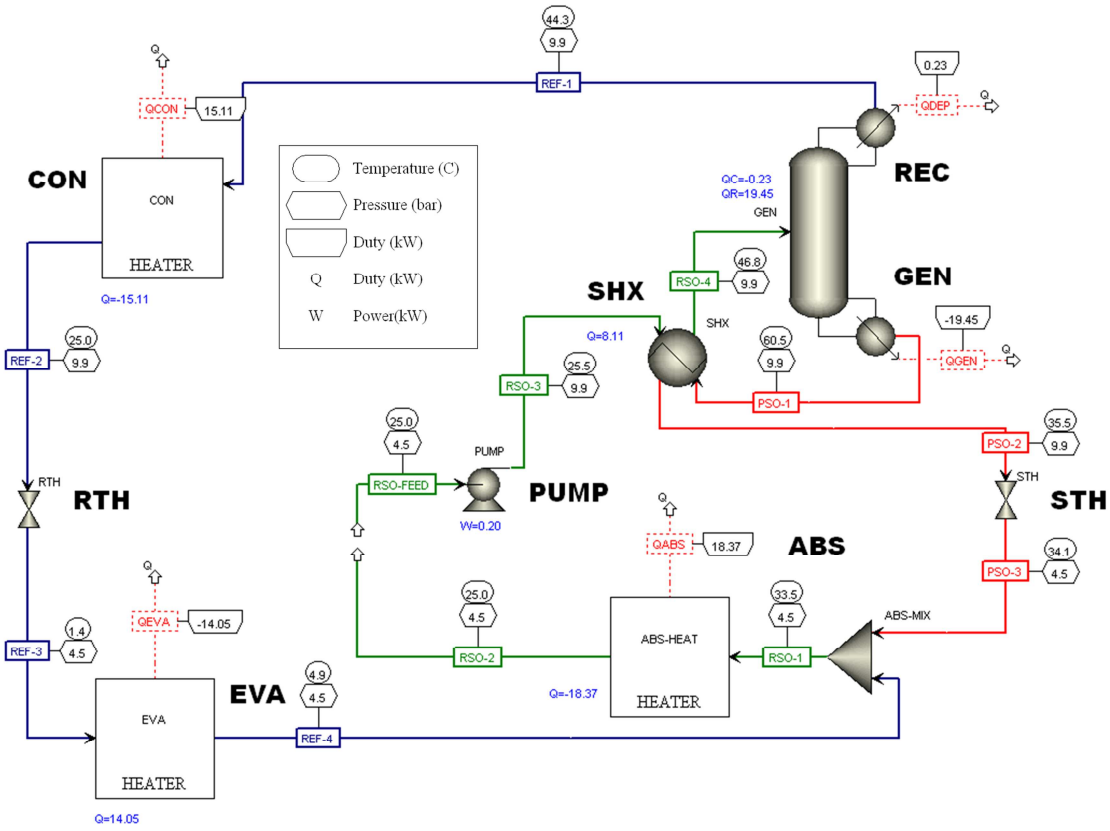

Figure 3-12: Schematic of the NH_3 / H_2O AHP-process using NaOH as additive in ASPEN Plus

For the simulation, no heat or pressure drops were taken into account. The components of the process were specified as follows:

1. *Absorber (ABS)*: consists of the ASPEN-models “Mixer” and “Heater”. In the “Mixer” the poor solution and the refrigerant vapor are mixed using VLE-equilibrium. At the outlet from the “Heater” the temperature of the working mixture of NH_3 / H_2O / *NaOH* is fixed to t_{ABS_OUT}.
2. *Condenser (CON)*: consists of the ASPEN-model “Heater” and at its outlet the NH_3 / H_2O solution has the vapor fraction 0.
3. *Evaporator (EVA)*: the evaporator consists of the ASPEN-model “Heater”. The vapor fraction of the working mixture at its outlet is 0.99.

4. *Generator and rectification column (GEN and REC)*: Both components are modeled using one ASPEN-model "RadFrac" consisting of 4 theoretical stages (see Figure 3-13): generator (GEN), stripping (STR) and rectifying (REC) sections and dephlegmator (DEP). The rich solution enters between the stripping and rectifying stages. The NH_3 / H_2O vapor with the NH_3 mass concentration of 99.9% leaves via the top of the "RadFrac" and the poor solution in the bottom of the "RadFrac".

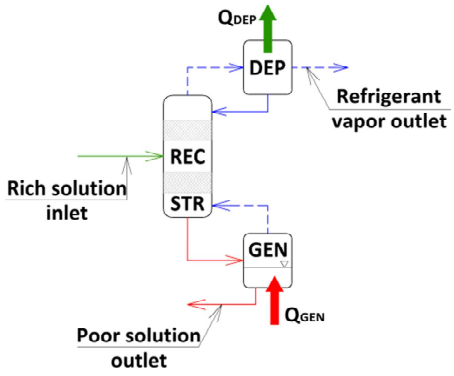

Figure 3-13: Schematic of the generator, rectification column and dephlegmator in ASPEN Plus

5. *Pumps (PUMP-1 and PUMP-2)*: at the outlet of the pumps (ASPEN-model "Pump") the binary mixture is at a high level of pressure.
6. *Expansion valves (RTH and STH)*: For both expansion valves, the ASPEN-model "Valve" has been used. Both valves are specified as "adiabatic flash for specified outlet pressure" and at their outlet the binary mixtures are at low level of pressure.
7. *Solution heat exchanger (SHX)*: The internal heat exchanger consists of the ASPEN-model "HeatX". The temperature difference between the rich solution inlet and poor solution outlet is 5 K.

The calculated COP_C are shown depending on the generator outlet temperature in Figure 3-14. It can be seen that there is an increase in the COP_C and a decrease in the required generator temperature when *NaOH* is used as an additive to the working mixture NH_3 / H_2O. For instance, at t_{ABS_OUT} / t_{EVA_OUT} = 45 / 5℃ the COP is 0.53 at a generator outlet temperature of 125℃. If 5% *NaOH* is added to the rich solution the generator outlet temperature can be reduced to 112℃ achieving the s ame COP_C.

As is mentioned above, it was considered that the temperature difference between rich solution inlet temperature with regards to the solution heat exchanger and poor solution outlet temperature from the solution heat exchanger was set equal to 5 K. When using *NaOH* the specific solution flow rate increases and therefore there is an increase in the ratio of the solution heat exchanger capacity to the generator heat capacity ($\dot{Q}_{SHX}$ / $\dot{Q}_{GEN}$). In real applications this means that the solution heat exchanger with a greater capacity must be

used when using *NaOH* as an additive. Furthermore, an increase in the solution flow rate requires a larger heat and mass transfer area in the absorber. The use of the same absorber for both processes with and without *NaOH* might cause a decrease in the absorber performance, which was equal to 100% in all simulations.

The simulation results depend on the binary parameters assumed for the working pairs. For the data regression, the VLE-Data of the NH_3 / H_2O / *NaOH* mixture were used. These data are valid for a temperature range of 20 - 80°C. However, the AHP-process was calculated at generator outlet temperatures of up to 130°C. The caloric data of the mixture, such as the heat of vaporization, could not be found in the literature. Thus, the simulation results have to be confirmed by means of experimental investigation.

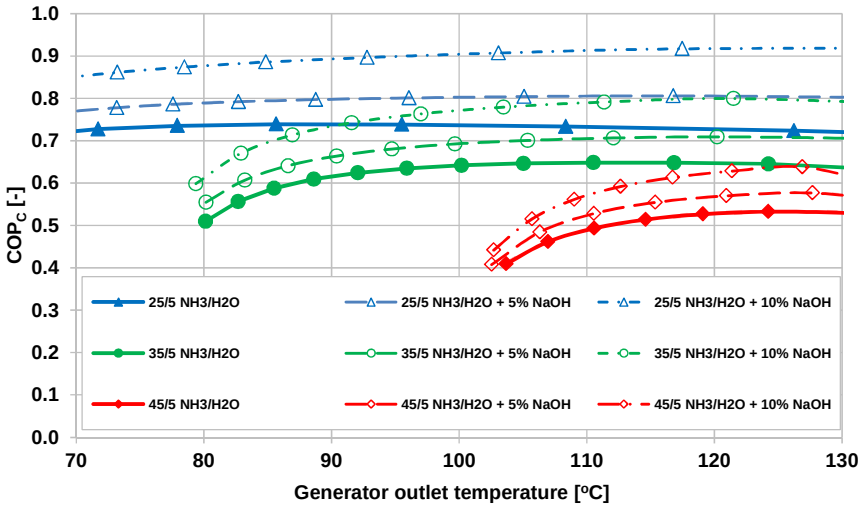

Figure 3-14: COP_C of the NH_3 / H_2O AHP-process using NaOH as additive at t_{ABS_OUT} / t_{EVA_OUT} = 25 / 5°C, 35 / 5°C and 45 / 5°C, NaOH mass concentrations of 0, 5 and 10% depending on the generator outlet temperature

Furthermore, an increase in the viscosity of the working fluid mixture when using strong bases could affect the absorption process negatively and corrosion could have a negative influence on the operation and should be also taken into account.

Within the master thesis of Kalkgruber (2009), the corrosion problem was experimentally investigated with the help of experiments using sample containers (austenitic stainless steel 1.4401) with PTFE seals and material samples (austenitic steel 1.4301 and 1.4571). The sample containers were filled with an NH_3 / H_2O / *NaOH* mixture with a *NaOH* mass concentration of 10 and 20 wt.-% and left in an oven at a temperature of 160°C for 3-7 weeks. No corrosion was detected in the samples with 10 wt.-% *NaOH*. However, corrosion issues have been observed in the samples with 20-% *NaOH*. Therefore, for further experimental investigations in an AHP test rig (see Chapter 5) the maximal *NaOH* concentration in the working mixture charge was 10 wt.-% *NaOH*.

3.2 Absorption heat transformer using partially miscible working mixtures

An alternative to a conventional AHT discussed in Chapter 2.1.1 is the AHT-process using partially miscible working mixtures, which was suggested and analyzed by Niang et al., (1997, 1998) and Alonso et al. (2002, 2003). The operating principle of such a process is based on the separation of the working mixture without evaporation.

3.2.1 Literature review

In this subchapter, the partial miscibility of mixtures will be explained and a detailed survey of related literature on AHT-process using partially miscible working mixtures will be presented.

Partial miscibility

As is well known, the demixing of a binary liquid mixture into two liquid phases occurs when the mixture is thermodynamically unstable. If a binary liquid mixture is immiscible, it demixes into two pure components. In the case of partial miscibility a binary mixture demixes into two liquid phases consisting of both components. The criterion for this is based on the notion of the Gibbs free energy (*G*), which is at a minimum when the binary system is in equilibrium.

Figure 3-15 shows the Gibbs free energy of three binary mixtures depending on the concentration at constant pressure and temperature. The curve “a” corresponds to a completely miscible mixture. Its Gibbs free energy cannot be decreased by demixing at any concentration. The curve “b” shows a partially miscible mixture. If the mixture concentration is between $x_{1\alpha}$ and $x_{1\beta}$ (for instance x_1) its Gibbs free energy G_{1m} can be reduced to G_{2m} and the liquid phase is demixed into two liquid phases with concentrations of $x_{1\alpha}$ and $x_{1\beta}$. The curve “c”, shows a completely immiscible mixture, because its Gibbs free energy is always higher than those of pure phases (G_1 and G_2).

Different types of working mixtures with partial miscibility are shown in Figure 3-16. The phase (*Txy*-) diagram “a” represents a mixture with an upper critical solution temperature (UCST). Below this temperature the mixture is partially miscible, above this temperature, it is completely miscible. In the diagram “b”, a mixture with a lower critical temperature (LCST) is shown. This mixture is partially miscible at temperatures higher than LCST. The diagrams “c” and “d” show mixtures with both upper and lower critical solution temperatures. The mixture in the diagram “c” has a closed area of immiscibility. The areas of immiscibility of the mixture in the diagram “d” lie over the UCST and below LCST. The last type of partial immiscibility, without critical solution temperatures, is shown in diagram “e”.

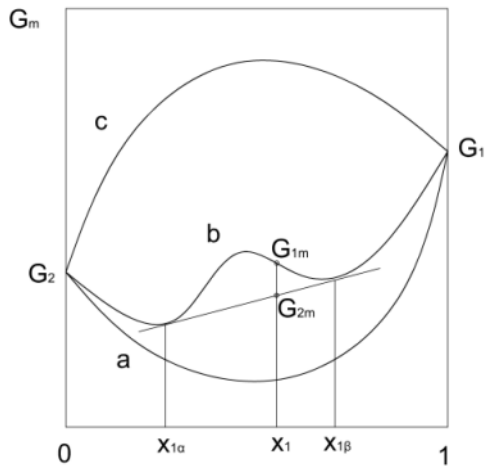

Figure 3-15: The Gibbs free energy of three binary mixtures depending on its concentration at constant pressure and temperature: a – completely miscible mixture; b – partially miscible mixture; c – immiscible mixture (according to Luedecke and Luedecke, 2000)

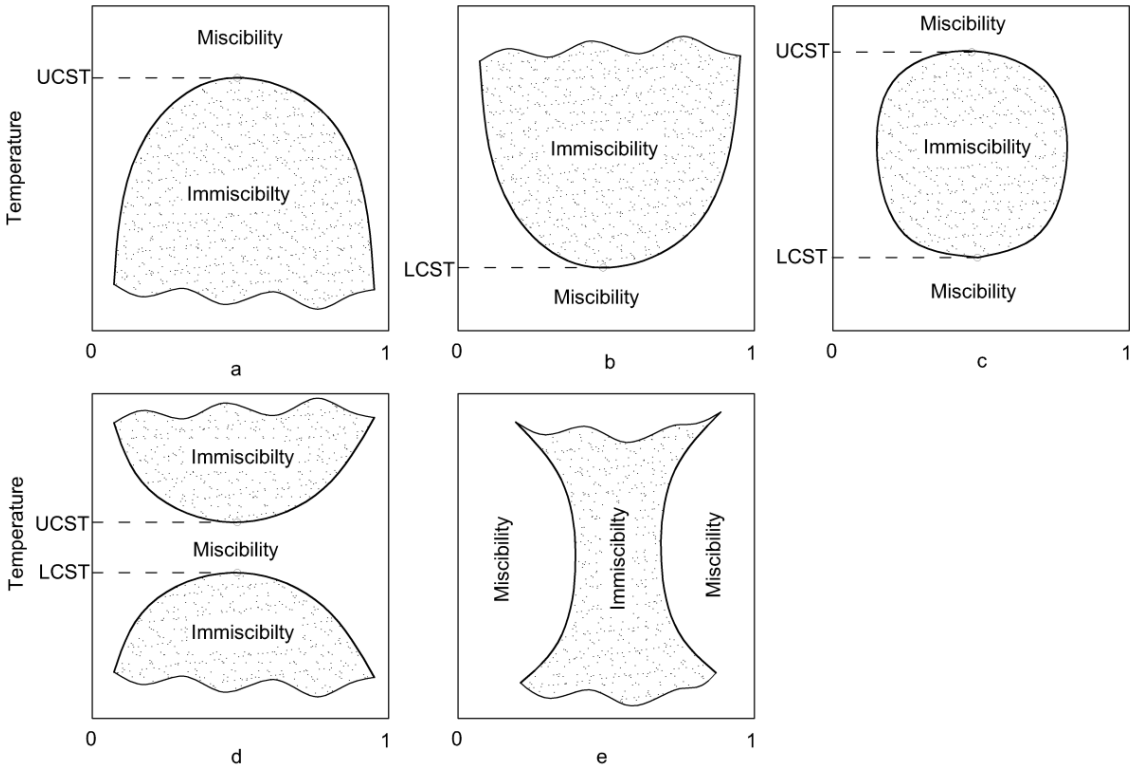

Figure 3-16: Different types of mixtures with partial miscibility (according to Luedecke and Luedecke, 2000)

Process description

The AHT-process suggested by Niang et al. (1998) uses partially miscible working mixtures which possess an UCST and consist of two components, with one being much more volatile than the other (Figure 3-16a). At temperatures higher than the UCST, the mixture is completely miscible; below this temperature it is partially miscible. In order to utilize this phenomenon in an AHT, absorption must occur at temperatures above the USCT and demixing (desorption) at temperatures lower than the USCT.

In the literature, three different working mixtures have been suggested for this process (Table 3-2): water / furfural (Niang et al., 1998); cyclohexane / DMSO (dimethylsulfoxide) (Alonso et al., 2002); n-heptane / DMF (dimethylformamide) (Alonso et al., 2002, 2003).

For the calculation of the AHT-process using water / furfural, Niang et al. (1998) had used experimental LLE-data. The process is highly efficient, i.e. at heat sink inlet / heat source outlet temperatures of 183 / 157 °C it has a COP of 0.86.

The working mixture cyclohexane / DMSO has the highest COP (0.96) of the three above-mentioned working mixtures. However, owing to a lack of experimental data, Alonso et al. (2002) had used ideal gas model for vapor phase calculation, meaning that their calculation uncertainties might be high.

The second working mixture investigated by Alonso et al. (2002) was n-heptane / DMF. The process calculation was based on experimental VLE-data and the calculated COP is 0.93. This mixture has been investigated in a test rig by Alonso et al. (2003). The measured COP was much lower (0.40) than its calculated value.

Table 3-2: Investigated AHT-processes using partially miscible working mixtures (literature review)

Working pair (literature)	**Heat sink inlet/ heat source outlet temperatures, °C**	**COP**	**Used binary properties for data regression**
Water/furfural (Niang et al., 1998)	183 / 157	0.86	Experimental LLE-Data from DECHEMA (Gmehling et al., 1981)
Cyclohexane/DMSO (Alonso et al., 2002)	180 / 123	0.96	UNIFAC predictive model (Ideal gas model for vapor phase)
N-heptan/DMF (Alonso et al., 2002; 2003)	109 / 97	0.93 (calculation) 0.40 (experiment)	Experimental VLE-Data (Quitzsch et al. 1969)

The schematic of the AHT-process using partially miscible working mixture is shown in Figure 3-17 and its principle of operation is explained by means of a phase diagram in Figure 3-18. For explaining the process, the working pair water / furfural is chosen, with water the more volatile component.

The working pair of water and furfural (M_1) enters the separator (SEP), where it demixes (M_2) into two liquid mixtures by rejecting heat at low temperature ($\dot{Q}_{SEP}$) to an external heat sink: liquid phase rich in water (W_1) and liquid phase rich in furfural (F_1). Both mixtures are pumped to the high pressure level by two pumps (PUMP-1, PUMP-2) and heated up in two internal heat exchangers (IHX-1, IHX-2). The mixture rich in water (W_3) evaporates (W_4) in the evaporator (EVA) by supplying heat ($\dot{Q}_{EVA}$) at a middle temperature level from an external heat source and flows to the lower part of the absorber (ABS). The mixture rich in furfural (F_3) enters the absorber in the upper part.

The absorber is assumed to be a plate column, where the vapor (W_4) is in counter-flow with the liquid (F_3). The concentration of water in the vapor flow decreases and its temperature increases along the dew-point curve (W_5). At the same time concentration of furfural in the liquid phase increases and its temperature decreases along the boiling curve (F_4). As a result, the vapor mixture exits from the upper part of the absorber at a higher temperature than at the inlet. The rest of the liquid mixture (F_4) exits from the lower part of the absorber. It is necessary to mention that the mixtures F_{3A} and W_{4A} are the liquid and vapor phases that are in vapor-liquid-equilibrium with the vapor mixture W_5 and liquid mixture F_4 respectively.

The liquid mixture F_4 is cooled in the internal heat exchanger (IHX-1), throttled (V1) to the low pressure level and enters the separator (SEP).

The vapor mixture (W_5) generated in the absorber enters the condenser (CON), condenses (W_6) and rejects heat ($\dot{Q}_{CON}$) at high temperature to an external heat sink. Afterwards, it is cooled (W_7) in the internal heat exchanger (IHX-1) and throttled (V-2) to the low pressure level. Finally the mixture rich in water (W_8) flows into the separator and mixes there with the rest of the mixture (F_6).

The COP of this AHT-process can be defined as the ratio of the condenser capacity ($\dot{Q}_{CON}$) to the evaporator capacity ($\dot{Q}_{EVA}$).

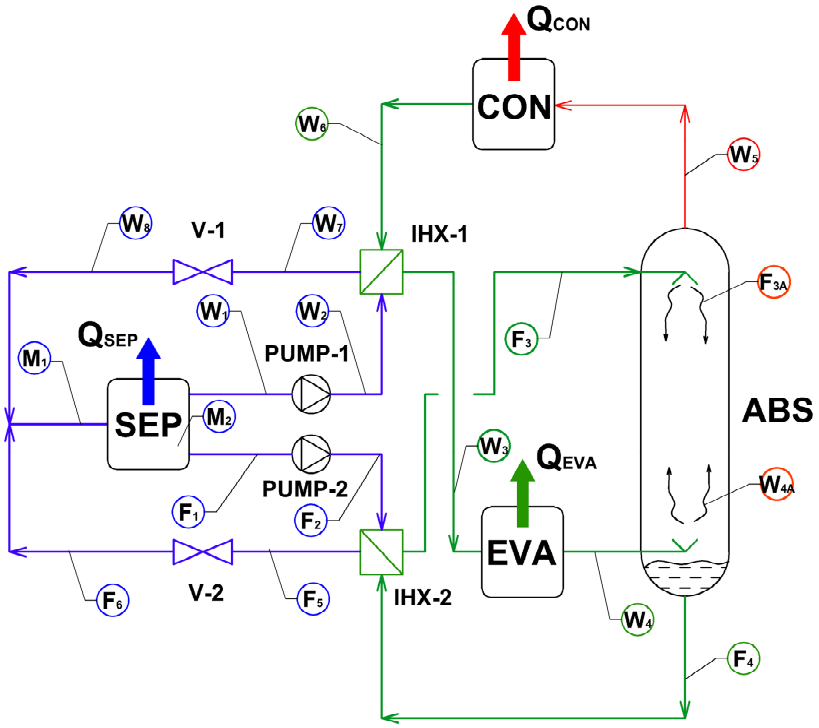

Figure 3-17: Schematic diagram of the AHT-process using partially miscible working mixtures with upper critical solution temperature

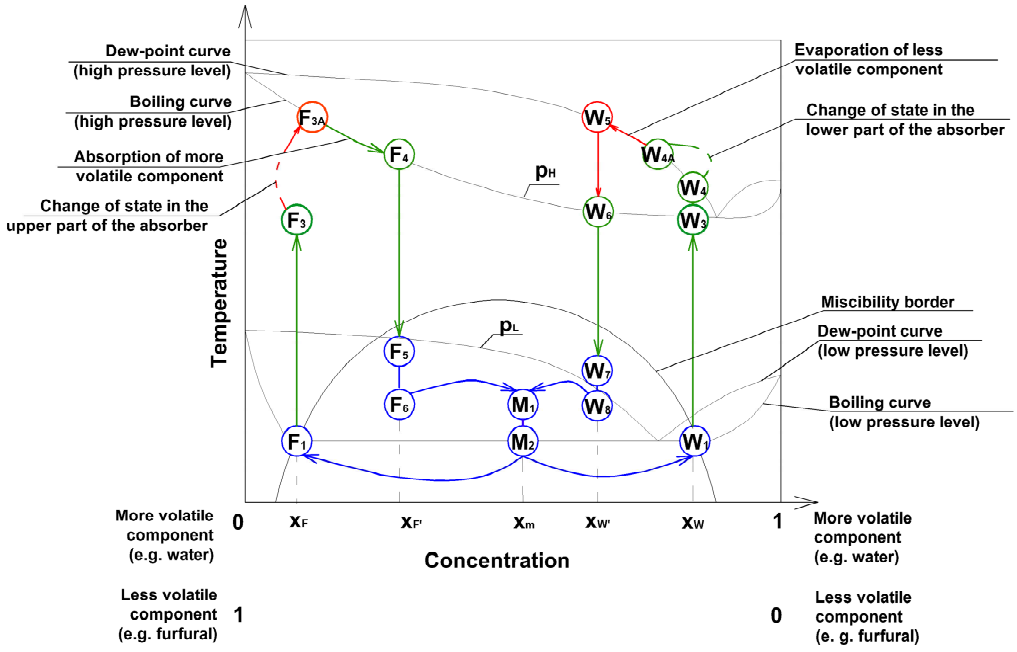

Figure 3-18: AHT-process using partially miscible working mixtures with upper critical solution temperature (UCST) in the phase-diagram

3.2.2 Process analyses in ASPEN Plus

Within this work the AHT-process using water / furfural as a working mixture has been chosen for investigation by means of thermodynamic simulation in ASPEN Plus. In the following, the calculation of properties of the working mixture water / furfural will be discussed and the process will be analyzed with regard to areas for its possible application.

Calculation of properties of the working mixture water / furfural

For calculation of properties of the water / furfural, the built-in ASPEN library "ASPEN-LLE" was used. The comparison of the calculated LLE-data with experimental LLE-data measured by Sorensen and Artl (1979) for the temperature range between 20-120℃ is shown in Figure 3-19. It can be seen that by means of ASPEN Plus, calculated LLE-data coincides well with the experimental data. The calculation uncertainty ranges from -0.001 mol·mol^{-1} to +0.02 mol·mol^{-1}. However, it is necessary to mention that no experimental data of other thermodynamic properties, such as boiling and condensation curves, as well as enthalpies of vaporization, could be found. Thus, the calculated COP may obtain uncertainties.

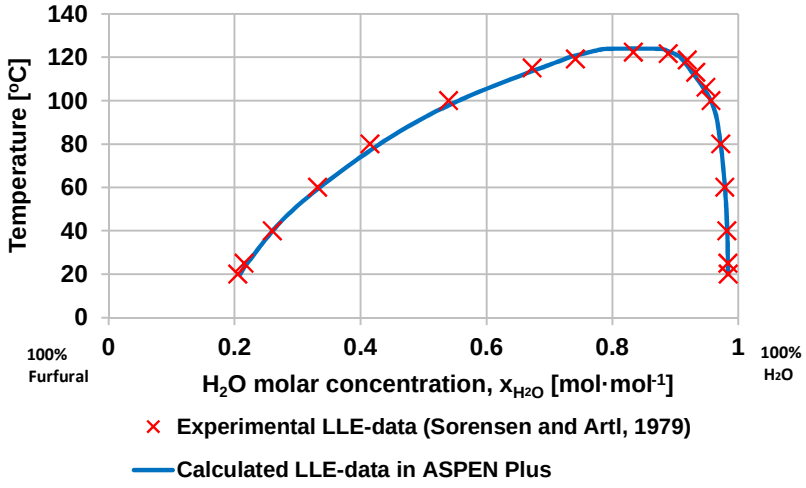

Figure 3-19: Calculated LLE-data of the mixture water / furfural using ASPEN library "ASPEN-LLE" in comparison to the experimental data measured by Sorensen and Artl (1979)

Thermodynamic model and simulation results

The schematic of the water / furfural AHT-process in ASPEN Plus is shown in Figure 3-20. For the thermodynamic simulation, no pressure drops or heat losses have been taken into account. The components of the investigated AHT-process have been specified as follows:

1. *Absorber (ABS)*: the absorber consists of the ASPEN-model "RadFrac" with 10 theoretical stages. The vapor mixture enters the lower part (Stage 10) and the liquid mixture the upper part (Stage 1) of the absorber.

2. *Condenser (CON)*: at the condenser outlet the binary mixture is liquid in a state at of boiling.
3. *Evaporator (EVA)*: the evaporator consists of the ASPEN-model “Heater”. At its outlet, the working mixture is vapor in a saturation state.
4. *Expansion valves (RTH* and *STH)*: For both expansion valves, the ASPEN-model “Valve” has been used. At the outlet from the valves, the binary mixtures is at a low level of pressure.
5. *Internal heat exchangers (IHX-1 and IHX-2)*: the internal heat exchangers consist of the ASPEN-model “HeatX”. The temperature differences between P-2 and R-6 and between P-6 and R-2 are set equal to 5 K.
6. *Pumps (PUMP-1 and PUMP-2)*: at the outlet of the pumps (ASPEN-model “Pump”) the binary mixture is at a high level of pressure.
7. *Separator (SEP)*: the separator consists of two components SEP-CON (“Heater”) and SEP (“Decanter”). At the outlet from the SEP-CON, the working mixture is liquid in a state of boiling. The working mixture is separated adiabatically using liquid-liquid-equilibrium in SEP.

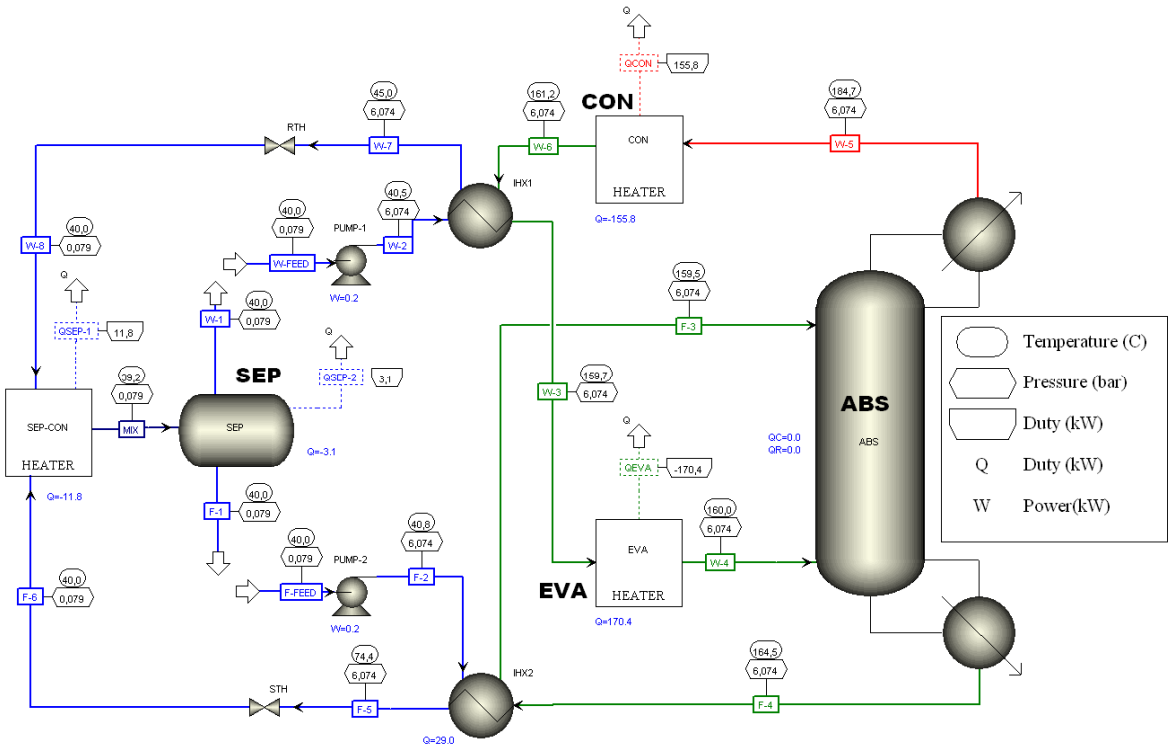

Figure 3-20: Schematic of the AHT-process with the working pair water / furfural in ASPEN Plus

The cycle has been calculated at evaporator / separator outlet temperatures of 160 / 40℃. The high / low pressure levels that correspond to these temperatures are 6.0 / 0.08 bar. The

simulation results have shown that a condenser inlet temperature of 185℃ can be obtained and the cycle has a COP of 0.82. At first glance, the results taken from the literature (Niang et al, 1998) are confirmed.

As is already shown in Figure 3-18, the temperature lift – the difference between the condenser inlet and evaporator outlet temperatures – is defined by the thermodynamic properties of the working mixture, mostly by the shape of the dew point curve and bubble point curve. However, as can be seen from Figure 3-21 there is a big temperature glide in the condenser, i.e. the water / furfural working mixture is condensing by rejecting heat at temperatures from 185℃ to 161℃. In the evaporator , the temperature difference is only 1 K (159-160℃), due to the preheating of the mixture i n the internal heat exchanger (IHX-1) and in the separator, the heat is rejected at a temperature of 40℃. Thus, the temperature difference between the condenser inlet and evaporator inlet is 25 K while between the condenser outlet and evaporator outlet the different is only 1 K.

The temperature profile in the condenser is shown in Figure 3-21. It has been assumed that the working mixture has a vapor fraction of 0 at the outlet from the condenser. From these results it can be inferred that approximately 75% of the heat is rejected between 161℃ and 166℃ and only 25% between 166℃ and 185℃. Further more, the temperature difference between the evaporator outlet and the condenser outlet is only 1 K. For this temperature profile, it is not appropriate to utilize the total condenser capacity by using a heat transfer fluid with constant heat capacity as a heat sink. In order to utilize the entirety of the heat, one can use different heat sinks or to use just a certain amount of the heat, i.e. the working mixture must be partially condensed in the condenser.

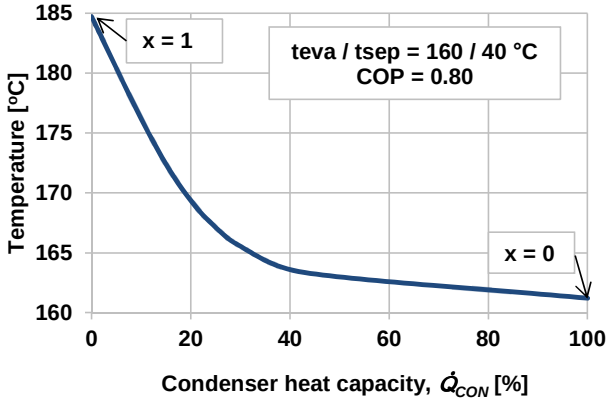

Figure 3-21: Temperature profile in the condenser of the AHT-process with the working pair water / furfural (full condensation)

In order to overcome this drawback, partial condensation of the water / furfural mixture in the condenser is suggested within this work. The condensation of the working mixture is then completed in an internal heat exchanger (IHX-2, see Figure 3-20). In order to investigate the operation with the partial condensation in the condenser the AHT-process with the working mixture water / furfural was simulated at different boundary conditions:

1. The vapor fraction of the working mixture at the outlet from the condenser varies from 0 to 0.999;
2. It was assumed that the vapor fraction of the working mixture at the outlet from the IHX-2 is 0;
3. The AHT-process using water / furfural with partial condensation has been calculated at three different evaporator outlet temperatures of 130℃, 160℃ and 180℃ and a separator temperature of 40℃;
4. The high pressure levels defined by the evaporator temperatures are 2.7, 6.0, 9.4 bar respectively;
5. The low pressure level is defined by the temperature level in the separator and is 0.08 bar.

The simulation results are shown in Figure 3-22. The diagram shows the COP depending on the condenser outlet temperature. As expected, the COP decreases significantly with increasing condenser outlet temperature. For instance, at evaporator / separator outlet temperatures of 160 / 40℃ and at a condenser outlet temperature of 161℃, the COP is 0.80. When increasing the condenser outlet temperature up to 170℃, the COP is just 0.25.

Figure 3-23 shows the temperature profile in the condenser with partial condensation. The vapor fraction of the working mixture at the condenser outlet is 0.72. It can be seen, that the temperature glide is lower in comparison to the total condensation and is roughly linear with the condenser capacity. However, the calculated COP is just 0.10.

It is necessary to mention that the temperature lift of the AHT-process using partially working mixtures depends only on the dew-point curve of the working mixtures at a high level of pressure (see Figure 3-18). This means that when fixing the evaporator temperature to a certain value, the condenser inlet temperature is also fixed and cannot be varied.

It can be concluded from these investigations, that currently, the AHT-process with the partially miscible mixture of water /furfural is not competitive compared to a conventional AHT. Even if alternative working mixtures, which enable operating the process at lower temperature levels with higher efficiency, will be found, its practical use will be rather unrealistic, owing to the high temperature glide in the condenser and the fact that the

temperature lift of this process depends only on the shape of the dew-point curve of the working mixture.

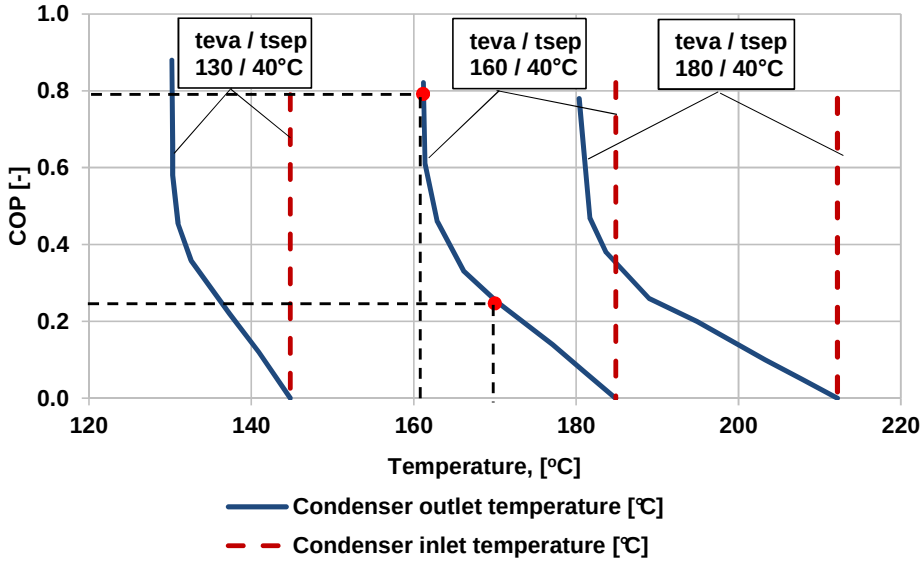

Figure 3-22: COP of the AHT-process with the working pair water / furfural depending on the condenser outlet temperature

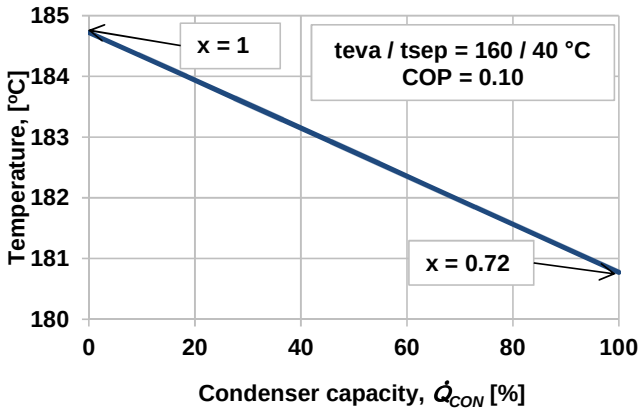

Figure 3-23: Temperature profile in the condenser of the AHT-process with the working pair water / furfural (partial condensation in the condenser; vapor fraction at the outlet from the condenser is 0.72)

3.3 The Rojey cycle

An alternative AHP-process using an auxiliary condensable fluid has been considered by Rojey (1975). Different working mixtures have been investigated for this cycle (Rojey, 1975, 1979, 1983, etc.). The most promising of them is a ternary mixture of NH_3 / H_2O / C_4H_{10}, where ammonia is the refrigerant, water is the absorbent and butane is the auxiliary fluid.

3.3.1 Principle of operation

Figure 3-24a shows the Rojey cycle in the pressure / temperature diagram. The rich NH_3/ H_2O solution leaves the absorber (ABS), is pumped by the solution pump (PUMP) to the high pressure level (p_H) and enters the generator (GEN). In the generator heat ($\dot{Q}_{GEN}$) from a high temperature heat source is supplied to the rich solution generating almost pure NH_3 vapor and poor solution.

The pressure of the poor solution is reduced again to the low pressure level (p_L) in the solution throttle valve (STH) and it enters the absorber. The NH_3 vapor enters the condenser (CON) and condenses there by rejecting heat ($\dot{Q}_{CON}$) at the middle temperature level to a heat sink. The condensed NH_3 is throttled then (RTH) to the low pressure level and partially evaporates.

The partially evaporated NH_3 and liquid C_4H_{10} (flowing from the absorber) enter the evaporator (EVA) and evaporate by absorbing heat ($\dot{Q}_{EVA}$) from the low temperature heat source. Due to the presence of the C_4H_{10} the partial pressure of the NH_3 (p_{EVA}) in the evaporator decreases and evaporation occurs at the low temperature level. It is necessary to mention, that in order to obtain a similar temperature profile in the evaporator of the Rojey cycle as in the evaporator of a conventional NH_3/ H_2O AHP, the concentration of C_4H_{10} must be to the concentration of the azeotropic NH_3/ C_4H_{10} mixture.

The NH_3 / C_4H_{10} vapor enters the absorber and the NH_3 is absorbed by the poor solution coming from the generator. The absorption heat ($\dot{Q}_{ABS}$) at the middle temperature level is rejected to an external heat sink. The partial pressure of C_4H_{10} increases and it condenses. Due to the immiscibility of the liquid C_4H_{10} and the NH_3/ H_2O solution at temperatures below 50℃, they are separated in the absorber. The parti al pressure of NH_3 in the absorber (p_{ABS}) is lower than in the evaporator (p_{EVA}) and, therefore, the NH_3-concentration in the rich solution is lower compared with a conventional NH_3/ H_2O AHP.

The cooling COP of the Rojey cycle is defined as the ratio of the evaporator capacity to the generator capacity.

It can be concluded that the presence of an auxiliary fluid within the Rojey cycle, on the one hand, increases the evaporator capacity while decreasing the evaporator temperature and, on the other hand, affects the absorption negatively by decreasing the NH_3 partial pressure in

the absorber. This results in a lower COP_C than that of a conventional NH_3/H_2O AHP (Rojey, 1979; Coronas, 1995). In order to improve the cycle performance, the condensation of the gaseous NH_3/C_4H_{10} mixture in different stages has been investigated by Rojey (1979).

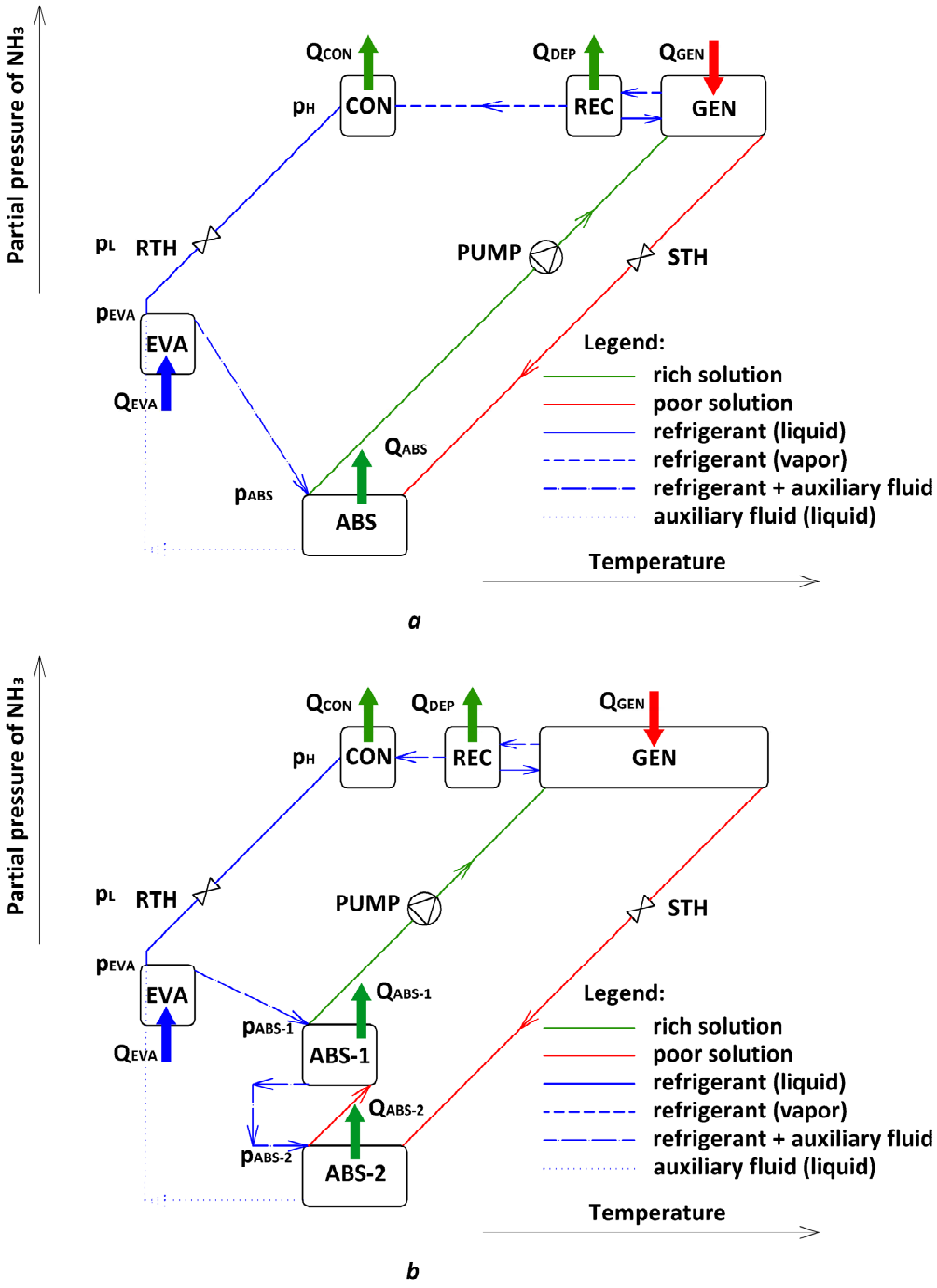

Figure 3-24: Rojey cycle in the pressure / temperature diagram: a – with 1 stage absorption; b – with 2-stage absorption

The Rojey cycle with two-stage absorption in the pressure / temperature diagram is shown in Figure 3-24b. In the first absorber stage (ABS-1) the NH_3 is partially absorbed at the partial pressure p_{ABS-1} by the NH_3 / H_2O solution coming from the second absorber stage (ABS-2). The partial pressure of the C_4H_{10} increases, but is still less than the condensation pressure. In the second stage, the rest of the NH_3 is absorbed at the partial pressure p_{ABS-2} by the poor solution coming from the generator. The partial pressure of C_4H_{10} increases up to the condensation pressure and butane condenses. At the outlet from the first stage (ABS-1) the rich solution and at the outlet from the second stage (ABS-2) the C_4H_{10} leave the absorber. The main advantage of this two-stage absorption is that NH_3 is absorbed at different partial pressures and the rich solution leaving the absorber has a higher NH_3 concentration than that of the Rojey cycle with one-stage absorption.

The efficiency of the Rojey cycle using the working mixture NH_3 / H_2O / C_4H_{10} with 1- and 2-stage absorption has been calculated and compared with that of a conventional NH_3 / H_2O AHP by Coronas (1995). The investigated processes have been analyzed at t_{ABS_OUT} / t_{EVA_OUT} = 30 / -5°C. Figure 3-25 shows that the Rojey cycl e with 1-stage absorption has a lower COP_C (0.50) in comparison to a conventional process (0.60). The use of the 2-stage absorption leads to an increase in the COP_C up to 0.75.

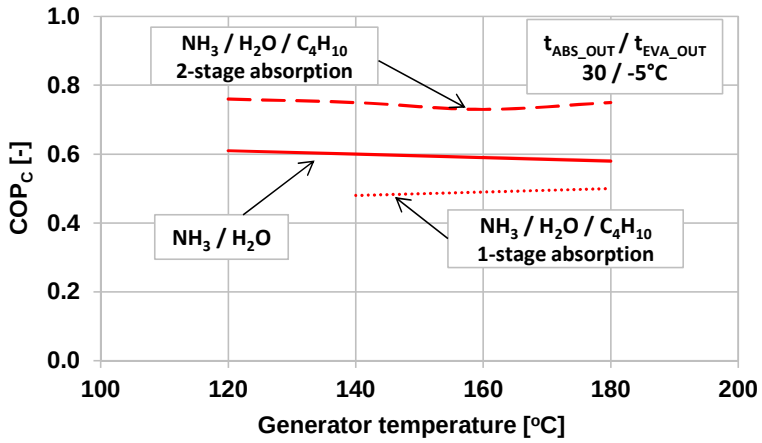

Figure 3-25: Simulation results of Coronas (1995) for the Rojey cycle with 1- and 2-stage absorption and a conventional NH_3 / H_2O AHP (according to Coronas, 1995)

The technical feasibility of the NH_3 / H_2O / C_4H_{10} Rojey cycle with 2-stage absorption has been shown by Cheron and Rojey (1986). Two air / water AHP test rigs with a thermal output of 100 kW and 300 kW have been built and experimentally investigated. The authors reported the COP_H of 1.68 measured at the following boundary conditions: $t_{AIR\_EVA\_IN}$ / $t_{AIR\_EVA\_OUT}$ = 5 / 0°C; $t_{SNK\_ABS\_IN}$ / $t_{SNK\_CON\_OUT}$ = 37 / 50°C. However, no information concerning generator temperatures and the concentration of the NH_3 / H_2O / C_4H_{10} mixture has been reported.

Furthermore, the authors mention, that the absorber construction had to be optimized in order to improve the separation of the liquid C_4H_{10} from the rich solution. Even though the feasibility of the Rojey cycle has been confirmed by Cheron and Rojey (1986), no data concerning further experimental investigations on this process have been found.

3.3.2 Properties calculation of the working mixture NH_3 / H_2O / C_4H_{10}

The calculation of the properties of the working mixture NH_3 / H_2O / C_4H_{10} were made using the Redlich-Kwong-Soave equation of state with Boston-Mathias modifications. The binary parameters for the mixture NH_3 / C_4H_{10} were regressed using the experimental vapor-liquid-liquid-equilibrium (VLLE) data of Widling et al. (1996). The regression data results for the temperature range of 0 - 50℃ and pressure range of 1 - 24 bar are shown in Figure 3-26. It can be seen that the experimental and calculated VLLE-data of the mixture NH_3 / C_4H_{10} coincide well and the calculation uncertainty varies from -3.7 % to +5.9 %.

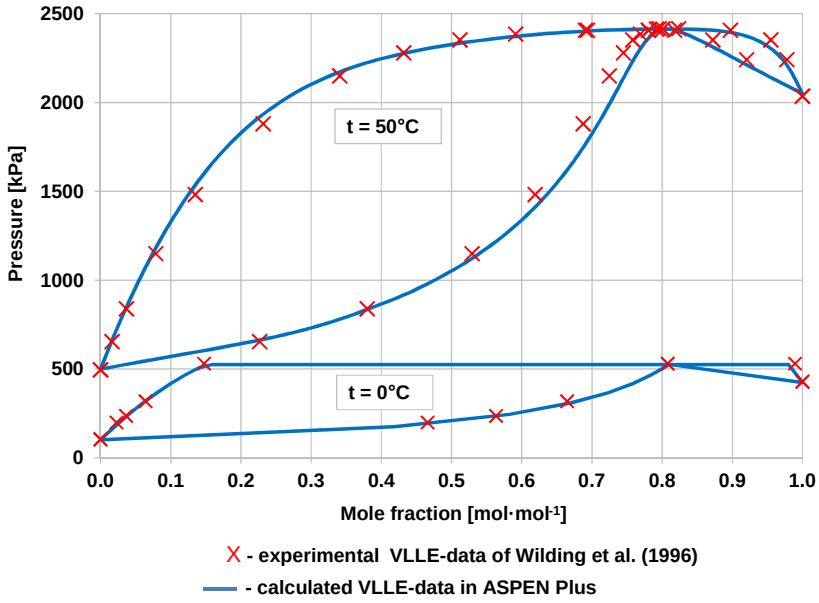

Figure 3-26: Calculated VLLE-data for the mixture NH_3 / C_4H_{10} using the Redlich-Kwong-Soave equation of state with Boston-Mathias modifications in comparison to the experimental data measured by Widling et al. (1996)

3.3.3 Thermodynamic model and simulation results

Principally, the evaporation of a NH_3 / C_4H_{10} mixture takes place at gliding temperature. In order to prevent this, the composition of the NH_3 / C_4H_{10} mixture in the evaporator has been chosen equal to the azeotropic mixture (NH_3 / C_4H_{10} 55.0 / 45.0 wt.-% at p=4.5 bar). Due to

the presence of a small amount of water in the evaporator, the temperature profile in the evaporator of the Rojey cycle is similar to a conventional NH_3 / H_2O-AHP.

Figure 3-27 shows the temperature profile of the evaporator of a NH_3 / H_2O-AHP at a low pressure level of 4.50 bar and for the NH_3 / H_2O composition of 99.9 / 0.1 wt.-% and the temperature profile of the evaporator of the Rojey cycle (NH_3 / H_2O / C_4H_{10}) at a low pressure level of 5.55 bar and for the NH_3 / H_2O / C_4H_{10} composition of 55.0 / 0.05 / 44.95 wt.-% for a vapor fraction in the outlet from the evaporator of 0.99. Evaporation in a conventional NH_3 / H_2O AHP occurs at temperatures between 1.5 - 5.0℃ and in the Rojey cycle between 1.5 - 3.5 ℃. The temperature profile in the evaporator of the Rojey cycle differs from one of a conventional NH_3 / H_2O-AHP due to the presence of butane. However, the average evaporator temperature (t_{EVA}) in both processes is 1.7℃.

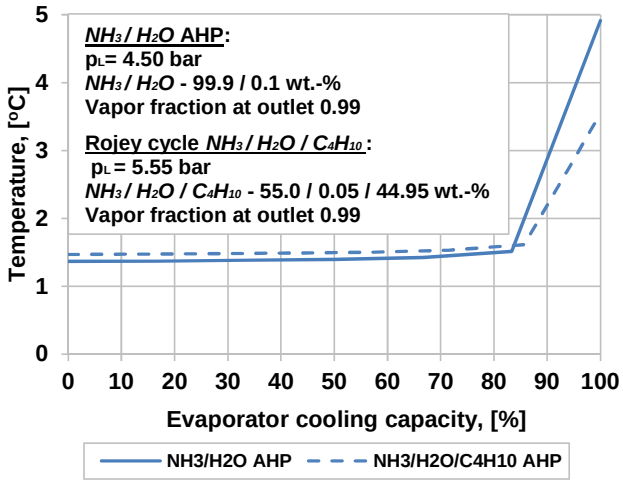

Figure 3-27: Comparison of the temperature profile of the NH_3 / H_2O / C_4H_{10} Rojey cycle and a conventional NH_3/H_2O-AHP

Both the Rojey cycle with 2-stage absorption, and a conventional NH_3 / H_2O AHP cycle were calculated at absorber outlet temperatures (t_{ABS_OUT}) of 25, 35 and 45℃. The boundary conditions in the evaporator were set as discussed above. The schematic of the Rojey cycle with 2-stage absorption in ASPEN Plus is shown in Figure 3-28.

For the simulations of both processes no heat losses or pressure drops were taken into account. The components of the investigated Rojey cycle were specified as follows:

1. *The first stage of the absorber (ABS-1)*: consists of the ASPEN-models “Heater” and “Flash”. At the outlet from the “Heater” the temperature of NH_3 / H_2O / C_4H_{10} is set equal to t_{ABS_OUT} and at the outlet from the “Flash” the vapor and liquid phases are separated using VLE-equilibrium.

2. *The second stage of the absorber (ABS-2)*: consists of the ASPEN-models “Heater” and “Decanter”. At the outlet from the “Heater” the vapor fraction of the NH_3 / H_2O / C_4H_{10} is set equal to 0 and in the “Decanter” the NH_3 / H_2O solution and liquid C_4H_{10} are separated using LLE-equilibrium.
3. *Condenser (CON)*: is simulated by using the ASPEN-model “Heater” and in its outlet the NH_3 / H_2O solution has the vapor fraction of 0.
4. *Evaporator (EVA)*: is represented by the ASPEN-model “Heater”. The vapor fraction of the working mixture at its outlet is 0.99.
5. *Generator and rectification column (GEN and REC)*: Both components are modeled using one ASPEN-model “RadFrac” consisting of 5 theoretical stages. The lowest stage (5th stage) is the generator followed by 3 theoretical stages and the dephlegmator (1st stage). The rich solution enters between the 2nd and 3rd stages. The NH_3 / H_2O vapor with the NH_3-mass concentration of 99.9% leave at the top of the “RadFrac” and the poor solution from the bottom of the “RadFrac”.
6. *Pumps (PUMP-1 and PUMP-2)*: at the outlet of the pumps (ASPEN-model “Pump”) the binary mixture is at a high level of pressure.

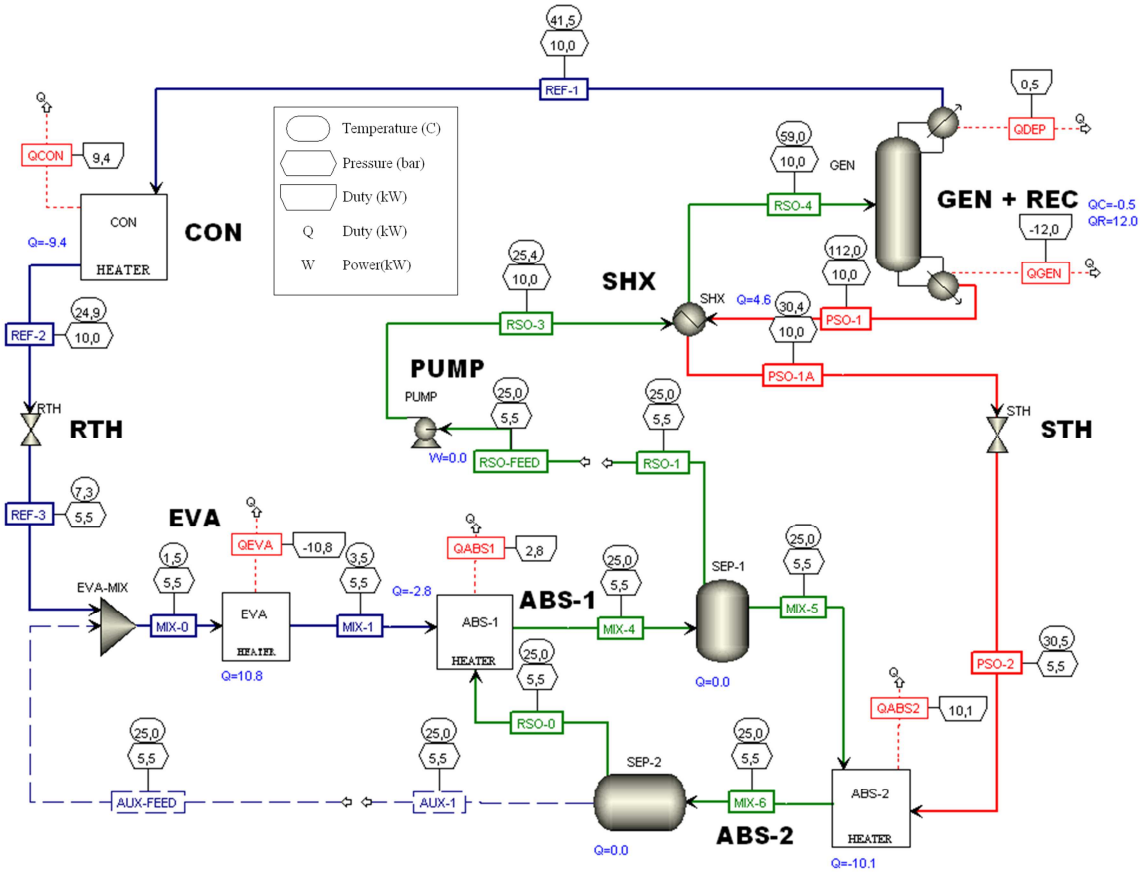

Figure 3-28: Schematic of the Rojey cycle with 2-stage absorption in ASPEN Plus

7. *Expansion valves (RTH and STH)*: For both expansion valves the ASPEN-model "Valve" were used. At the outlet of the valves the binary mixtures are at low level of pressure.
8. *Solution heat exchanger (SHX)*: The internal heat exchanger consists of the ASPEN-model "HeatX". The temperature difference between the rich solution inlet and poor solution outlet is 5 K.

Figure 3-29 shows the calculated COP_C of both cycles depending on the generator temperature. The simulation results in a temperature lift of approximately 30 K (t_{ABS_OUT} / t_{EVA} = 30 / 1.7℃) with the generator outlet temperatur es ranging from 120℃ to 150℃ being similar to those obtained by Coronas (1 995). In his paper, Coronas has reported COP_C of 0.73 - 0.76 for the Rojey cycle with 2-stage absorption and 0.60 - 0.62 for a conventional NH_3 / H_2O AHP at similar boundary conditions. As can be seen in Figure 3-29 the calculated COP_C for the Rojey cycle with 2-stage absorption ranges from 0.75 to 0.76 and for a conventional NH_3 / H_2O AHP from 0.63 to 0.66.

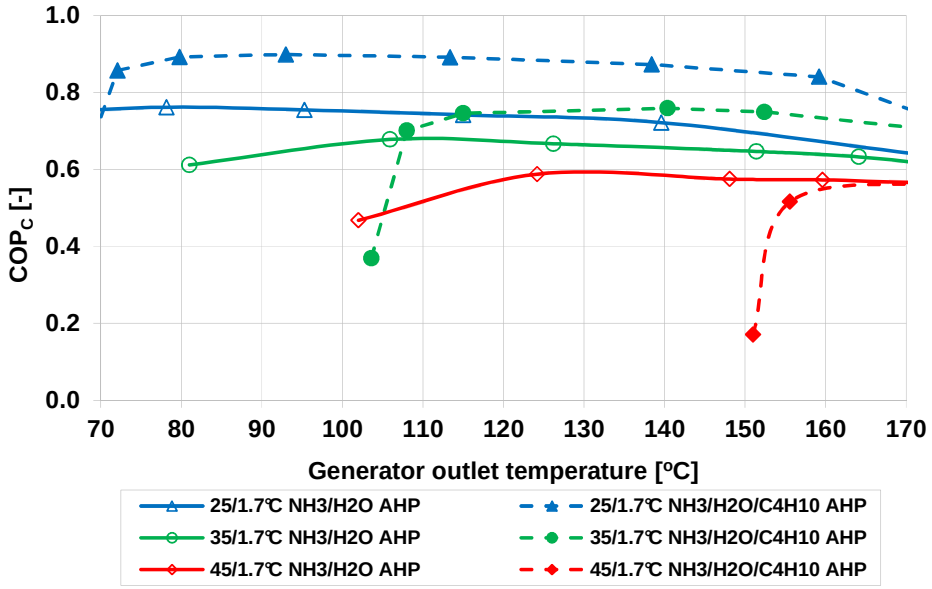

Figure 3-29: Calculated COP_C of the Rojey cycle (NH_3 / H_2O / C_4H_{10}) with 2-stage absorption and of a conventional NH_3 / H_2O AHP at t_{ABS_OUT} / t_{EVA} = 25 / 1.7℃, 35 / 1.7℃ and 45 / 1.7℃ depending on the generator outlet temperature

However, when analyzing the Rojey cycle at other temperature lifts and generator temperatures, it can be inferred, that it has higher efficiency than a conventional NH_3 / H_2O AHP operating only at low temperature lifts and high generator temperatures. The COP_C of the Rojey cycle decreases more than that of a conventional NH_3 / H_2O AHP with the increasing temperature lift. For instance, at t_{ABS_OUT} / t_{EVA} = 45 / 1.7℃ both cycles have

similar COP_C but the Rojey cycle requires a generator temperature of 165℃ instead of 120℃.

A decrease in COP_C with the decreasing generator temperature occurs because of an increase in the solution flow rate and a decrease in the difference between NH_3 concentrations in the rich and poor solution. Thereby, the difference between the NH_3 partial pressure at the first and second absorber stage is low and, furthermore, the NH_3 concentration of the strong solution decreases.

Figure 3-30 shows the Rojey cycle at two different generator temperatures, with one being lower (a) than the other (b). As can be seen, the difference between NH_3 partial pressures in the first (p_{abs-1}) and second (p_{abs-2}) absorber stages (because of high solution flow) is very low at low generator temperatures (Figure 3-30a). The concentration of the poor solution decreases with the increasing generator temperature and at the same time the concentration of the rich solution increases owing to the 2-stage absorption (Figure 3-30b).

From the simulation results, it can be concluded, that the Rojey cycle with 2-stage absorption and the working mixture $NH_3 / H_2O / C_4H_{10}$ is promising for application in systems with high generator temperatures and low temperature lifts. It is necessary to mention, that the NH_3 / C_4H_{10} concentrations in the evaporator of the Rojey cycle were set equal to the composition of the azeotropic mixture. When changing the C_4H_{10} concentration in the evaporator, evaporation will occur at gliding temperature. On the one hand, the comparison of the Rojey cycle with a conventional NH_3 / H_2O AHP will be difficult, while on the other hand, new application areas for the cycle can be found. Therefore, the investigation of the Rojey cycle at different C_4H_{10} concentrations is of interest.

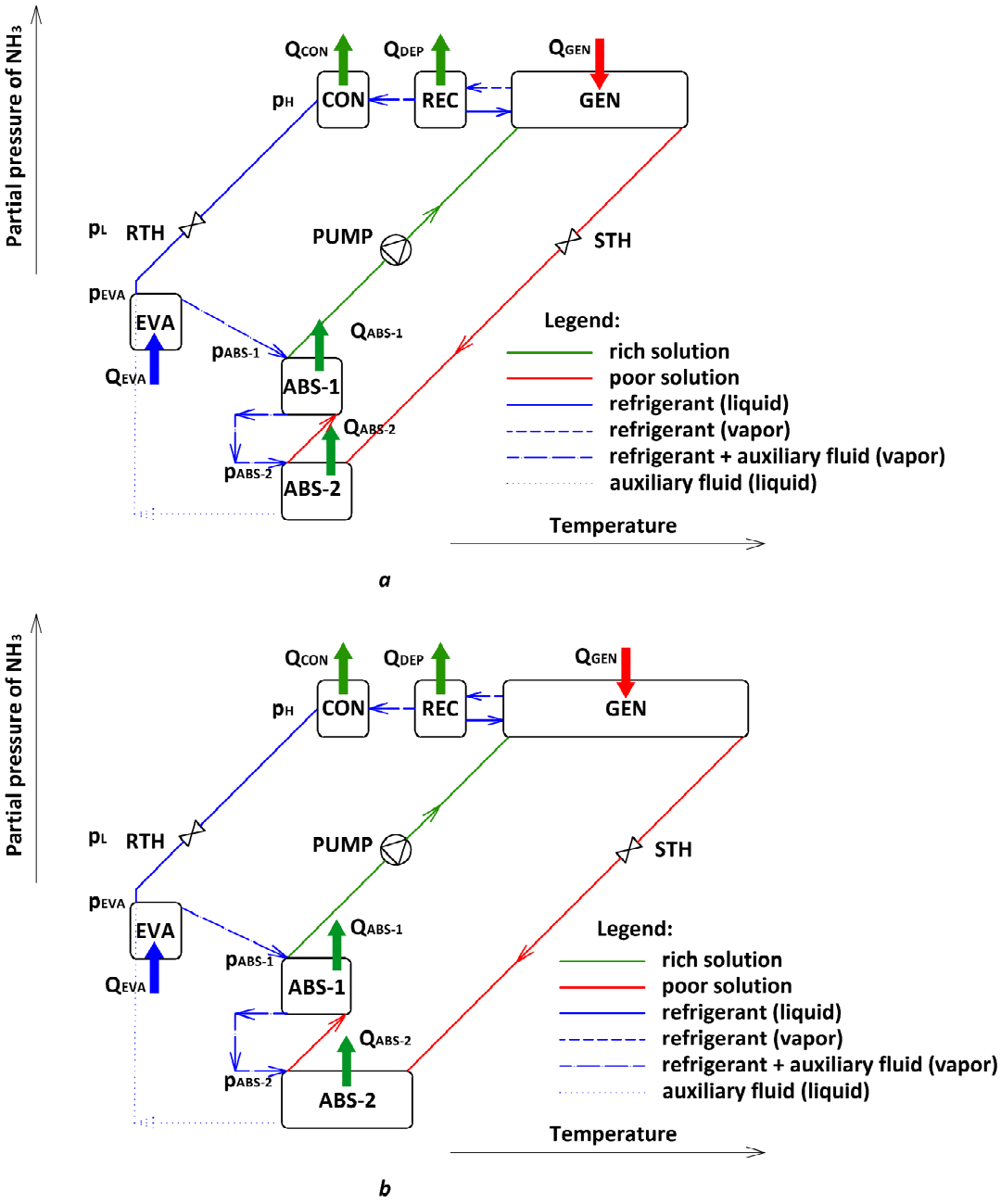

Figure 3-30: Rojey cycle in the pressure / temperature diagram at different generator temperatures: a – lower generator temperature; b – higher generator temperature

3.4 The Einstein-Szilard cycle

Another AHP-process using an auxiliary fluid has been proposed by Einstein and Szilard (1930). The commonly used working mixture in this cycle is C_4H_{10} / H_2O / NH_3, where NH_3 is the auxiliary fluid, H_2O is the absorbent and C_4H_{10} is the refrigerant. The advantage of this cycle in comparison to a conventional NH_3/ H_2O AHP is that no solution pump, condenser or throttle valve are necessary. Therefore, the Einstein- Szilard cycles operates at a single system pressure level.

3.4.1 Principle of operation

The Einstein-Szilard cycle using the mixture C_4H_{10} / H_2O / NH_3 is shown in the pressure / temperature diagram in Figure 3-31a. The rich NH_3 / H_2O solution enters the generator (GEN) at the system pressure level (p_S). In the generator heat ($\dot{Q}_{GEN}$) is supplied from a high temperature heat source generating NH_3 vapor and the poor solution. The poor solution flows back to the absorber (ABS) and the NH_3 vapor to the evaporator where it mixes with liquid C_4H_{10}. This leads to a decrease in the C_4H_{10} partial pressure and C_4H_{10} evaporation. The NH_3 partial pressure in the evaporator is lower than the system pressure due to the presence of the C_4H_{10}. Therefore, evaporation occurs at the lower temperature.

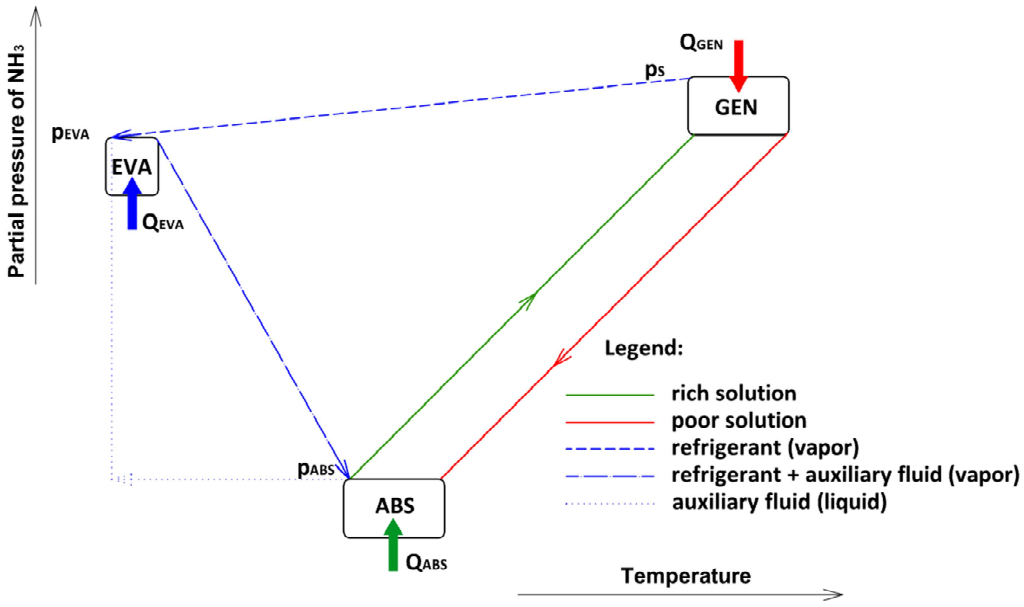

Figure 3-31: Einstein-Szilard cycle in the pressure / temperature diagram

The NH_3 / C_4H_{10} vapor enters the absorber and NH_3 is absorbed there by the poor solution. The absorption heat ($\dot{Q}_{ABS}$) is relegated at the middle temperature level to an external heat sink. The C_4H_{10} partial pressure increases, so that the C_4H_{10} condenses and is separated in the liquid phase from the rich solution. Due to an increase in the partial pressure of the C_4H_{10}, there is a decrease in the partial pressure of the NH_3 between the absorber and evaporator.

The Einstein-Szilard cycle has been theoretically and experimentally investigated for heating (Schaefer, 2000) and cooling (Delano, 1998; Mejbri et al., 2005) applications. Mejbri et al. (2005) reported the COP_C of 0.15 calculated at the following boundary conditions: t_{GEN_OUT} = 125°C; t_{ABS_OUT} = 30°C; t_{EVA_OUT} = 5°C; p_S = 5 bar. The main market barrier for this cycle seems to be its low efficiency.

3.4.1 Thermodynamic model and simulation results

Similar to the Rojey cycle (see Chapter 3.3) the efficiency of the Einstein-Szilard cycle could be increased, when the absorption of ammonia and condensation of butane occurs in two stages. This absorber modification was considered within this work for the Einstein-Szilard cycle (Figure 3-32).

The Einstein-Szilard cycle with 1- and 2-stage absorption and with the working mixture C_4H_{10} / H_2O / NH_3 was analyzed by means of thermodynamic simulations in ASPEN Plus and compared with a conventional NH_3 / H_2O AHP. The modification of the Einstein-Szilard cycle with 2-stage absorption investigated within this work is shown in Figure 3-33.

Both processes have been compared at absorber outlet temperatures (t_{ABS_OUT}) of 25, 35 and 45°C. In the evaporator of the Einstein-Szilard cycle, a mixture of C_4H_{10} / H_2O / NH_3 is present and thus the temperature difference between the evaporator inlet and outlet as well as the composition of the C_4H_{10} / H_2O / NH_3 mixture has been set as described for the Rojey cycle (see Chapter 3.3). Both processes (the Einstein-Szilard cycle and the conventional NH_3 / H_2O AHP) were analyzed at an evaporator temperature (t_{EVA_LOG}) of 1.7°C and the vapor fraction in the outlet of the evaporator of 0.99. Further, no heat or pressure losses were assumed for the simulations of both processes.

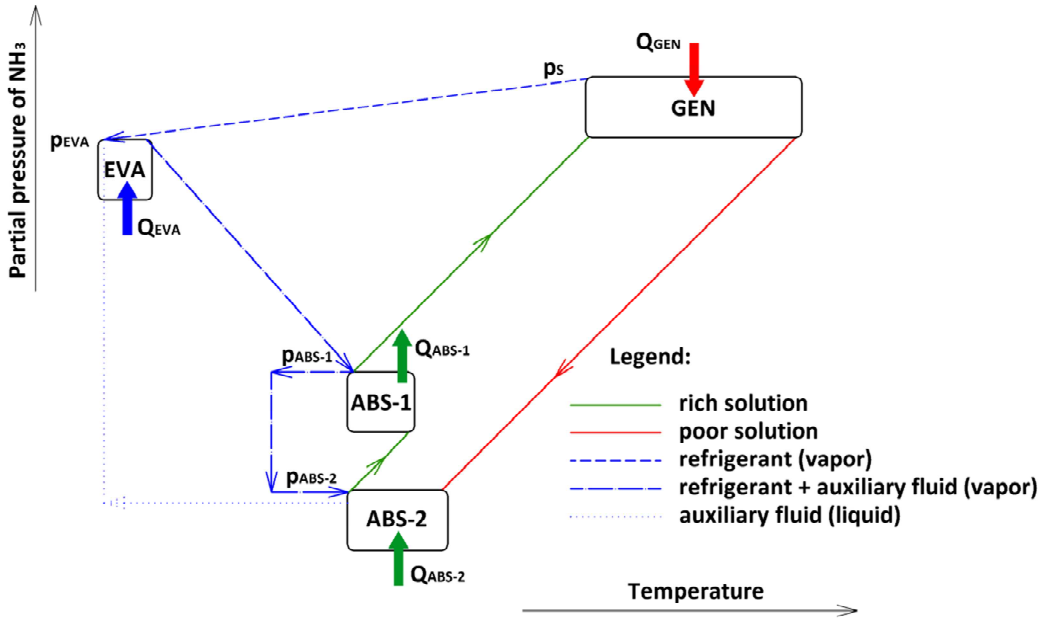

Figure 3-32: Einstein-Szilard cycle with 2-stage absorption in the pressure / temperature diagram

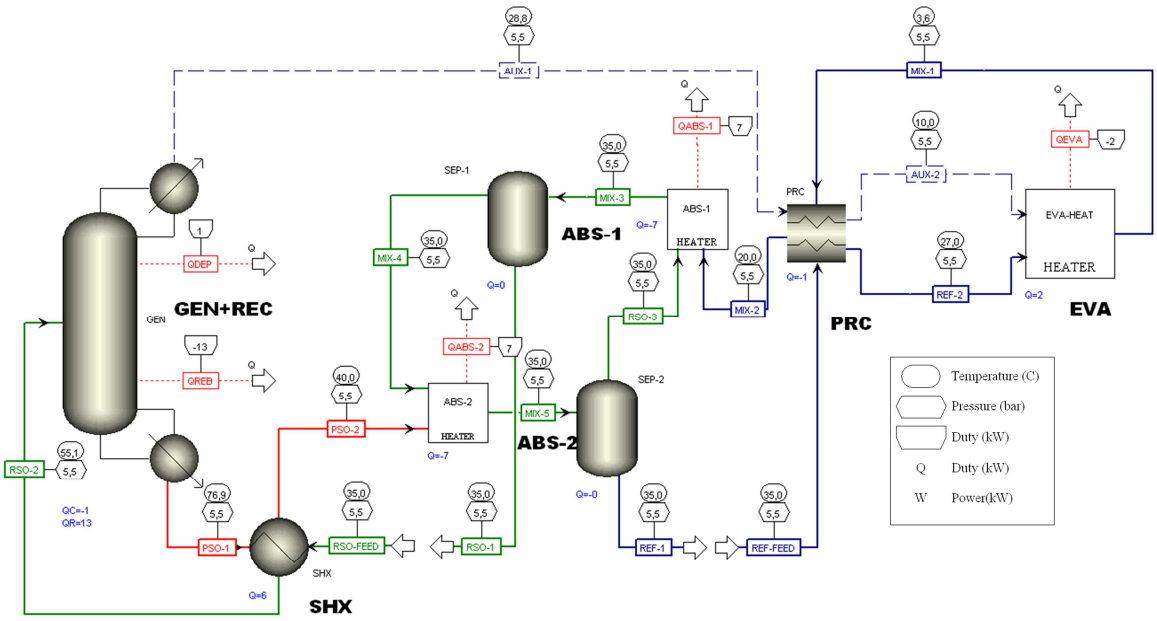

Figure 3-33: Schematic of the Einstein-Szilard cycle with 2-stage absorption in ASPEN Plus

For the simulation of a conventional AHP-process (see Figure 2-1) the same assumptions as discussed in Chapter 3.3.3 were made. The components of the investigated Einstein-Szilard cycle were specified as follows:

1. *The first stage of the absorber (ABS-1)*: consists of the ASPEN-models “Heater” and “Flash”. At the outlet from the “Heater” the temperature of the 2-phase mixture of C_4H_{10} / H_2O / NH_3 is fixed to t_{ABS_OUT} and at the outlet from the “Flash” the vapor and liquid phases are separated using VLE-equilibrium.
2. *The second stage of the absorber (ABS-2)*: consists of the ASPEN-models “Heater” and “Decanter”. At the outlet from the “Heater” the vapor fraction of C_4H_{10} / H_2O / NH_3 solution is 0 and in the “Decanter” two liquid phases (NH_3 / H_2O solution and liquid C_4H_{10}) are separated using LLE-equilibrium.
3. *Evaporator (EVA)*: the evaporator consists of the ASPEN-model “Heater”. The vapor fraction of the working mixture at its outlet is 0.99.
4. *Generator and rectification column (GEN and REC)*: Both components are modeled using one ASPEN-model “RadFrac” consisting of 5 theoretical stages. The lowest stage (5th stage) is the generator followed by 3 theoretical stages and the dephlegmator (1st stage). The rich solution enters between the 2nd and 3rd stages. The NH_3 / H_2O vapor with an NH_3 mass concentration of 99.9% leaves at the top of the “RadFrac” and the poor solution from the bottom of the “RadFrac”.
5. *Pre-cooler (PRC)*: The pre-cooler consists of the ASPEN-model “HeatX”. The temperature of the auxiliary fluid at the outlet from the pre-cooler is set equal to 10°C and the temperature of the vapor of the refrigerant and auxiliary fluid to 20°C.
6. *Solution heat exchanger (SHX)*: The solution heat exchanger consists of the ASPEN-model “HeatX”. The temperature difference between the rich solution inlet and poor solution outlet is 5 K.

The difference in the specification of the Einstein-Szilard cycle with 1-stage absorption is that the absorber consists of only the ASPEN-models “Heater” and “Decanter”.

The simulation results, at a temperature lift of approximately 25 K (t_{ABS_OUT} / t_{EVA_LOG} = 25 / 1.7°C) and a generator temperature of 125°C, are similar to those reported by Mejbri et al. (2006) for the Einstein-Szilard process with 1-stage absorption. Mejbri et al. (2006) reported a COP_C of 0.15 while in this work, that same number was calculated at 0.16.

It is obvious, that by means of 2-stage absorption the COP_C of the Einstein-Szilard cycle could be increased and the driving energy could be supplied at lower generator temperatures. However, the efficiency of the “improved” Einstein-Szilard cycle is still much lower than that of a conventional NH_3 / H_2O AHP. For instance, at t_{ABS_OUT} / t_{EVA}=25 / 1.7°C the Einstein-Szilard cycle has a COP_C of 0.19 and a conventional NH_3 / H_2O AHP of 0.75 (see Figure 3-34).

At present the Einstein-Szilard cycle with the C_4H_{10} / H_2O / NH_3 mixture does not seem to be competitive in efficiency with conventional technologies.

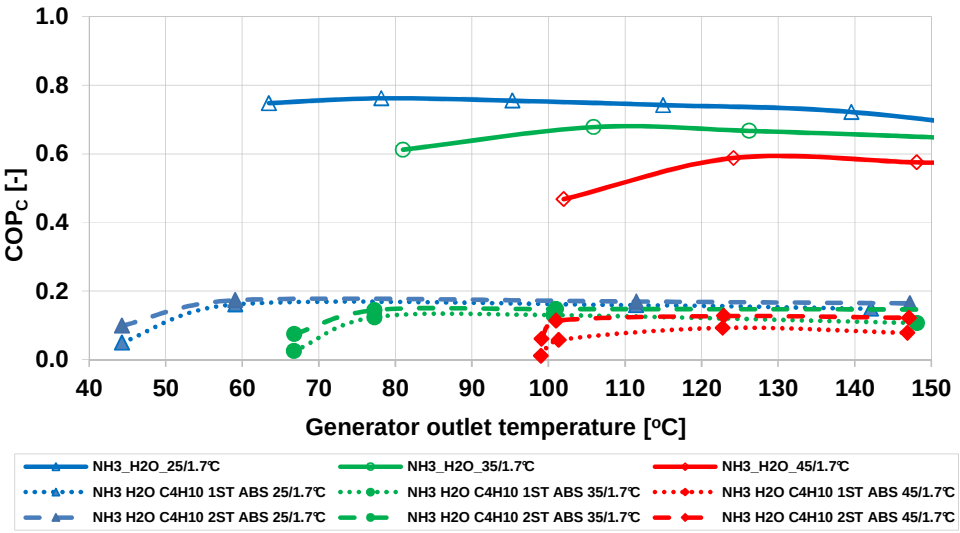

Figure 3-34: COP of the Einstein-Szilard cycle with 1- and 2-stage absorption and of a conventional NH_3/ H_2O AHP depending on absorber, evaporator and generator temperatures

3.5 Absorption heat pumping processes using ionic liquids as absorbents

In order to overcome some drawbacks of the working pair NH_3 / H_2O, such as the need for rectification, the use of ionic liquids (*IL*) as absorbents has been discussed by several authors (Yokozeki and Shiflett, 2007a, b; 2008). *ILs* are commonly described in the literature as substances composed entirely of ions with melting points below 100℃.

The majority of research on AHP-processes using *IL* aims to measure certain binary properties, e.g. VLE-data, in order to use them for process calculations. However, up to now, not much information on the efficiency of AHP-processes using *IL* at different boundary conditions as well as on the influence of *IL* on component design could be found.

3.5.1 NH_3 / IL absorption heat pumping processes

The use of *IL* with NH_3 as a refrigerant in an AHP-process has been discussed by Yokozeki and Shiflett (2007a, b). According to them, the main advantage of this AHP-process in comparison with a conventional NH_3/ H_2O AHP is that due to the low vapor pressure of *IL*, no rectification column is necessary.

The operating principle of the NH_3 / *IL* AHP-processes is similar to a conventional NH_3 / H_2O AHP. The difference is that in the sorption part (between the absorber and generator) an *IL* as absorbent is used instead of H_2O (see Figure 3-35).

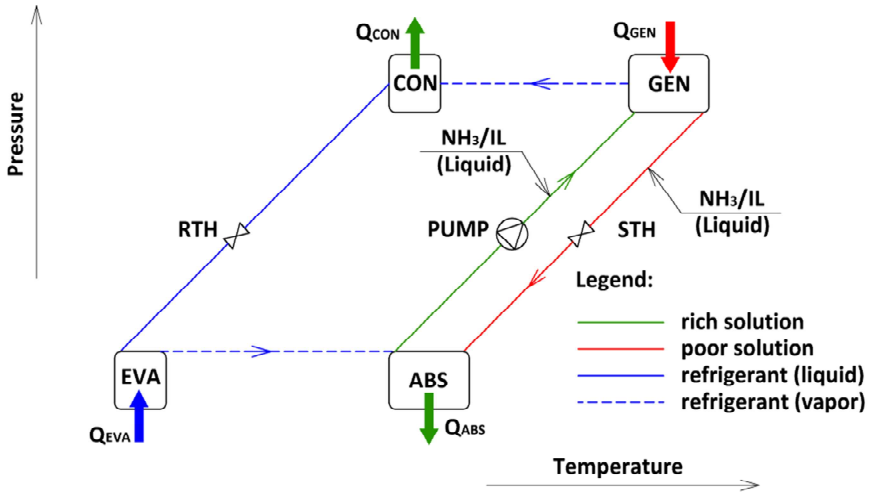

Figure 3-35: Schematic diagram of the NH_3 / IL AHP-process

Yokozeki and Shiflett (2007a, b; 2008) have theoretically investigated different *IL* with NH_3. In order to regress binary parameters, authors have measured VLE-data of 8 mixtures of ILs with NH_3 (see Table 3-3). The measurements have been conducted for the temperature range between 9 - 99℃ and pressure ran ge between 0.4 - 50.0 bar.

The measured VLE-data have been used by Yokozeki and Shiflett (2008) for the COP_C calculation of the investigated NH_3 / *IL* AHP-processes. The data was regressed using the Redlich-Kwong equation of state.

Table 3-3: NH_3 / IL working mixtures for AHP-processes (according to Yokozeki and Shiflett, 2008)

No.	Working mixture	Temperature range [℃]	Pressure range [bar]	IL manufacture
1	NH_3 / *[bmim][PF_6]*	10 - 83	1.4 - 27.0	Sigma-Aldrich Chemie GmbH (Fluka Buchs, Switzerland)
2	NH_3 / *[hmim][Cl]*	10 - 75	0.4 - 25.0	
3	NH_3 / *[emim][Tf_2N]*	10 - 75	1.1 - 29.0	
4	NH_3 / *[bmim][BF_4]*	9 - 82	0.9 - 26.0	
5	NH_3 / *[emim][Ac]*	9 - 75	3.2 - 29.0	
6	NH_3 / *[emim][$EtOSO_3$]*	9 - 99	2.9 - 48.0	
7	NH_3 / *[emim][SCN]*	9 - 99	2.4 - 50.0	
8	NH_3 / *[DMEA][Ac]*	9 - 99	1.4 - 42.0	Bioniqs (York, England)

The investigated processes were analyzed at t_{GEN_OUT} / t_{CON_OUT} / t_{ABS_OUT} / t_{EVA_OUT} = 100 / 40 / 30 / 10℃ and compared with a conventional NH_3 / H_2O AHP. The calculated COP_C as well as NH_3 mass concentrations in the rich and poor solution and specific solution flow rates are listed in Table 3-4. From the simulation results, it can be inferred that the COP_C is somewhat lower when using investigated *IL* instead of H_2O in an AHP-process. However, no rectification column for the NH_3 generation is necessary. This leads to a decrease in the investment costs and easier process regulation.

It must also be noted that the low difference between the NH_3 mass concentration in the rich and poor solution causes high specific solution flow rates when using the above mentioned *IL*.In regard to simulation uncertainties it is necessary to mention that no caloric data for the data regression of binary parameters were used. Further, the specific heat capacities of pure *IL* have been calculated according to the Harrison-Seaton method (heat capacity estimation based on the information of the type and number of different elements comprising a molecule) and not regressed from experimental data.

Table 3-4: Cooling COP of AHP-processes with ILs (according to Yokozeki and Shiflett, 2008)

No.	Working mixture	Specific solution flow rate, f [-]	NH_3 mass concentration in the rich solution, ξ_{RSO} [kg·kg^{-1}]	NH_3 mass concentration in the poor solution, ξ_{PSO} [kg·kg^{-1}]	COP_C [-]
1	NH_3 / [bmim][PF_6]	17.27	0.11	0.055	0.575
2	NH_3 / [hmim][Cl]	14.26	0.127	0.061	0.525
3	NH_3 / [emim][Tf_2N]	24.57	0.076	0.037	0.589
4	NH_3 / [bmim][BF_4]	12.98	0.117	0.043	0.557
5	NH_3 / [emim][Ac]	12.55	0.15	0.077	0.573
6	NH_3 / [emim][$EtOSO_3$]	12.42	0.148	0.073	0.557
7	NH_3 / [emim][SCN]	17.55	0.102	0.048	0.485
8	NH_3 / [DMEA][Ac]	7.60	0.269	0.159	0.612
9	NH_3 / H_2O	2.54	0.639	0.405	0.646

In the following subsections, the use of *IL* as absorbents with the refrigerant NH_3 in an AHP-process will be analyzed. The calculated properties of pure *IL* and their mixtures with NH_3 and the thermodynamic model developed in ASPEN Plus will be discussed. The obtained simulation results will be analyzed in regard to the influence of *IL* on the process efficiency and component's capacities.

3.5.2 Properties calculation of the working mixtures NH_3 / IL

For the calculations of the properties of *IL* and their mixtures with NH_3 the thermodynamic model "NRTL" was used. The simulation of a conventional NH_3 / H_2O AHP was carried out

using the “Peng-Robinson” thermodynamic model with built-in binary parameters. Due to the lack of experimental data of specific heat capacities of pure *IL*, out of 8 working mixtures discussed in Chapter 3.5.1, the following mixtures were chosen for the thermodynamic analysis: NH_3 / *[bmim][*BF_4*]*, NH_3 / *[bmim][*PF_6*]*, NH_3 / *[emim][*$EtSO_4$*]* and NH_3 / *[emim][*TF_2N*]*. For calculating the properties, the following data were used:

- experimental data of pure *IL*: critical data and vapor pressure (Valderrama and Robles, 2007), molar volume or density (Seddon et al., 2002; Rodriguez and Brennecke, 2006; Fernandez et al., 2008; Krummen et al., 2008), thermal conductivity (Van Valkenburg et al., 2005; Ge et al., 2007; Tomida et al., 2007), viscosity (Seddon et al., 2002; Sanchez et al., 2009), specific heat capacity (Holbrey et al., 2003; Rebelo et al., 2004; Ge et al., 2008) and heat of evaporation at 298K (Verevkin, 2008). The relative error of the data regression ranges from -3.5% to +4.5%;
- experimental VLE-data for the investigated NH_3 / *IL* mixtures (Yokozeki and Shiflett, 2007a, b). The relative error of the data regression ranges from -7.4% to + 12.6%.

Figure 3-36 compares the VLE-data calculated and measured by Yokozeki and Shiflett (2007 a) for the investigated working mixture. For the working mixtures NH_3 / *[bmim][*BF_4*]*, NH_3 / *[bmim][*PF_6*]* and NH_3 / *[emim][*TF_2N*]* a sufficient number of measurements were used for the data regression. For the working mixture NH_3 / *[emim][*$EtSO_4$*]* only 2 measurements lie within the area of the simulation of the AHP-process. Furthermore, the experimental VLE-data used are valid for a temperature range from 9 to 99°C. Thus for the simulation of higher temperatures (up to 140°C) the experimental data used were extrapolated.

In spite of the calculation uncertainties arising from the data regression and extrapolation of the experimental data the calculated thermodynamic properties seem to be useful for:

- pre-selection of *IL* for use as absorbents with the refrigerant NH_3 in an AHP-process;
- analysis of the influence of variable boundary conditions on the COP_C;
- comparison of the component’s capacities of the investigated NH_3 / *IL* AHP-processes with those of a conventional NH_3 / H_2O AHP.

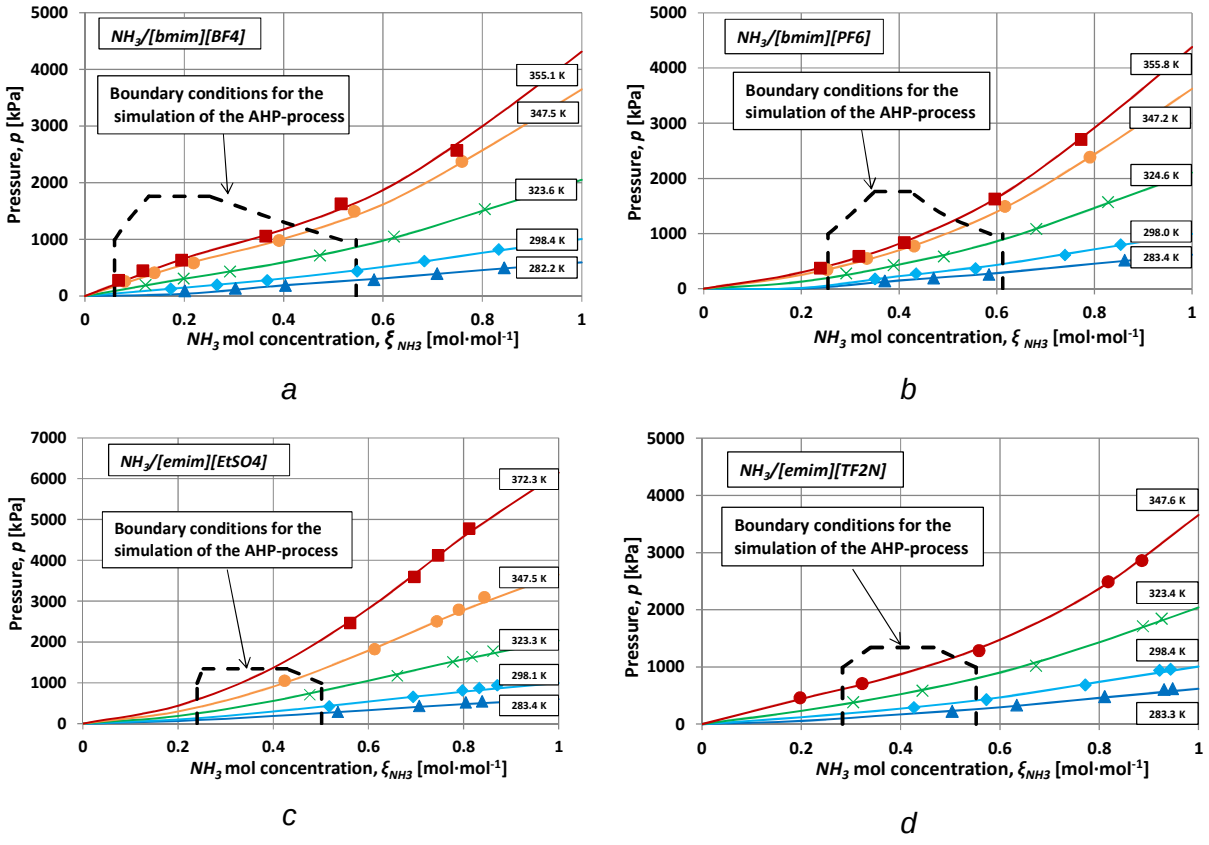

Figure 3-36: Comparison of the calculated and measured by Yokozeki and Shiflett (2007 a) VLE-data: a – NH_3 / [bmim][BF_4]; b –NH_3 / [bmim][PF_6]; c –NH_3 / [emim][$EtSO_4$]; d –NH_3 / [emim][TF_2N]

3.5.3 Thermodynamic model and simulation results

As mentioned above, the use of *IL* within an AHP-process ensures the generation of the refrigerant vapor with sufficient purity without using a rectification column. Therefore two thermodynamic models were developed in ASPEN Plus: AHP-process with rectification column (simulation of a conventional NH_3 / H_2O AHP) and AHP-process without rectification column (simulation of NH_3 / *IL* AHP-processes). For both processes, no heat losses or pressure drops were taken into account.

AHP-processes with NH_3 / *IL* and NH_3 / H_2O working mixtures were calculated at absorber / evaporator outlet temperatures (t_{ABS_OUT} / t_{EVA_OUT}) of 25 / 5℃, 35 / 5℃ and 45 / 5℃ and at generator outlet temperatures (t_{GEN_OUT}) ranging from 60℃ to 140℃. The calculated COP_C are shown in Figure 3-37. As can be seen the dependence of the COP_C of the investigated NH_3 / *IL* AHP-processes on boundary conditions differs from one another.

The COP_C of the NH_3 / [bmim][BF_4] AHP-process is comparable with that of a conventional NH_3 / H_2O AHP only at t_{ABS_OUT} / t_{EVA_OUT} = 25 / 5℃ and t_{GEN_OUT} = 80 - 105℃ (see Figure 3-37a). At higher generator temperatures, there is a large decrease in the COP_C. The reasons for this are a relatively low normal boiling temperature of the *IL* (thus a certain part of

IL evaporates together with the NH_3) and the non-use of a rectification column. Therefore, a certain amount of *[bmim][BF_4]* ends up in the refrigerant circuit and decreases the evaporator capacity.

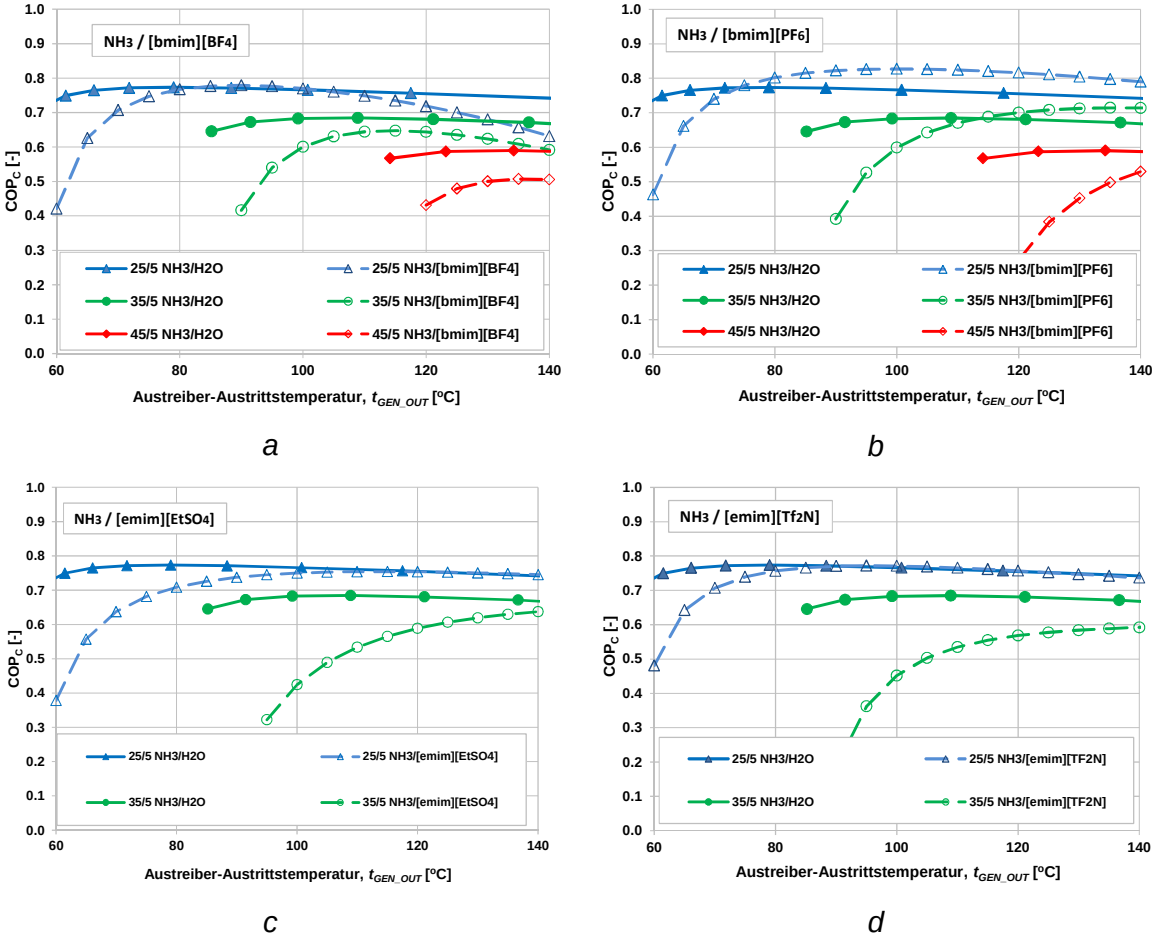

Figure 3-37: Calculated COP_C of the NH_3 / IL AHP-processes without rectification column in comparison to a conventional NH_3 / H_2O AHP-process with rectification column at t_{ABS_OUT} / t_{EVA_OUT} =25 / 5℃, 35 / 5℃ and 45 / 5℃: a – NH_3 / [bmim][BF_4]; b – NH_3 / [bmim][PF_6]; c – NH_3 / [emim][$EtSO_4$]; d – NH_3 / [emim][TF_2N]

The mixture with the highest calculated COP_C was *NH_3 / [bmim][PF_6]* (see Figure 3-37b). The AHP-process using *NH_3 / [bmim][PF_6]* seems to be more efficient than a conventional *NH_3 / H_2O* AHP at certain boundary conditions: t_{ABS_OUT} / t_{EVA_OUT} = 25/5℃ and t_{GEN_OUT} > 75℃; t_{ABS_OUT} / t_{EVA_OUT} = 35/5℃ and t_{GEN_OUT} > 115℃. However, at t_{ABS_OUT} / t_{EVA_OUT} = 45/5℃ the COP_C are lower than those of a conventional *NH_3 / H_2O* AHP.

The dependence of the COP_C on the generator temperature and temperature lift for the AHP-processes using *NH_3 / [emim][$EtSO_4$]* and *NH_3 / [emim][TF_2N]* are similar (see Figure 3-37c and d). Apparently, the COP_C decreases more than those of a conventional *NH_3 / H_2O* AHP with an increasing temperature lift.

This happens due to the small difference between the NH_3 concentrations in the rich and poor solution and, therefore, the high specific solution flow rate. Table 3-5 lists the NH_3 mass concentrations in the rich and poor solution and the specific solution flow rate at t_{GEN_OUT} = 140℃ for the NH_3 / *[bmim][PF$_6$]* AHP-process and for a conventional NH_3 / H_2O AHP. When using *[bmim][PF$_6$]* the NH_3 mass concentration in the rich solution is significantly lower (0.05 – 0.09) in comparison to the working pair NH_3 / H_2O (0.41 – 0.57). Therefore, the specific solution flow rate of the NH_3 / *IL* AHP-processes is much higher (14.5 – 61.8) than those of a conventional NH_3 / H_2O AHP (2.0 – 4.5).

Table 3-5 – NH_3 mass concentration in rich and poor solution and specific solution flow rate for the investigated working pairs (at t_{GEN_OUT} = 140℃)

	Absorber / evaporator outlet temperatures, t_{ABS_OUT} / t_{EVA_OUT} [℃]	NH_3 / H_2O	NH_3 / *[bmim][PF$_6$]*
NH_3 mass concentration in the rich solution, ξ_{RSO} [kg/kg]	25 / 5	0.568	0,087
	35 / 5	0.479	0.062
	45 / 5	0.408	0.047
NH_3 mass concentration in the poor solution, ξ_{PSO} [kg/kg]	25 / 5	0.137	0.020
	35 / 5	0.186	0.025
	45 / 5	0.221	0.031
Specific solution flow rate, *f* [-]	25 / 5	2.0	14.5
	35 / 5	2.9	26.2
	45 / 5	4.5	61.8

The high solution flow rate is tied to the shape of the boiling curve of the working mixture (see Figure 3-38). In order to decrease the solution flow rate, *IL* with a steeper boiling curve at high NH_3 mass concentrations have to be found.

The high solution flow rate causes an increase in the components capacity at the constant rich solution flow rate. For instance, the calculated evaporator capacity is shown depending on the generator outlet temperature for the operation with the working mixture NH_3 / H_2O and NH_3 / *[bmim][PF$_6$]* in Figure 3-39a. It can be seen, that to achieve the same cooling capacity, the AHP-process using *IL* requires bigger components of the sorption circuit, i.e. absorber, generator, solution heat exchanger, solution pump and solution throttle valve.

Figure 3-39b compares the specific solution pump capacity of the NH_3 / *[bmim][PF$_6$]* AHP-process with a conventional NH_3 / H_2O AHP. Apparently, the solution pump capacity increases when using *IL* and therefore must be taken into account when calculating the process performance.

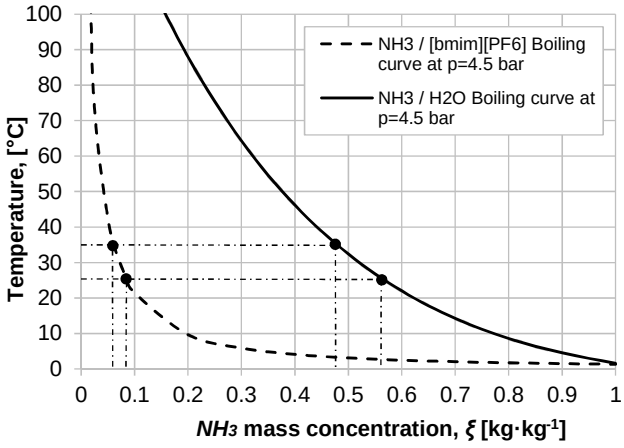

Figure 3-38: Phase diagram of the mixtures NH_3 / [bmim][PF_6]and NH_3 / H_2O at 4.5 bar

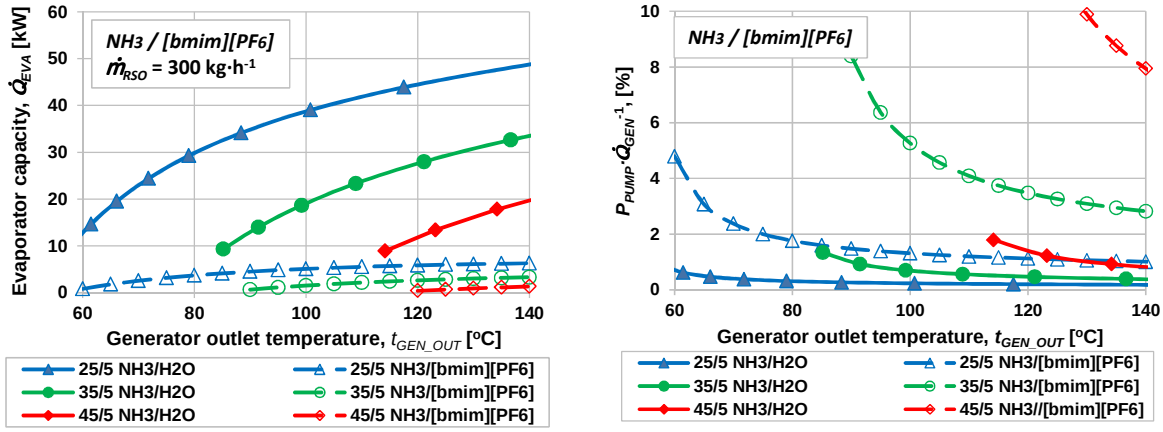

a *b*

Figure 3-39: Ratio of the capacity of the solution pump to the generator capacity of the NH_3 / [bmim][PF_6] AHP-process in comparison to a conventional NH_3 / H_2O AHP depending on the generator outlet temperature

From the simulation results, it can be inferred that the use of the investigated *IL* instead of H_2O influences the AHP-process and its components as follows:

- no rectification column is necessary;
- to get the same cooling capacity of the AHP-process, the bigger components of the sorption circuit, i.e. absorber, generator, solution heat exchanger, solution pump and solution throttle valve, are required;
- to overcome the issue of the high solution flow rate, new IL with a steeper boiling curve at high NH_3 mass concentrations have to be found.

Finally, it is necessary to mention that an increase in the viscosity when using *IL* instead of H_2O leads to a decrease of the absorber efficiency and poor wetting of the absorber surface

(Römich et al., 2009). Concerning the *IL* discussed within this work, their viscosities vary from 0.039 Pa·s to 0.37 Pa·s at a temperature of 20℃ and are significantly hi gher than those of H_2O (0.001 Pa·s) at the same temperature.

3.6 Cycle selection for experimental investigation

From the thermodynamic analysis of innovative AHP-processes, it was concluded that the preferred cycle for further experimental investigation is the NH_3 / H_2O AHP-process using *NaOH* as an additive. This cycle consists of the same components as a conventional NH_3 / H_2O AHP and therefore no additional costs are needed. The cycle was found to be promising for the cooling applications at low generator temperatures.

Another cycle found to be competitive in efficiency with a conventional NH_3 / H_2O AHP is the Rojey cycle. However, the Rojey cycle is more efficient only at low temperature lifts and high generator temperatures. In regard to additional costs, this cycle needs an additional circuit between absorber and evaporator for the circulation of a condensable auxiliary fluid and the absorber has to provide the separation of the liquid auxiliary fluid from the rich solution. Thus, the absorber design has to be analyzed concerning its technical feasibility. Furthermore, at the present time, the application area at low generator temperatures, e.g. solar cooling, is more favorable and promising for practical use than that at high generator temperatures.

4 NH_3 / H_2O / NAOH TEST RIG

The purpose of this chapter is to describe the AHP test rig built for the investigation of *NaOH* as an additive to the working mixture *NH_3 / H_2O*, to comment on the design of its components and to discuss the process regulation and data processing and acquisition. The design chosen for the AHP test rig has to fulfill the following requirements of the experimental investigations:

1. To ensure data acquisition for the analysis by means of thermodynamic simulations using ASPEN Plus;
2. to validate the simulation results of the *NH_3 / H_2O / NaOH* AHP-process presented in Chapter 3.1.4;
3. to analyze the influence of *NaOH* on the performance of the AHP test rig;
4. to analyze the operation of the cycle components.

Figure 4-1 shows the schematic of the *NH_3 / H_2O / NaOH* AHP test rig in the pressure / temperature diagram. It consists of the absorber (ABS), condenser (CON), generator (GEN), rectification column with stripping section (STR), rectification section (REC) and dephlegmator (DEP), solution heat exchanger (SHX), rich solution (RSAC), poor solution (SAC) and refrigerant (RAC) accumulators and throttle valves (STH and RTH). Furthermore, there are two bypasses to enable operation with or without SHX. The design of the rectification column also permits operation using both the rectification and stripping sections or only the rectification section.

Also three external loops are used to enable the operation of the test rig at different temperature levels. The heat to the evaporator is supplied by the brine loop, while the heat to the generator is supplied by the hot water loop. The absorber, condenser and dephlegmator are cooled by the cooling loop.

The photograph of the AHP test rig is shown in Figure 4-2. It can be seen that access to each component of the AHP test rig is provided.

It must be noted that the AHP test rig has been built within the project “InnovAP” and afterwards several changes in its construction were made within the project “Hydroxid-AWP”. The detailed operation of each component as well as the regulation of the AHP test rig will be discussed in detail in the following sub-chapters.

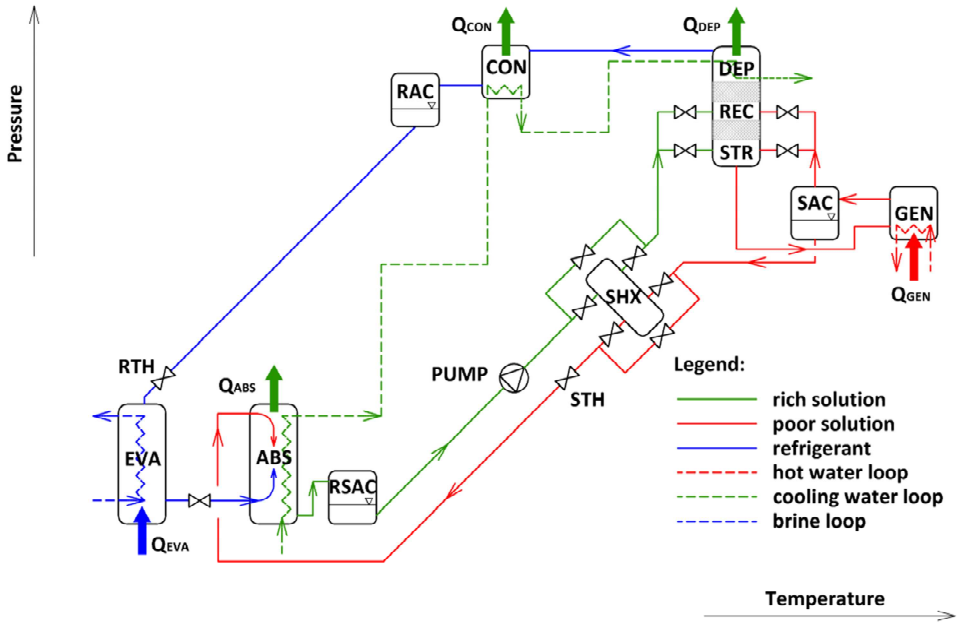

Figure 4-1: Schematic of the NH_3 / H_2O / NaOH AHP test rig

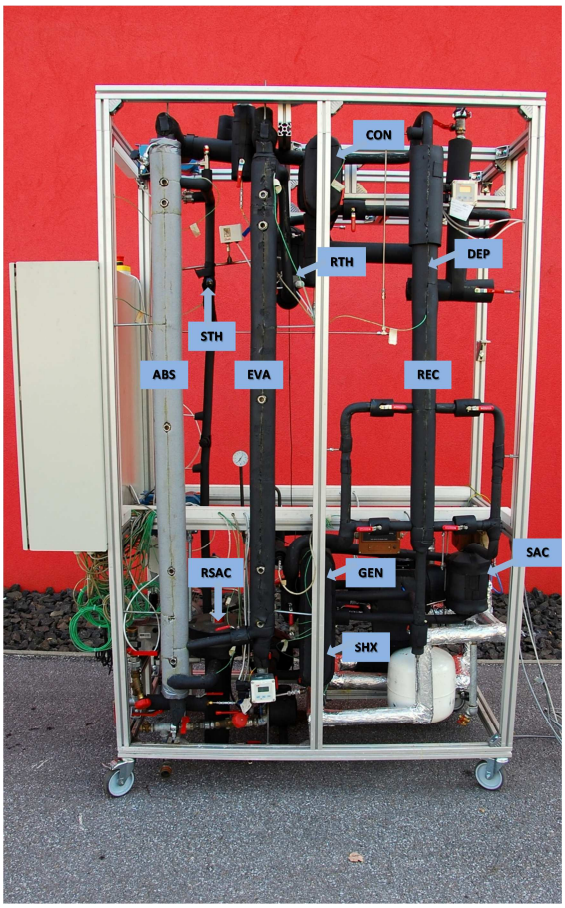

Figure 4-2: Photograph of the NH_3 / H_2O / NaOH AHP test rig

4.1 Absorber

The performance of the absorber is critical to the AHP efficiency. Its development is challenging and it has contradictory requirements concerning its construction. On the one hand, the solution side must provide both adequate heat and mass transfer, and the cooling-water side good heat transfer. On the other hand, the pressure drop on both sides has to be as low as possible to minimize parasitic electrical power (according to Garimella at al., 2011).

Within this work there were no restrictions concerning the pressure drop on the cooling water side, as the power consumption of the external circulation pumps was not taken into account. The main objective of the absorber construction was to provide adequate heat and mass transfer on both sides and to get proper wettability on the solution side when operating with the working mixture *NH_3 / H_2O* with and without *NaOH*.

Basically, there are two types of absorbers that are used in conventional AHP: falling film and bubble absorbers. The falling films absorbers, have relatively high U-values and are stable during operation. However, the design of the liquid distributor at the poor solution inlet to the absorber is crucial to ensure proper wettability of the solution side surface. The bubble absorbers have very high U-values and proper wettability. However, to achieve good mixing between the poor solution and refrigerant vapor, a distributor for refrigerant vapor is necessary (according to Kang et al., 2000).

Within this work the vertical falling film absorber with optical access to the absorption process was chosen for the AHP test rig.

A schematic of the realized falling film absorber is shown in Figure 4-3. The construction of this absorber consists of three vertical pipes inserted one into another: the external pipe of Ø 60.3 x 3 mm and two internal pipes of Ø 33.7 x 3.2 mm and Ø 21.3 x 3.2 mm.

Cooling water is introduced at the bottom of the absorber. It flows through four openings (Ø 6.0 mm) and then upward between two internal pipes and leaves at the top of the absorber. The regulation of the cooling water flow rate occurs by means of the regulation valve. As there were no restrictions on the cooling water pressure drop, a wire (Ø 2.5 mm) with a pitch angle of 20° was installed along the cooling water flow, to enhance the cooling-water side heat transfer.

The *NH_3 / H_2O* poor solution is introduced at the top of the absorber through the pipe of Ø 8.0 x 2.0 mm to the header. As it flows through the header, the flow is distributed in parallel through the openings of the distribution device (see Figure 4-4) on the surface of the first internal pipe (Ø 33.7 x 3.2 mm). In order to provide proper wettability of the absorber surface, the wire mesh (see Figure 4-4) with a mesh diameter of Ø 0.1 mm and a mesh width of 0.265 mm was welded to the surface of the first internal pipe and is additionally fixed by a

wire (Ø 1.5 mm) with a pitch angle of 16°. The gravity-driven *NH_3 / H_2O* solution, with a negligible absorption-side pressure drop, flows in the falling-film mode counter-current to the cooling water and *NH_3* vapor. The absorption of *NH_3* vapor by *NH_3 / H_2O* solution takes place on the surface of the first internal pipe (Ø 33.7 x 3.2 mm). The heat of absorption is conveyed to the cooling water.

Optical access to the absorption process was provided by installing five sight glasses along the height of the absorber as is shown in Figure 4-3.

It is important to note that the following changes to the absorber construction were made during the development phase in order to increase its capacity, to improve the wettability of the absorber surface and to achieve better optical access to the absorption process:

- the wire mesh was installed;
- the diameter of the cooling water side wire was increased from 2.0 mm to 2.5 mm;
- the pitch angle of the cooling water side wire was decreased from 21° to 16°;
- an additional sight glass in the lower part of the absorber was installed.

The solution-side heat transfer analysis was made according to Niebergall (1981) (see Eq. 4-1) and on the cooling water side according to VDI Waermeatlas (2006).

$$\alpha_{falling\ film\ ABS} = K \cdot Re^{0.5} \cdot Pr^{0.15} \cdot H^{-0.065} \cdot \lambda \qquad 4\text{-}1$$

The UA-values and the absorber capacities calculated at typical boundary conditions are shown in Table 4-1. The properties of the *NH_3 / H_2O* mixture were calculated by means of ASPEN Plus. The logarithmic temperature difference in the absorber was calculated using inlet and outlet temperature on the solution and cooling water sides. The *NH_3* mass concentration in the solution in the absorber is the arithmetic mean value of the *NH_3* mass concentrations in the rich and poor solution.

As can be seen, the UA-values of the absorber vary from 143 to 202 $W \cdot K^{-1}$ and the absorber capacities from 1000 to 1400 W. When comparing these calculated results with those calculated using the experimental data (see Figure 5-14) it can be inferred that the predicted heat capacities at 1100 W have been achieved. However, the absorber efficiency was somewhat lower than predicted. The reason for this is the sub-cooling of the rich solution at the outlet from the absorber and, therefore, a decrease in the absorber efficiency. A detailed analysis of the operation of the absorber based on the experimental results will be given in Chapter 5.2.3.

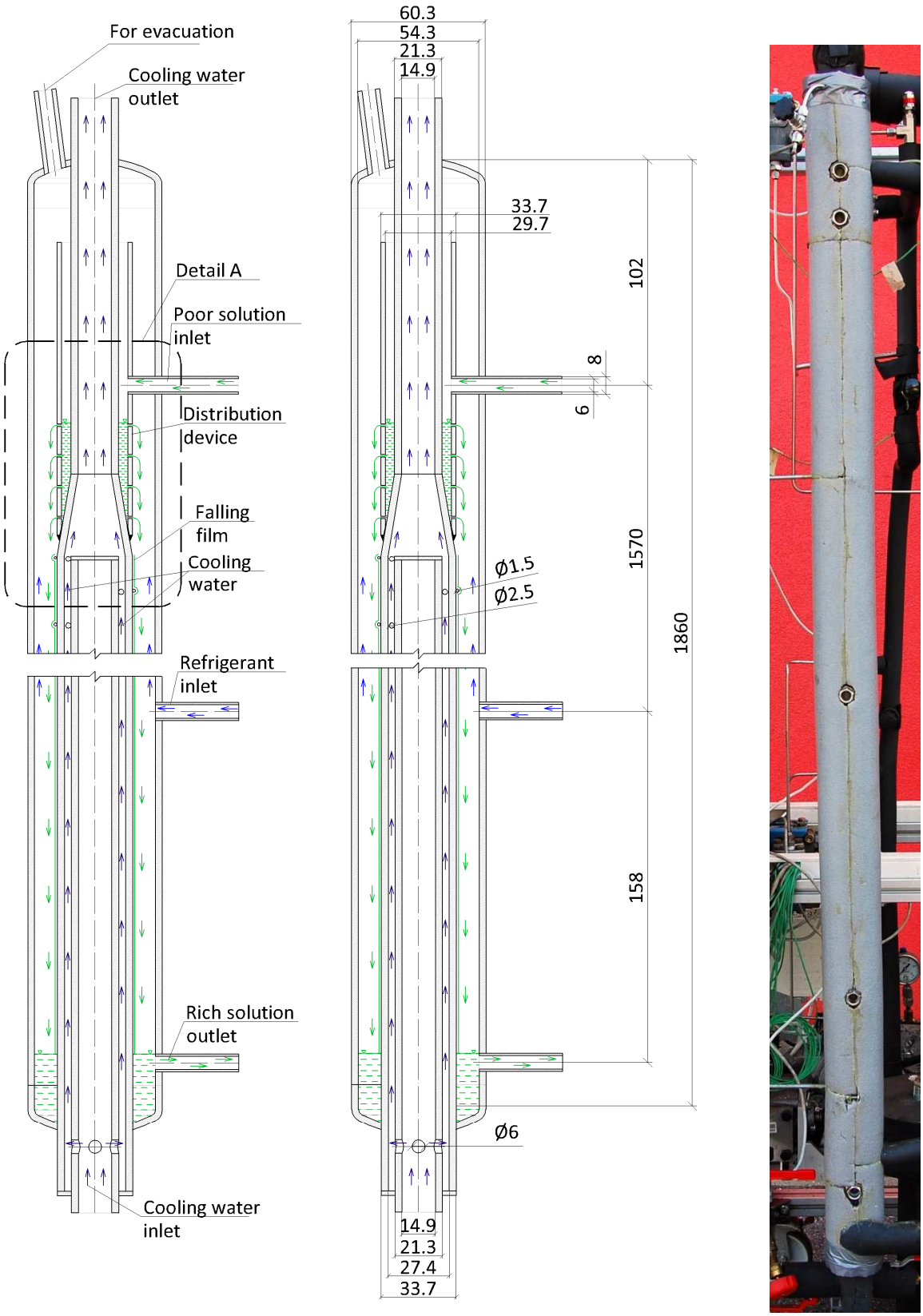

Figure 4-3: Schematic of the falling film absorber: left – operating principle; center – design details; right – photograph of the installed absorber

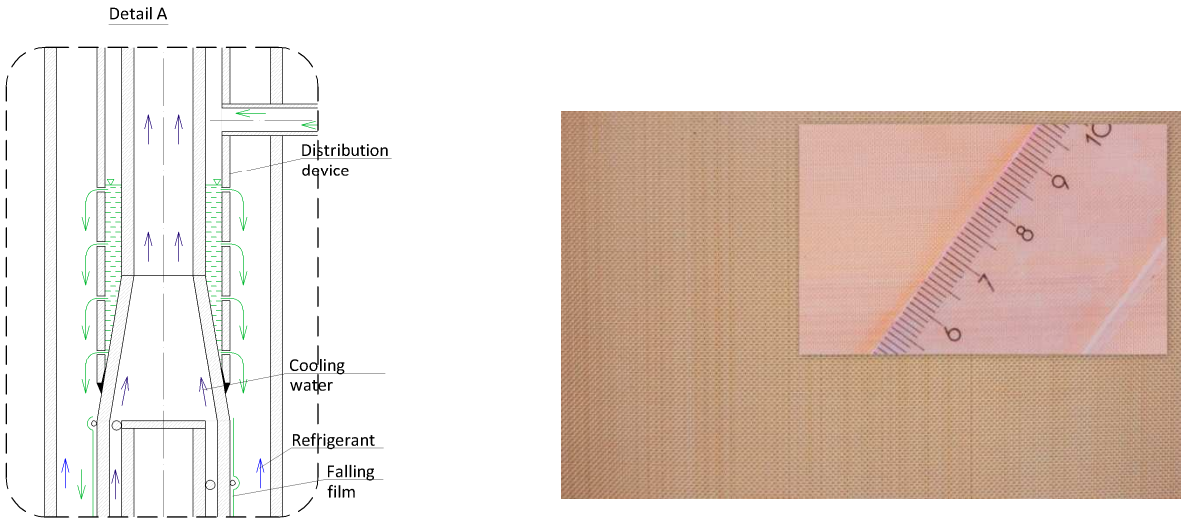

Figure 4-4: Schematic of the poor solution distribution device of the absorber (left), photograph of the installed wire mesh (right)

Table 4-1: Calculated absorber capacities and UA-values

Value	Operation conditions and calculated values			Units
Falling film area	0.191			m^2
Cooling water mass flow rate	220	220	220	$kg \cdot h^{-1}$
Low pressure	4	4	3.5	bar
Cooling water inlet temperature	32	32	23	℃
Cooling water outlet temperature	36.2	37.5	27.8	℃
Poor solution inlet temperature	45	60	57	℃
Rich solution outlet temperature	35	34	25	℃
Average NH_3 mass concentration in the solution in the absorber	47	48	41	wt.-%
Solution mass flow rate	11.3	6.7	4.6	$kg \cdot h^{-1}$
Logarithmic temperature difference	5.3	8.2	9.5	K
Heat transfer coefficient (cooling water)	4383	4444	3957	$W \cdot (m^2 \cdot K)^{-1}$
Heat transfer coefficient (falling film)	851	658	531	$W \cdot (m^2 \cdot K)^{-1}$
Absorber UA-value	**202**	**171**	**143**	$\mathbf{W \cdot K^{-1}}$
Absorber capacity	**1075**	**1405**	**1363**	**W**

4.2 Evaporator

Nowadays two types of evaporators are used in conventional AHP: flooded and falling film evaporators. According to Gonzalez et al. (1992) the use of the falling film evaporators has several advantages in comparison to the flooded ones:

- reduction in the refrigerant charge;
- more uniform U-value along the falling film;
- smaller temperature difference between the refrigerant and tube;
- high heat transfer performance.

The main drawback of the falling film evaporator, is that they require good distributors for the *NH_3 / H_2O* mixture at the inlet to the evaporator. Successful designs for falling film evaporators must, apart from the requirement of permitting good *NH_3 / H_2O* distribution, also address the requirements of providing adequate heat and mass transfer and low pressure drop on both the refrigerant and brine sides.

Within this work, the vertical falling film evaporator has been designed and built. Its construction is similar to the above described absorber construction (see Chapter 4.1) and is shown in Figure 4-5. It consists of three vertical pipes inserted one in another: the external pipe of Ø 48.3 x 3 mm and two internal pipes of Ø 21.3 x 2.0 mm and Ø 10.0 x 2.0 mm.

The brine is introduced at the bottom of the evaporator. It flows through four openings (Ø 4.0 mm) and then upward between two internal pipes and leaves at the top of the evaporator. For an enhancement of the brine-side heat transfer a wire (Ø 2.5 mm) with a slop of 30 mm was installed along the brine flow.

The refrigerant is introduced at the top of the evaporator through the pipe of Ø 10.0 x 2.0 mm. To ensure uniform distribution along the height of the evaporator, the refrigerant flows to the header and then is distributed in parallel through the openings of the distribution device. To perform an adequate wetting of the evaporator surface, a wire (Ø 1.5 mm) with a pitch angle of 35° was welded to the surface of the first inter nal pipe. The gravity-driven *NH_3 / H_2O* solution flows in the falling-film mode counter-flow to the brine. Its evaporation occurs on the surface of the first internal pipe (Ø 21.3 x 2.0 mm) and the heat of evaporation is supplied from the brine.

Five sight glasses were installed along the height of the evaporator to provide optical access to the evaporation process (see Figure 4-5).

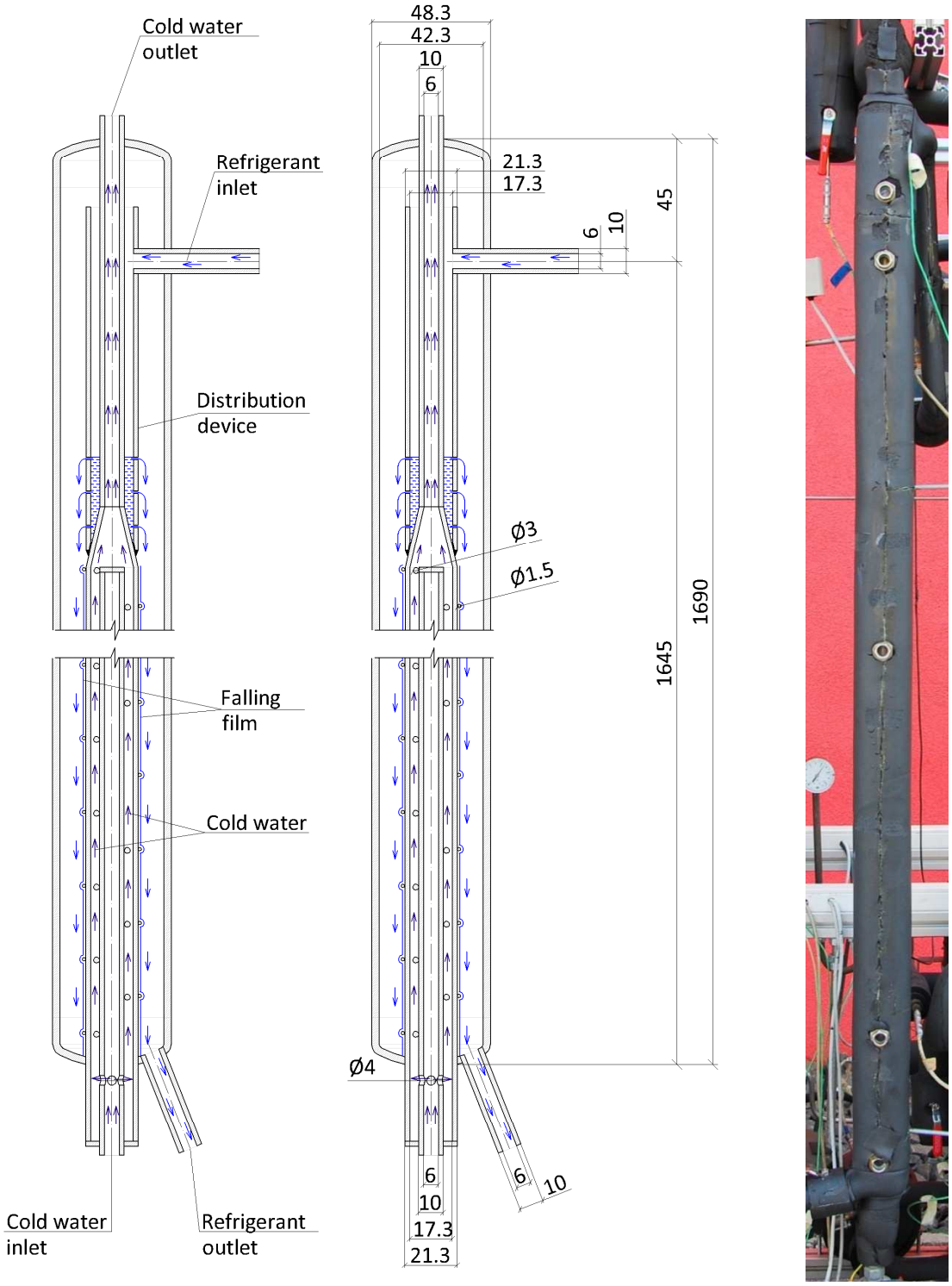

Figure 4-5: Schematic of the falling film evaporator: left – operating principle; center – design details; right – photograph of the installed evaporator

It must be noted that following changes were made to the evaporator construction in order to increase its capacity from approximately 700 W to 1000 W:

- the diameter of the brine side wire was increased from 2.5 mm to 3.0 mm;
- the pitch angle of the brine side wire was decreased from 35° to 20°;
- an additional sight glass was installed in the lower part of the evaporator.

In order to evaluate the evaporator capacity and the UA-values of the evaporator, a heat transfer analysis was conducted. The calculation of the heat transfer on the refrigerant side was made according to the work of Niederhauser und Trepp (1994) (see Eq. 4-2), and that on the brine side according to VDI Waermeatlas (2006).

$$\alpha_{falling\ film\ EVA} = \frac{Nu \cdot \lambda}{\left(\frac{v^2}{g}\right)^{\frac{1}{3}}} \qquad 4\text{-}2$$

The calculation results for typical boundary conditions are shown in Table 4-2. The properties of the refrigerant were calculated using ASPEN Plus. It was assumed, that the NH_3 concentration in the refrigerant vapor is 100% and therefore it evaporates at constant temperature. The logarithmic temperature difference in the evaporator was calculated using refrigerant temperature and cold water inlet and outlet temperatures.

As can be seen, the UA-values of the evaporator range from 99 to 105 $W \cdot K^{-1}$ and the evaporator capacities from 400 to 950 W. The measurement results presented in Chapter 5 show that evaporator capacities as high as 850 W were achieved when operating at a generator capacity of 1300 W, corresponding to a refrigerant mass flow rate of 2.5 $kg \cdot h^{-1}$ to 3.0 $kg \cdot h^{-1}$.

Table 4-2: Calculated evaporator capacities and UA-values

Value	Operation conditions and calculated values			Units
Falling film area	0.100			m^2
Brine mass flow rate	290			$kg \cdot h^{-1}$
Low pressure	3.5	4	4.5	bar
Brine inlet temperature	6.0	6.0	6.0	℃
Brine outlet temperature	2.5	3.5	4.6	℃
Refrigerant temperature	-5.3	-1.8	1.6	℃
Logarithmic temperature difference	9.4	6.5	3.6	K
Refrigerant mass flow rate	3	1.5	1	$kg \cdot h^{-1}$
Heat transfer coefficient (cold water)	1530	1547	1564	$W \cdot (m^2 \cdot K)^{-1}$
Heat transfer coefficient (falling film)	6287	7669	8685	$W \cdot (m^2 \cdot K)^{-1}$
Evaporator UA-value	**99**	**103**	**105**	**$W \cdot K^{-1}$**
Evaporator capacity	**935**	**667**	**382**	**W**

4.3 Rectification column

The rectification column aims to provide the highest possible concentration of NH_3 (approximately 99.9 wt.-%) in the generated vapor. The construction of the rectification column designed for the AHP test rig is shown in Figure 4-6. It consists of the following components: the stripping section, rectification section, dephlegmator and droplet separator. This design of the rectification column was chosen in order to enable two operating modes namely, with and without the stripping section.

When operating with the stripping section, the rich solution is introduced to the rectification column (Ø 48.3 x 2.8 mm) between both sections through the pipe with Ø 10.2 x 2.0 mm. The NH_3 / H_2O vapor generated in the generator is introduced at the bottom of the rectification column (Ø 10.2 x 2.0 mm), flows upward and condenses at the top.

In the stripping section, the rich solution and the NH_3 vapor are in counter-flow to each other, so that the vapor is cooled and a certain part of the H_2O condenses. The condensed H_2O then mixes with the rich solution and flows back to the generator. Both the stripping and rectification sections have a height of 30 cm and are filled with Rashig rings (Ø 6.0 x 0.3 mm, height – 3 mm) placed over the sieve plate (Ø 42.7) (see Figure 4-7). The construction of the sieve plates reduces the cross-section of the column as low as possible, in order to prevent the flooding of the rectification column.

The NH_3 / H_2O vapor leaving the stripping section enters then the rectification section and flows to the dephlegmator, where it is cooled by rejecting the heat to the cooling water. In evaluating the measurement results, it has been shown that the NH_3 mass concentration in the generated vapor ranges from 0.994 to 0.999 when operating with the stripping section (see Chapter 5.2.5). At the outlet from the dephlegmator, the droplet separator (Ø 88.9 x 2.0 mm), which consists of the rolled wire netting (h = 150 mm), is installed. In order to reduce the flow velocity entering the droplet separator and to increase the separation rate, there is a free space of ca. 130 mm in front of the rolled wire netting.

During the operation with the bypassed stripping section of the rectification column, the rich solution enters through the bottom of the column and the NH_3 vapor between both sections.

Note that the previous droplet separator had the following dimensions: Ø 88.9 x 2.0 mm, with a height of 50 cm. The reason for the construction changes was the presence of droplets in the generated vapor.

The number of stages was determined by means of thermodynamic simulations in ASPEN Plus.

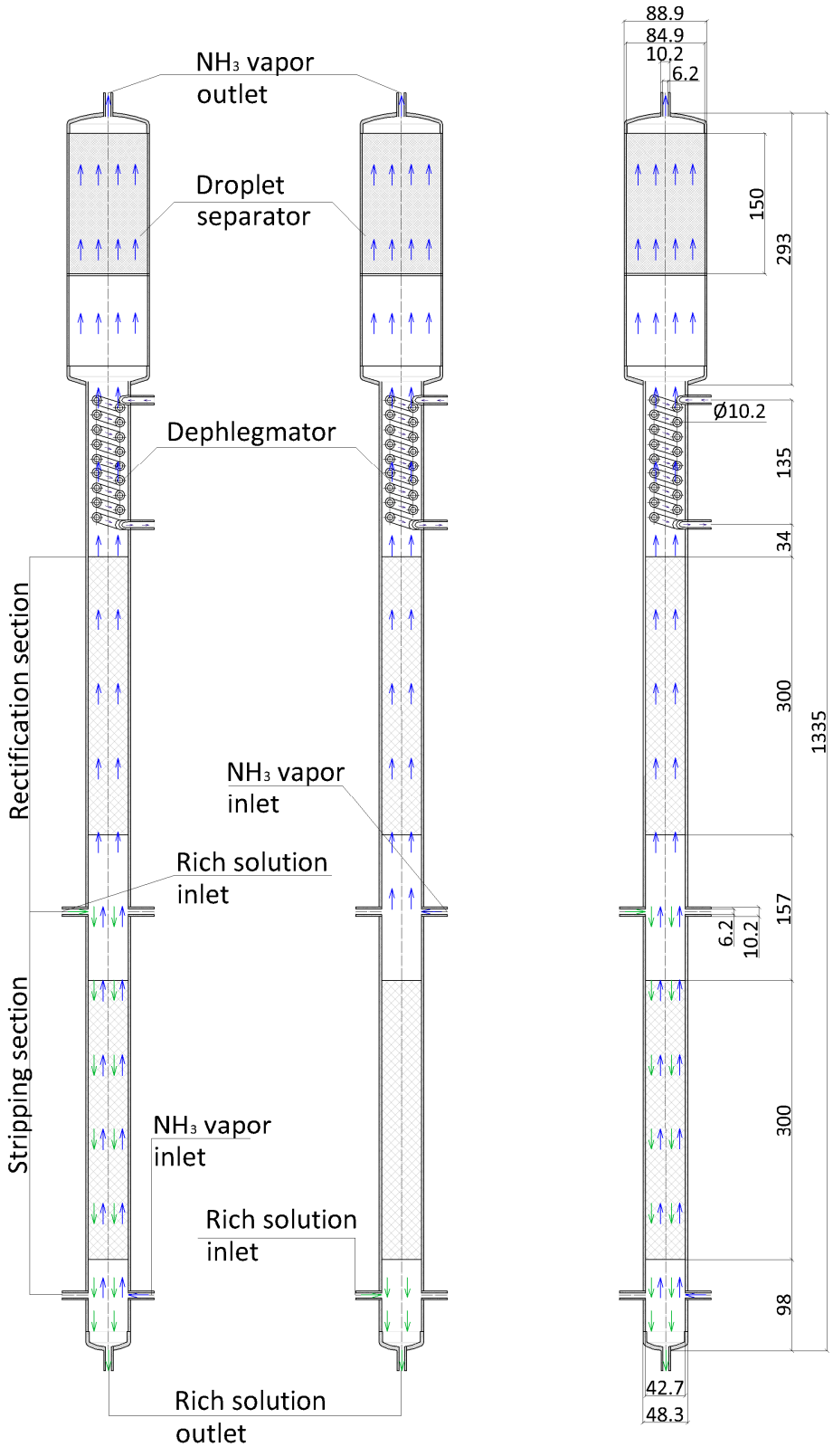

Figure 4-6: Schematic of the rectification column and dephlegmator: left – operation with the stripping section; center – operation without the stripping section; right – construction scheme

Figure 4-7: Rashig rings of the rectification column

The main requirement for the design of the rectification column is to ensure the operation with a comfortable margin of safety with regards to flooding. The calculation model used by Moser (2008) and based on his experimental data with water and air has been used for the prediction of the flooding area. It is based on the calculation of the dimensionless empty tube velocity of the vapor and liquid phase according to Eq. 4-3 and 4-4.

$$j_v^* = j_v \cdot \left(\frac{\rho_v}{(\rho_l - \rho_v) \cdot g \cdot D} \right)^{0.5} \qquad 4\text{-}3$$

$$j_l^* = j_l \cdot \left(\frac{\rho_l}{(\rho_l - \rho_v) \cdot g \cdot D} \right)^{0.5} \qquad 4\text{-}4$$

Where,

j_v , j_l	– empty tube velocity of the vapor (v) and liquid (l) phase, m·s^{-1}
ρ_v , ρ_l	– density of the vapor (v) and liquid (l) phase, kg·m^3
g	– free fall acceleration, m·s^{-2}
D	– hydraulic diameter, m

The empty tube velocity of the vapor and liquid phase in Eq. 4-3 and 4-4 is the ratio of the volumetric flow rate of the vapor (V_v, m^3·s^{-1}) or liquid (V_l, m^3·s^{-1}) phase to the area of the section (A_{REC}, m^2) of the rectification column:

$$j_v = \frac{V_v}{A_{REC}} \qquad 4\text{-}5$$

$$j_l = \frac{V_l}{A_{REC}} \qquad 4\text{-}6$$

The calculation results are shown in Figure 4-8. On the X-axis the square root of the empty tube velocity of the liquid phase is shown while on the Y-axis the square root of the empty tube velocity of the gas phase is visible. The expected hydraulic boundary conditions in the rectification column were calculated for the stripping section, rectification section and for the rectification section with total condensation.

All required properties of the *NH_3 / H_2O* solution and *NH_3* vapor, as well as mass flows, have been taken from the thermodynamic simulations made in ASPEN Plus. As one can see in Figure 4-8 the calculated hydraulic boundary conditions are within the operational area.

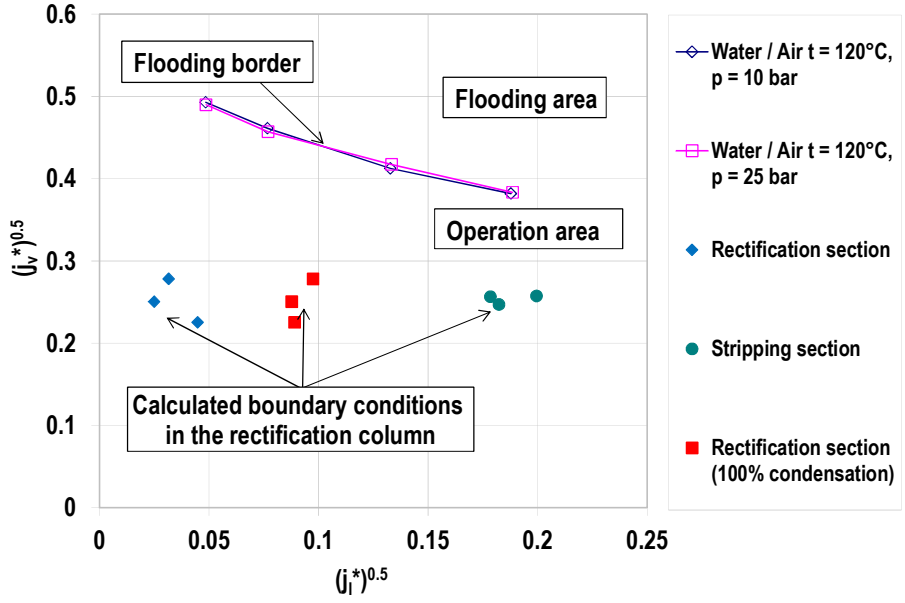

Figure 4-8: Comparison of the calculated flooding border with the expected hydraulic conditions in the rectification column

4.4 Other components and infrastructure

Apart from the above described absorber, evaporator and rectification column the AHP test rig consists of the following components: condenser (CON), generator (GEN), solution heat exchanger (SHX), solution pump (PUMP), refrigerant accumulator (RAC), solution accumulator (SAC), refrigerant throttle valve (RTH), solution throttle valve (STH) (see Figure 4-1). The operating principle of these components and of the external loops will be described below.

Condenser (CON)

The condensation of the NH_3-vapor coming from the rectification column occurs in the condenser (CON) by rejecting heat to the cooling water loop. In order to reduce the heat losses and therefore possible condensation of the NH_3-vapor in pipes, the condenser is installed directly above the rectification column. It is a plate heat exchanger of the type Alfa Nova 14-20H (“Alfa Laval”). The NH_3-vapor enters the condenser in the upper part, condenses there and flows to the evaporator from the lower part. The cooling water flows in counter flow to the refrigerant.

Generator (GEN)

In the generator (GEN), the NH_3-vapor is generated by supplying heat from the hot water loop to the rich solution. The rich solution and the hot water are in counter flow to each other. Thereby the two-phase mixture consisting of the poor solution and NH_3-vapor exits the generator. The two phases are separated from each other in the solution accumulator (SAC). The poor solution flows back to the absorber, and the NH_3-vapor to the rectification column. The generator is a plate heat exchanger of the type Alfa Nova 14-28H (“Alfa Laval”).

Solution heat exchanger (SHX)

In the solution heat exchanger (SHX), the poor solution is cooled by rejecting heat to the rich solution. The solution heat exchanger is a counter-flow plate heat exchanger, as well as the generator, of the type Alfa Nova 14-28H (“Alfa Laval”).

In order to analyze the influence of the SHX on the process efficiency and influence of use of *NaOH* on its operation, two bypasses, as is shown in Figure 4-1 were installed, in order to allow the operation to be conducted with or without the SHX.

Solution pump (PUMP)

The solution pump (PUMP) aims to increase the pressure of the rich solution from the low to the high pressure level. For the test rig, the plunger-membrane solution pump has been chosen (see Figure 4-9). The pressure on the oil side is built-up by means of a reciprocating motion of the plunger. It leads to the sucking and pumping of the rich solution to the chamber, which is separated from the oil side by means of a membrane.

The membrane is a PTFE-disc with a thickness of 0.5 mm, which separates the oil from the rich solution and acts as a seal. The main advantage of the plunger-membrane solution pump is that the plunger part of the pump does not come in contact with the NH_3 / H_2O solution, the pump operation is leak-free and possible contaminations from oil can be avoided.

The flow rate is regulated by means of the electronic frequency converter (ABB IP20, 0-500 Hz), which allows flow rate regulation independent of the pressure ratio.

For the pump operation the minimum pressure of 3 bar on the oil side is necessary. This means that the operation of the test rig is possible at evaporator temperatures higher than -9℃.

The test on the AHP test rig showed that for the considered PTFE membrane, the bolts of the flange have to be torqued with 35 Nm. If the torque is lower, the solution pump becomes loose; if higher, damage to the membrane can be expected (see Figure 4-10).

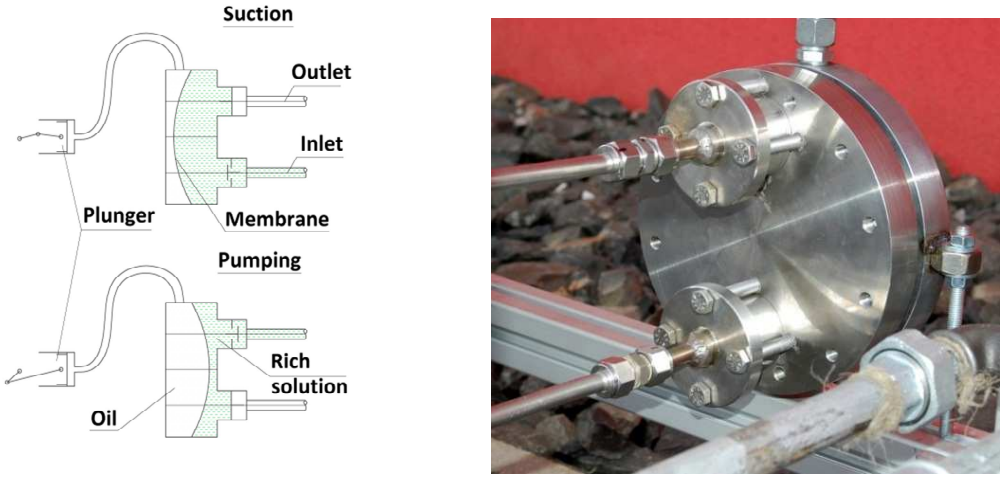

Figure 4-9: Plunger-membrane solution pump: left – operating principle; right – pump installed in the AHP test rig

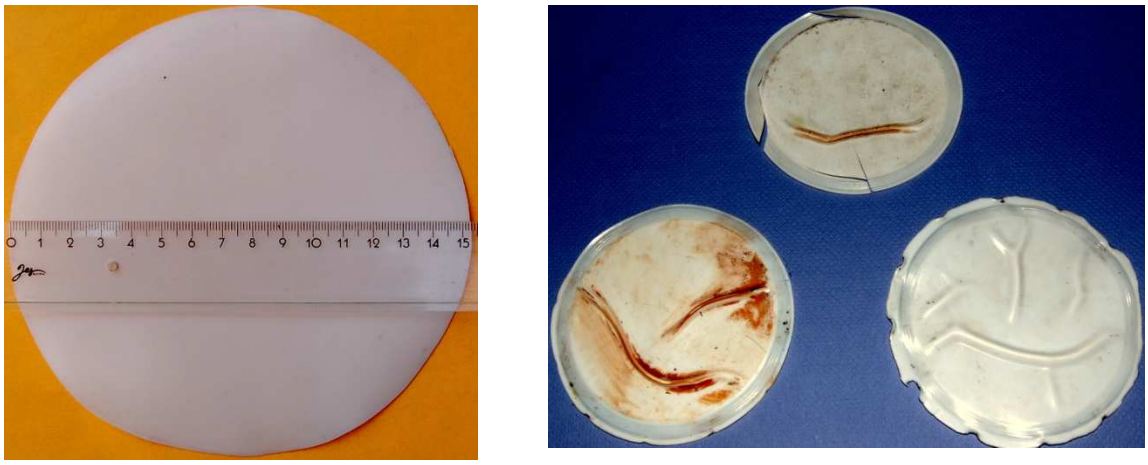

Figure 4-10: PTFE-membrane of the solution pump: left – before installation; right – damaged membranes

Refrigerant (RAC) and solution (SAC) accumulators

The refrigerant (RAC) and solution (SAC) accumulators are shown in Figure 4-11. The refrigerant accumulator is situated between the refrigerant throttle valve and condenser. This means that the NH_3-liquid coming from the condenser is sub-cooled in the refrigerant accumulator.

The solution accumulator is situated between the generator and rectification column. The two-phase mixture coming from the generator enters the solution accumulator in the upper part and is separated into NH_3-vapor and poor solution. The NH_3-vapor flows back to the rectification column and the poor solution to the absorber. The installed refrigerant and solution accumulators have a volume of 1.5 l and for temperature measurement thermometer pockets with PT100 are used.

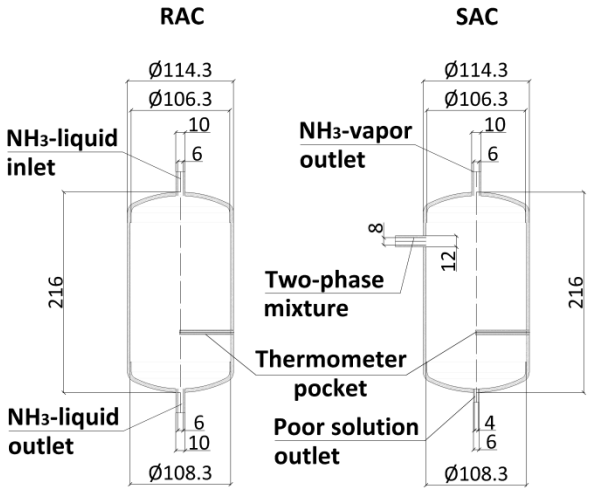

Figure 4-11: Schematic diagram of the refrigerant accumulator (left) and solution accumulator (right)

Refrigerant (RTH) and solution (STH) throttle valves

The refrigerant throttle valve regulates the mass flow of the NH_3-liquid coming from the refrigerant accumulator, as well as the temperature difference of the NH_3 between the inlet and outlet of the evaporator. For the AHP test rig, the electronic expansion valve type AKVA 10-1 (“Danfoss”) was installed. Valve regulation occurs by means of pulse-width modulation with in intervals of 6 sec. The valve regulation area lies between 5-100%.

For the AHP test rig, the smallest electronic expansion valve suitable for NH_3 applications has been used. However, its K_V-value is too high and, therefore, a manual throttle valve Type SS-1RS6MM (“Swagelok”) has been installed in series after the electronic expansion valve (see Figure 4-12).

The solution throttle valve is installed between the solution heat exchanger and absorber and reduces the poor solution pressure to the low pressure level. The solution throttle valve, SS-31RS6MM (“Swagelok”) has been used.

Rich solution accumulator with position sensor

In front of the solution pump, a rich solution accumulator (RSAC) with position sensor (PS; Temposonics G-Series) was installed. The position sensor measures the level of the solution in the accumulator; the measured value is used afterwards for the regulation of the speed of the solution pump (see Chapter 4.5).

Heat sources and heat sink

For the operation of the AHP test rig, the following external loops have been used: a hot water loop, a cooling water loop and a brine loop.

The hot water loop aims to supply heat at a high temperature (ca. 80-130℃) to the generator. The schematic diagram of the hot water loop is shown in Figure 4-12. The heating medium is distilled water, which is heated via an electric heating element with a heat capacity of up to 3500 W. The water circulation occurs by means of the circulation pump. The water mass flow is regulated by means of a regulation valve and measured by means of the coriolis mass flow meter (“Micro-Motion”). Additionally an expansion tank was installed in the loop.

To ensure heat rejection from the absorber, condenser and the dephlegmator, the central cooling water system of the institute has been used. To regulate the flow of this cool water, a regulating valve has been installed. The volume flow was measured by means of a magnetic inductive flow meter (“ABB”).

As the heat source for the evaporator the “mobile” heat source of the institute has been used. As a heat carrier a mixture of Glysantin and water (43 Vol.-% / 57 Vol.-%) was used. The required brine flow has been regulated by means of a control valve and measured by means of a magnetic inductive flow meter (“ABB”).

4.5 Control concept

In this chapter the control concept of the AHP test rig will be discussed. First, installed measurement equipment will be described. Afterwards experimental uncertainties will be discussed. Finally, control of different process parameters will be analyzed.

4.5.1 Installed measurement equipment

In order to measure all necessary state variables of the AHP test rig different measurement devices have been installed. The schematic diagram of the installed equipment is shown in

Figure 4-12. Further, when analyzing the experimental results (see Chapter 5), the abbreviations shown in Figure 4-12 will be used.

Temperature measurement

The temperature measurement within the AHP test rig has been made by means of thermocouples and platinum resistance thermometers Pt100.

The thermocouples were used for the measurement of the process temperatures of the AHP test rig and were installed on the pipes outer side. In order to provide better thermal conductivity for the thermocouples a heat transfer paste was used and they were fixed to the pipe surface using 1-mm wire. This leads to certain experimental uncertainties because of the difference of the measured temperature and temperature of the fluid in the pipe. In further calculations (see Chapter 5) these experimental uncertainties have not been taken into account.

The platinum resistance thermometers Pt100 were used for the measurement of the external temperatures (hot water, cooling water and brine) as well as for measuring the temperatures in the solution and refrigerant accumulators. They were installed directly inside of the pipes of external loops using thermometer pockets in the solution and refrigerant accumulators.

Pressure measurement

For the pressure measurement, three pressure transmitters “Alphaline” of the company “Rosemount” were installed. Two of them are absolute pressure transmitters and were used for measuring the high (PT_HP) and low (PT_LP) pressures. They were installed between the position sensor (PS) and electric conductivity sensor and between the refrigerant throttle valve (RTH) and refrigerant accumulator (RAC) (see Figure 4-12). The third one is a differential pressure transmitter which was used for measuring the pressure difference before the solution throttle valve. It was thought to use the measured pressure difference for the calculation of the poor solution flow rate. However, in the first experiments it was shown that the relative measurement errors were very high.

Additionally, a pressure switcher (PS_HP, “Danfoss”) was installed in order to shut down the AHP test rig, should the high pressure exceed 25 bar.

Mass and volume flow rate measurement

For the flow rate measurement in the external loops, three flow meters were used. For the flow rate measurement of the cooling water and brine two magnetic inductive flow meters from the company “ABB” were installed. The mass flow of the hot water has been measured by means of the coriolis mass flow meter from the company “Schwing”.

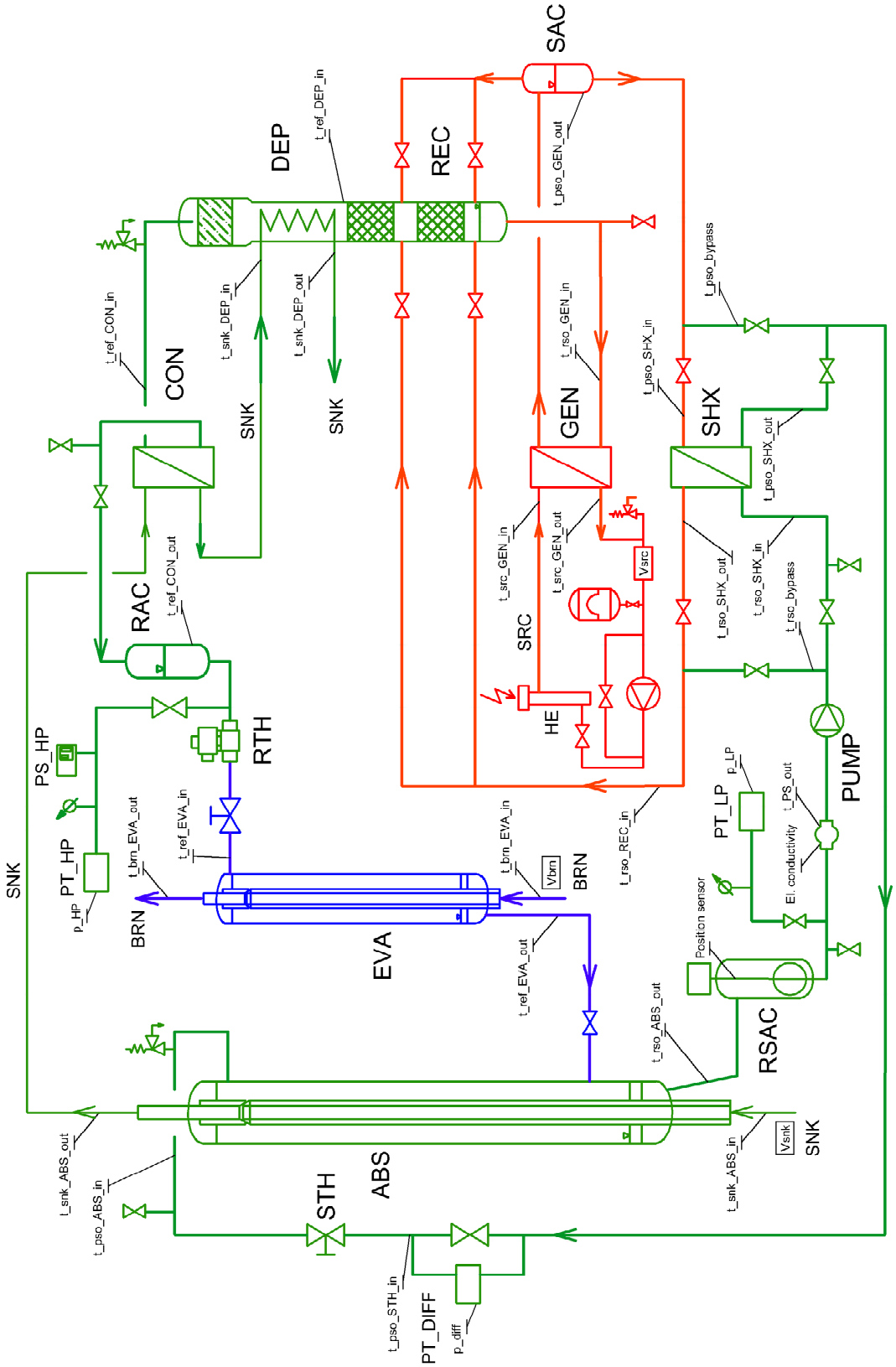

Figure 4-12: Schematic diagram of the installed measurement devices

4.5.2 Experimental errors

The experimental errors of heat / cold capacities and COPs depend both on temperatures, volume and mass flows, pressures measurements and on the calculated properties of water and the brine medium. In order to decrease the experimental errors all measurement devices were calibrated. For the calculation of experimental errors the normal (or Gaussian) distribution law has been used (see Eq. 4-7). The experimental errors of the measurement devices are shown in Table 4-3 and the properties calculation errors are shown in Table 4-4.

$$u(y) = \sqrt{\sum_{i=1}^{m} \left(\frac{\delta f}{\delta x_i}\right)^2 u^2(x_i)} \qquad 4\text{-}7$$

Table 4-3: Experimental errors

Measurement value	**Measurement device**	**Error**
External temperatures (heat source, heat sink, brine)	PT100	±0.05 K
External temperatures (absorption process)	thermocouple	±0.21 K
Mass flow of hot water	coriolis mass flow meter (Schwing)	±0.6 %
Volume flow of cooling water	magnetic inductive flow meter (ABB)	±0.5 %
Volume flow of brine	magnetic inductive flow meter (ABB)	±0.9 %
Pressure	“Alphaline” (Rosemount)	±36 mbar

Table 4-4: Properties calculation errors

Calculated property	**Error**
Cooling water density	±0.31 $kg \cdot m^{-3}$
Brine density	±2 $kg \cdot m^{-3}$
Cooling water enthalpy	±0.1 $kJ \cdot kg^{-1}$
Brine enthalpy	±0.4 $kJ \cdot kg^{-1}$
Hot water specific heat capacity	±0.02 $kJ \cdot kg^{-1} \cdot K^{-1}$

4.5.3 Process control

In the following the process regulation will be explained; the given and regulated values and the data processing will be described.

Given process values

When using a conventional AHP in a real application, the cooling water and brine temperatures are defined according to the application area. That is why these values were considered as given process values.

The temperature level in the evaporator and thereby the low pressure level depend on the given brine temperature. The high pressure level is set by the *NH_3* saturation temperature, which depends on the cooling water temperature. Furthermore, by setting the cooling and cold water temperature, the amount of the *NH_3* absorbed by the poor solution and, therefore the *NH_3* concentration of the rich solution, are fixed. Figure 2-1 shows that the *NH_3* concentration of the rich solution decreases with an increase in cooling water and decreasing brine temperatures.

Regulated process values

The regulated process values of the AHP test rig are the hot water inlet temperature, refrigerant throttle valve opening and solution throttle valve opening together with the solution pump capacity. The correlation of these values can be described by the following equations:

$$\dot{m}_{RSO} = \dot{m}_{PSO} + \dot{m}_{REF} \qquad 4\text{-}8$$

$$\dot{m}_{RSO} \cdot \xi_{RSO} = \dot{m}_{PSO} \cdot \xi_{PSO} + \dot{m}_{REF} \cdot \xi_{REF} \qquad 4\text{-}9$$

The hot water inlet temperature can be chosen manually; it defines the internal temperature in the generator and therefore the *NH_3* concentration of the poor solution, when the high pressure level is defined by the cooling water temperature. Also the *NH_3* concentration in the generated vapor depends on the generator temperature. It is necessary to mention that the cooling water temperature cannot be changed manually, because the absorber, condenser and dephlegmator are connected to the cooling water loop in series. So, the purity of the generated vapor depends only on the generator temperature and operating mode of the rectification column (with or without stripping section).

The refrigerant throttle valve regulates the refrigerant flow rate in the evaporator and therefore the temperature difference in the evaporator. If the temperature difference between $t_{REF\_EVA\_IN}$ and $t_{REF\_EVA\_OUT}$ is too high, the throttle valve opening time increases, and if too low it decreases.

When all above mentioned values are defined, the generator heat capacity can be regulated only by means of the solution pump and solution throttle valve. The solution throttle valve opening is set manually so that the level of the solution in the rich solution accumulator remains constant at the set generator heat capacity. The solution pump capacity is regulated by comparing the measured value of the level of the solution with its set value. If the measured level is too low, the frequency inverter reduces the pump capacity; if it is too high, the frequency inverter increases the speed of the pump.

Data acquisition and processing

The data acquisition was carried out by means of 3 IMPs (isolated measurement pod) of the type 35951J from the company “Solartron”. The regulation of the above described regulated process values and the heating element was conducted by an additional IMP of the type 35951D. The data gathered by IMPs are sent to a PC by means of the software program LabView and copied to a text-file with the measurement period of 2 sec. During the experiments the measured data can be visualized in various diagrams.

The AHP test rig is controlled through the window of LabView shown in Figure 4-13. All measured data is performed on the schematic diagram of the AHP test rig. In the upper part of Figure 4-13 two main switches can be seen. The “Hot water”-switch is used for turning on / off the circulation pump of the hot water loop and the “PUMP”-switch is used for the solution pump.

In the lower part of Figure 4-13, four regulation windows are shown. The first one is used for regulation of the brine water temperature if higher temperatures are necessary. The second one is responsible for the solution pump regulation by regulation of the electronic frequency converter. The third one regulates the generator heating capacity in order to keep constant a certain hot water inlet temperature. The fourth one is used for the refrigerant throttle valve opening regulation according to the required temperature difference in the evaporator.

For safety reasons, there is an alarm window over the fourth regulation window in which four alarm conditions can be defined: high pressure alarm, low pressure alarm, hot water inlet temperature alarm and refrigerant inlet temperature in the evaporator alarm.

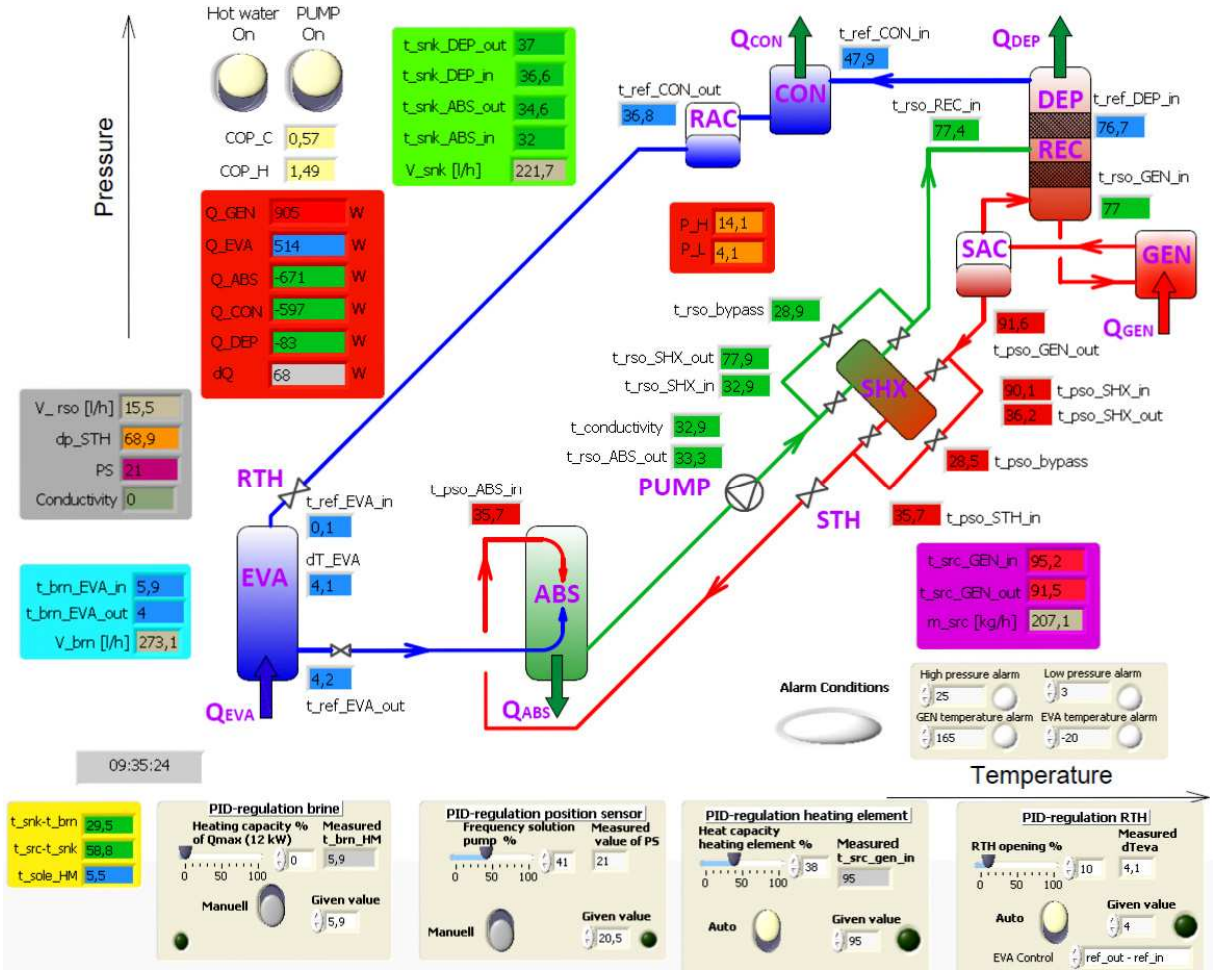

Figure 4-13: Regulation program of the AHP test rig

5 NH_3 / H_2O / NAOH TEST RESULTS AND ANALYSIS

The experimental investigations of the *NH_3 / H_2O / NaOH* AHP test rig will be analyzed within this chapter. The measured COP_C of the AHP test rig at different boundary conditions will be reported. All measurements were carried out with the *NH_3 / H_2O* mixture with 0, 5 and 10 wt.-% of *NaOH*.

To analyze the test results, the developed thermodynamic model in ASPEN Plus will be described as well as the simulation results in regard to the influence of *NaOH* on the absorption and desorption of *NH_3*. Finally, the outlook concerning the use of *NaOH* as an additive to the working mixture *NH_3 / H_2O* in the AHP-process and further work required will be given.

5.1 Test results

Before bringing the AHP test rig into operation, leak/tightness testing using nitrogen was carried out. Afterwards, the test rig was vacuumed to a pressure of 0.02 bar by means of the vacuum pump CSK DB.2 and charged with the *NH_3 / H_2O* working mixture. The quantity of the working mixture charge (3.2 kg) and the *NH_3* concentration (65 wt.-%) were calculated to provide the proper functioning of the AHP test rig over the range of conditions tested.

After the tests with the working mixture *NH_3 / H_2O* were accomplished, the AHP test rig was vacuumed again to charge it with the ternary working mixture *NH_3 / H_2O / NaOH* with a charge quantity of 3.2 kg and an *NH_3* concentration of 60 wt.-%. Depending on the tests carried out, the working mixture had a *NaOH* mass concentration of 5.3 wt.-% or 9.9 wt.-%.

It should to be noted that 5.3 wt.-% *NaOH* was the *NaOH* mass concentration in the working mixture when filling the AHP test rig. During operations, there was a slightly higher *NaOH* mass concentration in the rich solution (closer to 6%), owing to a certain amount of *NH_3* accumulating in the refrigerant accumulator. Furthermore, the *NaOH* mass concentration in the poor solution at the outlet from the generator is higher than in the rich solution and increases with the generator temperature.

All tests with and without *NaOH* were carried out at the following flow rates of the external loops:

- hot water mass flow rate ($\dot{m}_{SRC}$): 200 kg·h^{-1};
- cooling water volume flow rate ($\dot{V}_{SNK}$): 220 l·h^{-1};
- brine volume flow rate ($\dot{V}_{SNK}$): 270 l·h^{-1}.

In order to conduct a measurement at certain boundary conditions a steady-state operation of the AHP test rig has to be provided by following the next steps:

1. the hot water circulation pump and the heating element have to be turned on;
2. the heating element has to be heated up to a set hot water inlet temperature;
3. depending on the temperature lift (difference between the cooling water and brine inlet temperatures) the generation of the refrigerant vapor starts at a certain generator temperature. As soon as this happens the level of the rich solution in RSAC decreases and certain amounts of the refrigerant and poor solution will be accumulated in RAC and SAC. In order to keep the rich solution level in RSAC constant, the regulation of the solution pump capacity must be turned on.
4. the required generator capacity has to be manually set by changing the poor solution flow rate using STH;
5. the automatic regulation of the temperature difference between the refrigerant inlet and outlet from the evaporator using RTH must be turned on;
6. as soon as the steady state operation is provided a measurement can be taken. Figure 5-1 shows an example of the steady state operation with the working mixture *NH_3 / H_2O* without *NaOH* at t_{SRC_IN} / t_{SNK_IN} / t_{BRN_IN} = 90 / 32 / 6℃, with SHX and the stripping section of the rectification column. The steady state operation time for every measurement was 20 min.

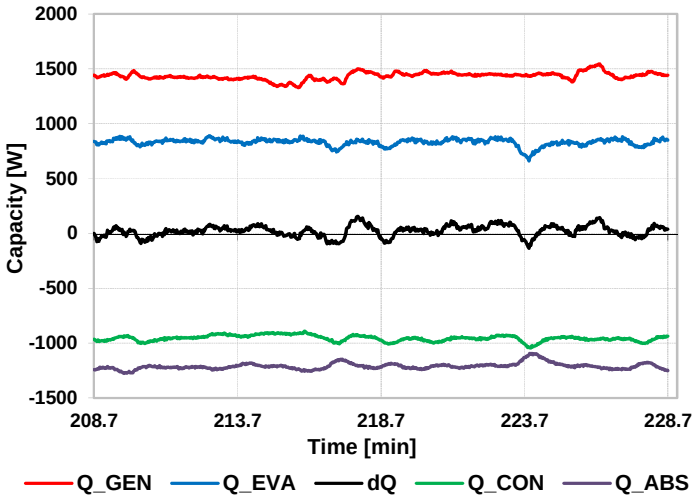

Figure 5-1: Example of the steady state operation of the AHP test rig (at t_{SRC_IN} / t_{SNK_IN} / t_{BRN_IN} = 90 / 32 / 6℃; with SHX and NH_3 / H_2O working mixture without additive)

The temperature difference between the refrigerant inlet and outlet from the evaporator was set equal to 5 K. During the operation, this temperature difference ranged between 1 K and 8 K. This occurred because the electronic expansion valve type AKVA 10-1 (“Danfoss”) used has a pulse-width modulation and thus the refrigerant flow rate was not constant. However,

the average value of the refrigerant temperature difference in the evaporator over the period of time chosen (20 min.) varied from 4 K to 6 K.

The minimal and maximal generator temperatures were limited due to a decrease in the absorber efficiency and due to a low solution flow rate and difficult regulation of the generator capacity.

The AHP test rig was operated at boundary conditions listed in Table 5-1. As was already mentioned in Chapter 4.4, for operating the solution pump, a minimum pressure of 3 bar on the oil side is necessary. In order to provide a low pressure higher than 3 bar during the operation, the brine inlet temperature was set to 6℃.

Table 5-1: Boundary conditions for tests on the AHP test rig

No.	Solution heat exchanger	Stripping section	Generator capacity, $\dot{Q}_{GEN}$ [W]	Hot water inlet temperature, t_{SRC_IN} [℃]	Cooling water inlet temperature, t_{SNK_IN} [℃]	Brine inlet temperature, t_{BRN_IN} [℃]
1	With	With	900 - 1300	105	32	6
2	With	With	1300	83 – 130 100 - 130	23 32	
3	With	With	900	95 – 130	32	
4	With	Bypassed	1300	100 – 130	32	
5	With	Bypassed	900	87 – 105	32	
6	Bypassed	With	1300	83 – 120 95 – 130	23 32	

5.1.1 Operation experience with the AHP test rig

Generally, concerning the operation experience with the AHP test rig, it is necessary to mention that long-term operation with the working mixture *NH_3 / H_2O* and 5 wt.-% *NaOH* could not be realized. Circa one week after the operation began, traces of *NaOH* crystals had been observed in the evaporator and the working mixture was deemed ripe for change.

The tests with the working mixture *NH_3 / H_2O* and 10 wt.-% *NaOH* could not be carried out, owing to *NaOH* crystals which had blocked the lower part of the evaporator and the pipe between the absorber and evaporator (see Figure 5-2). This crystallization issue was caused by high *NH_3* and *NaOH* concentrations and the immiscibility of the *NH_3 / NaOH* mixture.

Figure 5-2: Photograph of a sight glass in the lower part of the evaporator without (left) and with NaOH crystals (right)

5.1.2 Operation at different generator capacities

In order to analyze the influence of the generator capacity on the COP_C of the AHP test rig the measurements with the working mixture *NH_3 / H_2O* with and without 5 wt.-% *NaOH* were carried out at the following boundary conditions:

- hot water / cooling water / brine inlet temperatures (t_{SRC_IN} / t_{SNK_IN} / t_{BRN_IN}) of 105 / 32 / 6°C;
- generator capacities ($\dot{Q}_{GEN}$) ranging from 900 to 1300 W;
- with solution heat exchanger;
- with stripping section.

The measured COP_C relating to the generator capacity are shown in Figure 5-3. As can be seen, the COP_C ranges from 0.50 to 0.57, has a maximum at a generator capacity of approximately 1100 W and decreases at low and high generator capacities. The measured COP_C of the operations without *NaOH* are somewhat higher than with 5 wt.-% *NaOH* at a generator capacity of $\dot{Q}_{GEN}$ = 1300 W and approximately equal at $\dot{Q}_{GEN}$ = 900 W.

The COP_C decreases at low generator capacities due to the increasing impact of the heat losses, as their ratio to the generator capacity increases with decreasing generator capacity. At high generator capacities a decrease in the COP_C might be caused mainly by an increase in the solution flow rate. As will be shown in Chapter 5.2.3 the absorber efficiency decreases, when operating at high solution flow rates, due to the poor wettability and insufficient mass transfer area.

However, operating the AHP test rig at $\dot{Q}_{GEN}$ = 1300 W is favorable, due to low experimental errors and easier process control (solution flow rate). For instance, the experimental error of the COP_C at $\dot{Q}_{GEN}$ = 900 W is about 4.8% while at $\dot{Q}_{GEN}$ = 1300 W this is only about 3.7%. Such experimental data with low experimental errors is useful for the analysis by means of thermodynamic simulations in ASPEN Plus.

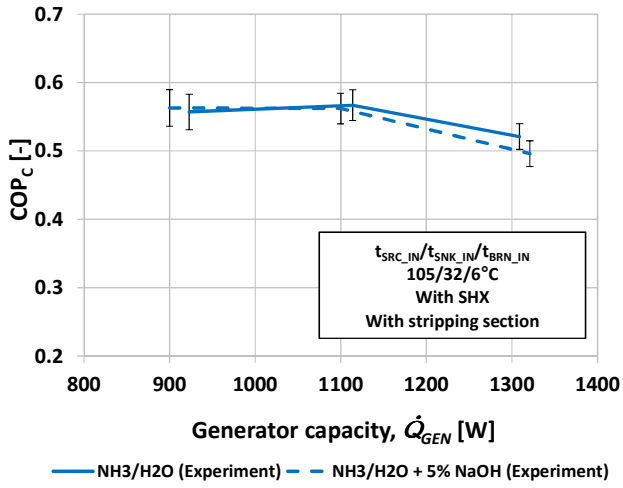

Figure 5-3: Measured cooling COP of the AHP test rig at t_{SRC_IN} / t_{SNK_IN} / t_{BRN_IN} = 105 / 32 / 6℃ and $\dot{Q}_{GEN}$ = 900 - 1300 W (with solution heat exchanger and stripping section)

5.1.3 Operation with and without solution heat exchanger

Figure 5-4a shows the COP_C depending on the hot water inlet temperature (t_{SRC_IN}) at cooling water / brine inlet temperatures (t_{SNK_IN} / t_{BRN_IN}) of 23 / 6 and 32 / 6℃ and a generator capacity of 1300 W. The test results with the working mixture *NH_3 / H_2O* without *NaOH* are shown as solid lines and those with 5 wt.-% *NaOH* as dashed lines.

The measured COP_C at the low temperature lift (23 / 6℃) varies from 0.53 to 0.60 when operating without *NaOH* and from 0.56 to 0.61 with 5 wt.-% *NaOH*. It can be seen, that there is a decrease in the COP_C at low and high generator temperatures. It achieves a maximum of 0.60 at t_{SRC_IN} = 100-120℃ when operating without *NaOH,* and of 0.61 at t_{SRC_IN} = 88-120℃ when operating with 5 wt.-% *NaOH*.

A decrease in the COP_C at low generator temperatures is caused by an increase in the solution flow rate and therefore a decrease in the absorption efficiency. A decrease in the COP_C at high generator temperatures is caused mainly by high heat losses of the generator and solution heat exchanger.

When increasing the cooling water inlet temperature up to 32℃ a decrease in the COP_C of 5 - 9% was recorded when adding 5 wt.-% *NaOH* to the working mixture (see Figure 5-4a). The main reason for this is a decrease in the absorber efficiency, which will be analyzed in detail in Chapter 5.2.3.

In order to reduce the solution flow rate and to evaluate its influence on the COP_C, the generator capacity was reduced to 900 W. The test results at cooling water / brine inlet temperatures (t_{SNK_IN} / t_{BRN_IN}) of 32 / 6℃ are presented in Figure 5-4b. These results show that the change in the COP_C when using the working mixture with and without 5 wt.-% *NaOH*

is within experimental error and therefore can be neglected. When comparing the experimental results presented in Figure 5-4a with those in Figure 5-4b, it can be seen, that there is no decrease in the measured COP_C when adding *NaOH* and the COP_C are approximately the same at $\dot{Q}_{GEN}$ = 900 W for both operating modes.

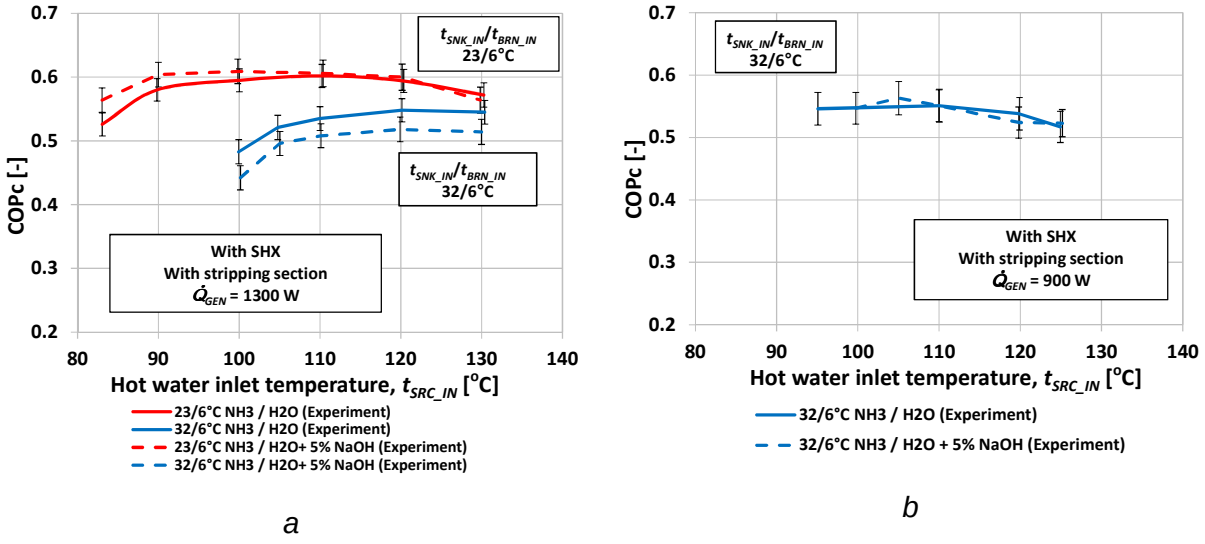

a *b*

Figure 5-4: Measured COP_C of the AHP test rig operated with solution heat exchanger and stripping section: a – at t_{SNK_IN} / t_{BRN_IN} = 23 / 6 and 32 / 6℃, $\dot{Q}_{GEN}$ =1300 W; b – at t_{SNK_IN} / t_{BRN_IN} = 32 / 6℃, $\dot{Q}_{GEN}$ =900 W

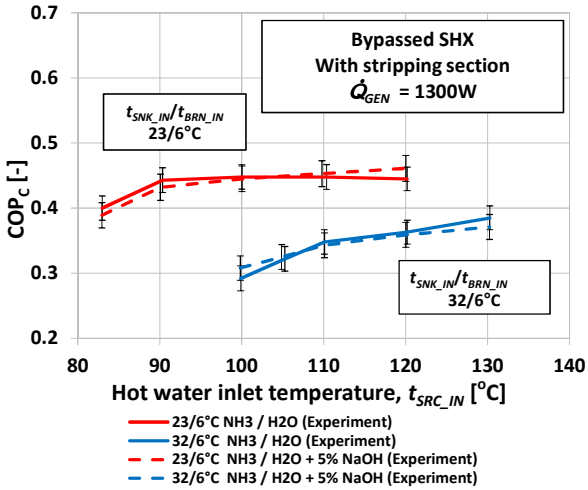

Figure 5-5: Measured COP_C of the AHP test rig operated with bypassed solution heat exchanger and with stripping section at t_{SNK_IN} / t_{BRN_IN} = 23 / 6 and 32 / 6℃, $\dot{Q}_{GEN}$ =1300 W

As the analysis of the influence of *NaOH* on the components of the AHP test rig by means of thermodynamic simulations using ASPEN Plus was found to be easier when operating with bypassed solution heat exchanger, the tests with the bypassed SHX were carried out (see Figure 5-5). In regard to the influence of *NaOH* on the COP_C, its values are similar at the

operation with and without 5 wt.-% *NaOH*. Finally, it has to be mentioned that when comparing the results presented in Figure 5-4 with those in Figure 5-5, a decrease in the COP_C of approximately 25% can be seen when the solution heat exchanger is bypassed.

5.1.4 Operation with and without stripping section

For the analysis of the influence of the stripping section on the COP_C the tests with a bypassed stripping section were carried out. Figure 5-6 shows the test results at a generator capacity of 1300 W. As expected, there is a large decrease in the COP_C at high hot water inlet temperatures when the stripping section is bypassed. The NH_3-concentration in the vapor at the outlet from the rectification column decreases with the increasing generator temperature and therefore less NH_3 / H_2O mixture can be evaporated in the evaporator. This results in a decrease of the evaporator capacity and of the COP_C.

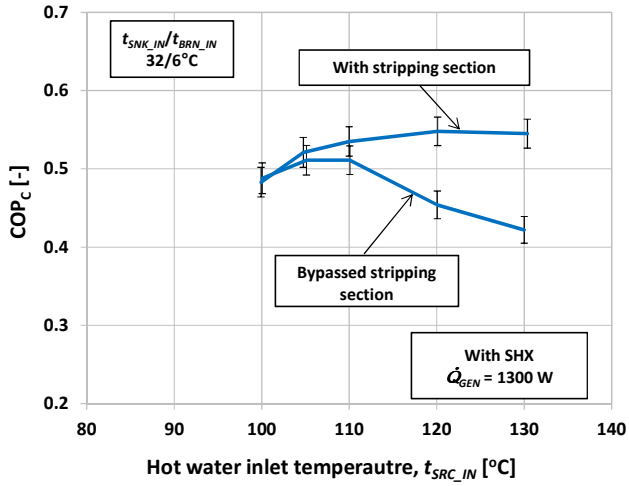

Figure 5-6: Measured COP_C of the AHP test rig operated with and without stripping section at t_{SNK_IN} / t_{BRN_IN} = 32 / 6℃, $\dot{Q}_{GEN}$ =1300 W

A decrease in the NH_3-concentration in the generated vapor can be also seen when comparing the absorber, condenser, evaporator and dephlegmator capacities (see Figure 5-7). There is almost no change in the condenser capacity for both operating modes. Meanwhile, there is a decrease in the evaporator capacity at high hot water inlet temperatures when the stripping section is bypassed. The non-evaporated part of the NH_3 / H_2O mixture is not absorbed by the poor solution. Therefore, a decrease in the absorber capacities also decreases (Figure 5-7). Furthermore, it is necessary to reject more heat from the dephlegmator in order to condense H_2O present in the generated vapor. This increase in the dephlegmator capacity is roughly linear with the increasing hot water inlet temperature and is also disadvantageous for the process performance.

It is necessary to note, that all measurements were carried out at the constant temperature glide in the evaporator (5 K). When increasing this temperature glide while operating with the bypassed stripping section, an increase in the evaporator capacity could be expected. However, this would lead to a decrease in the low pressure level and therefore could cause an increase in the generator and absorber capacities, due to lower NH_3 concentrations in the rich solution. Generally, one can say that even when optimizing the temperature glide in the evaporator while operating with the bypassed stripping section, there will still be a decrease in the COP_C; however, this could be shifted to the higher generator temperatures.

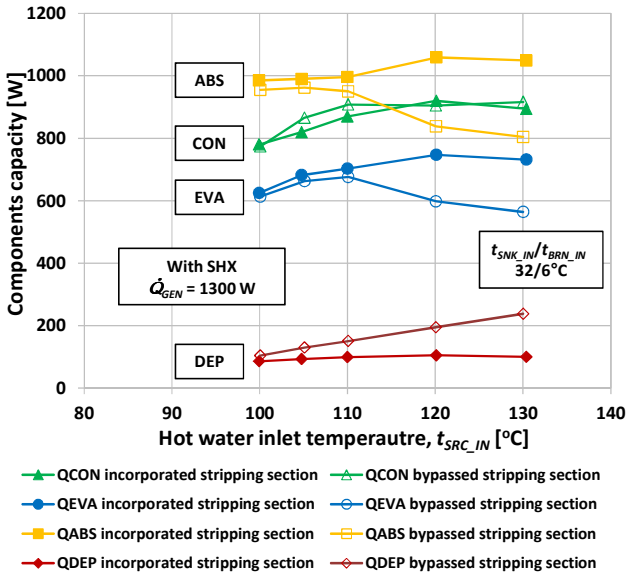

Figure 5-7: Measured components capacities the AHP-test rig operated with solution heat exchanger and with and without stripping section at t_{SNK_IN} / t_{BRN_IN} = 32 / 6℃, $\dot{Q}_{GEN}$ =1300 W

The comparison of the measured COP_C when operating with and without 5 wt.-% of *NaOH* is shown in Figure 5-8. It shows that the change in the COP_C when using the working mixture with and without 5 wt.-% *NaOH* is within experimental error and therefore can be neglected. The COP_C has the maximum of 0.52 at a hot water temperature of 105℃ with 5 wt.-% *NaOH*) and of 108℃ without *NaOH*). At hot water inlet temperatures over 110℃ there is a decrease in the process performance due to an increase in the H_2O concentration in the generated vapor.

The test results of the AHP test rig at the same cooling water / brine inlet temperatures, but at lower generator capacity (900 W), are shown in Figure 5-9. Lower solution flow rates enabled the AHP test rig to operate at lower, hot water inlet temperatures (87-105℃). However, as well as during the operation of generator at a capacity of 1300 W, a change in the COP_C when adding 5 wt.-% *NaOH* was within measurement uncertainties.

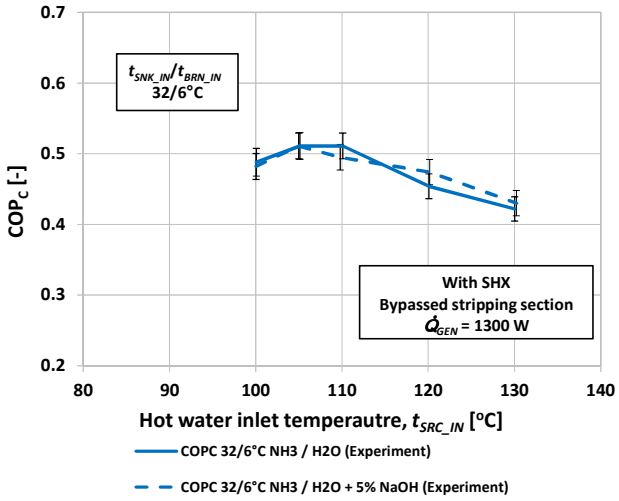

Figure 5-8: Measured COP_C of the AHP test rig operated with SHX and with bypassed stripping section at t_{SNK_IN} / t_{BRN_IN} = 32 / 6℃, $\dot{Q}_{GEN}$ =1300 W

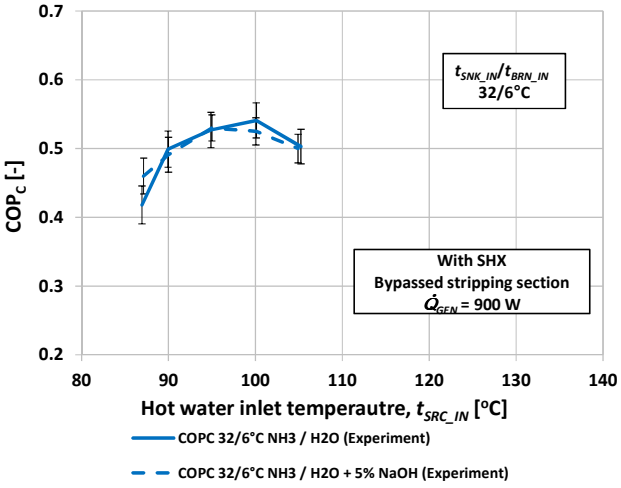

Figure 5-9: Measured COP_C of the AHP test rig operated with SHX and with bypassed stripping section at t_{SNK_IN} / t_{BRN_IN} = 32 / 6℃, $\dot{Q}_{GEN}$ = 900 W

5.2 System analysis using ASPEN Plus

This sub-chapter is dedicated to the system analysis by means of the developed thermodynamic model, using ASPEN Plus. The quality of the simulation results will be evaluated and the operation of the components of the AHP test rig will then be analyzed. The main focus will be on the influence of *NaOH* on the operation of the absorber and generator.

5.2.1 Simulation model

The calculation of the binary parameters of the mixture *NH_3* / *H_2O* / *NaOH* is presented in Chapter 3.1.3. Using the calculated data the thermodynamic model was developed in ASPEN Plus for the analysis of the test results. The schematic of the AHP test rig in ASPEN Plus is presented in Figure 5-10. The components are specified as follows:

1. *Absorber (ABS)*: The absorber consists of three components ABS, ABS-Mix and ABS-2. ABS consists of the ASPEN-model “RadFrac” and is specified as a plate column with 4 theoretical stages. The absorption heat is rejected uniformly from each stage. The rich solution at the saturated state leaves ABS in the lower part. In the upper part of ABS a negligible quantity (about 0.01% of the rich solution flow rate) of *NH_3* / *H_2O* solution leaves the absorber and is mixed with the rich solution in ABS-Mix. This is necessary due to the fact that for the ASPEN-model “RadFrac” both products top and bottom must be defined. The sub-cooling of the rich solution occurs in the heat exchanger ABS-2 (ASPEN-model “Heater”). The advantage for such a specification of the absorber is that it allows for the possibility to calculate the temperature profile along the falling film and to calculate the absorber UA-value and the sub-cooling of the rich solution.
2. *Condenser (CON)*: The condenser consists of the ASPEN-model “Heater” and at its outlet the refrigerant has a vapor fraction of 0.
3. *Generator and the rectification column (GEN and REC)*: The generator consists of the ASPEN-model “RadFrac” with 4 theoretical stages (dephlegmator, rectifying section, stripping section and generator). The rich solution enters the rectification column between the rectifying and the stripping section (operation with the stripping section) or goes directly into the generator (operation without the stripping section). The reflux ratio is set in order to achieve a certain *NH_3*-concentration in the vapor leaving the rectification column, which corresponds to the measured temperature and pressure at the outlet from the rectification column. Furthermore, the vapor fraction at the outlet from the rectification column was set equal to 1. It is assumed that there are no *H_2O* droplets in the generated vapor leaving the rectification column.
4. *Expansion valves (STH and RTH)*: both expansion valves are specified as the ASPEN-model (“Valve”). At the outlet from the expansion valve the pressure is equal to the measured low pressure level.
5. *Solution pump (PUMP)*: The solution pump (ASPEN-model “Pump”) increases the pressure of the rich solution to the measured high pressure level.
6. *Evaporator (EVA)*: For the specification of the evaporator (ASPEN-model “Heater”) the temperature difference between the refrigerant inlet and outlet was defined as being equal to the measured one.

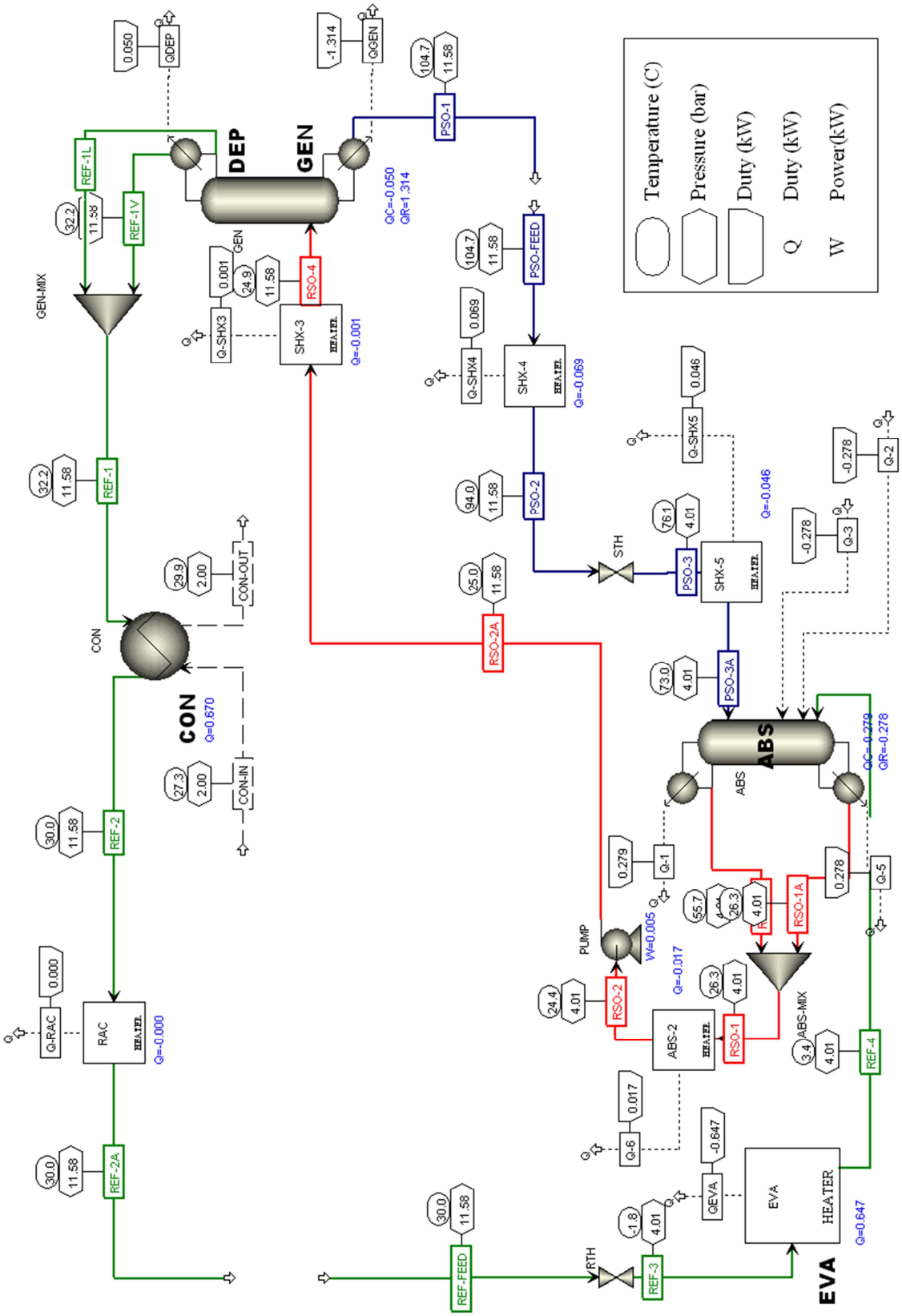

Figure 5-10: Schematic of the AHP test rig in ASPEN Plus

7. The heat losses in the pipes of the rich and poor solution were taken into account by means of measured temperature differences. For this, 4 ASPEN-Models “Heater” were specified (SHX-1, SHX-2, SHX-3 and SHX-4).

Additionally, the following assumptions were made:

- The heat losses in the rest of the components, as well as the pressure drops were not taken into account.
- The condenser and generator capacities were set equal to the measured values.
- The refrigerant at the outlet from the condenser and the poor solution at the outlet from the generator had a vapor fraction of 0.
- For the analysis of the test results with *NaOH*, its mass concentration in the rich solution was set equal to 6%.

5.2.2 Quality of the simulation model

In order to evaluate the quality of the simulation model the calculated and measured evaporator and absorber capacities were compared to each other (see Figure 5-11). For the capacities measurement, the flow rates and temperatures in the external loops (brine and cooling water) were used.

The comparison of the calculated and measured evaporator capacities is shown in Figure 5-11a. As can be seen, the difference between the calculation and measurement is positive over the range of conditions tested and varies from +2% to +11%. As the calculated capacities are higher than the measured ones, a certain part of these calculation uncertainties may be caused by heat inputs in the evaporator.

Figure 5-11b compared the calculated and measured absorber capacities. The difference between the calculation and measurement is within ±5%.

From the analysis of the quality of the simulation model, it can be concluded that the developed thermodynamic model in ASPEN Plus is suitable for the test results evaluation. However, this analysis has a certain level of uncertainties.

Over the following sections, the influence of *NaOH* on the components of the AHP test rig is analyzed for the operation with the bypassed solution heat exchanger.

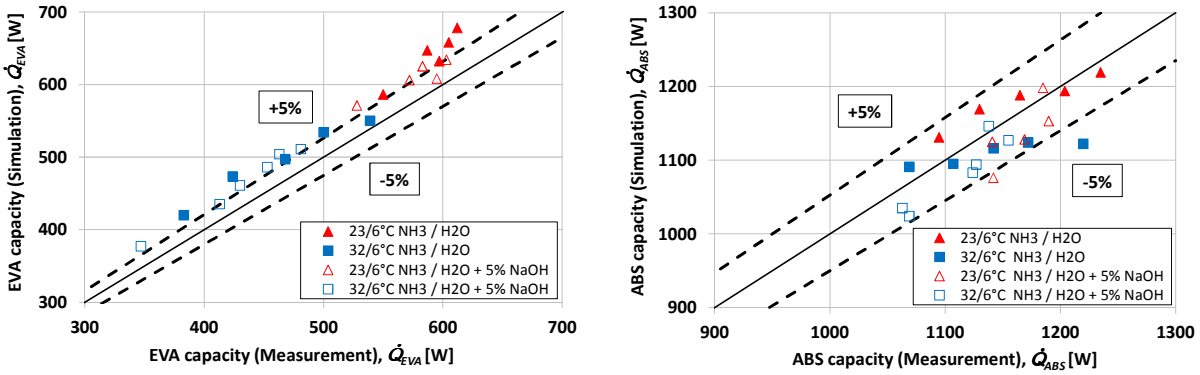

a *b*

Figure 5-11: Comparison of the measured and calculated evaporator (a) and absorber (b) capacities

5.2.3 Analysis of the influence of NaOH on the operation of the absorber

In order to evaluate the operation of the absorber, the absorber efficiency (η_{ABS}), sub-cooling of the rich solution (ΔT_{RSO}) and product of the heat transfer coefficient and area (UA-values) of the absorber were calculated and analyzed.

According to Niebergall (1981) the ideal absorption takes place at the saturation pressure of the rich solution. It is assumed that the absorption mass and heat transfer areas are infinitely large.

In reality, these areas are limited and a driving force (pressure or concentration difference) is necessary for the mass transfer. This means that the absorption of the refrigerant vapor occurs at a pressure (p_L-Δp) lower than the saturation one (p_L) (Figure 5-12). Due to this (that the rich solution temperature is defined by the cooling water temperature and the low pressure by the brine temperature) the rich solution concentration (ξ_{RSO}) is lower than its theoretical value (ξ_{RSO_THEOR}).

Commonly the sub-cooling (ΔT_{RSO}) is used instead of the low pressure decrease for the evaluation of the operation of the absorber. It is equal to the difference between the saturation temperature of the rich solution, calculated using thermodynamic equilibrium at the low pressure (p_L) and rich solution concentration (ξ_{RSO}), and the measured temperature of the rich solution:

$$\Delta T_{RSO} = t_{RSO\_THEOR} - t_{RSO} \qquad 5\text{-}1$$

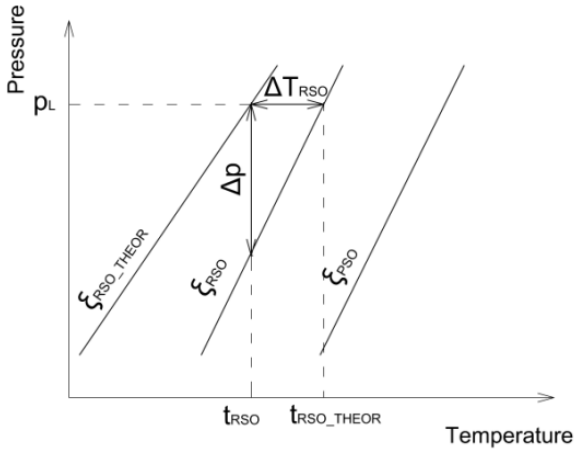

Figure 5-12: Sub-cooling of the rich solution and required partial pressure difference for the absorption of the refrigerant vapor in pressure / temperature diagram

Within this work, the temperature of the rich solution (t_{RSO}) was measured at the outlet from the absorber ($t_{RSO\_ABS\_OUT}$, see Figure 4-12). Its theoretical value (t_{RSO_THEOR}, RSO-1, see Figure 5-10) was calculated in ASPEN Plus using the measured value of the low pressure (p_{LP}, see Figure 4-12) and calculated concentration of the rich solution (ξ_{RSO}, *RSO-1*, see Figure 5-10).

The mass concentrations of the non-subcooled (ξ_{RSO_THEOR}) rich solution were calculated using the measured temperature and pressure of the rich solution ($t_{RSO\_ABS\_OUT}$ and p_{LP}, see Figure 4-12).

If the real and theoretical concentrations of the rich solution are known, the absorber efficiency can be calculated as follows:

$$\eta_{ABS} = \frac{\xi_{RSO} - \xi_{PSO}}{\xi_{RSO\_THEOR} - \xi_{PSO}} \qquad 5\text{-}2$$

For the heat transfer analysis in the absorber, the UA-values (product of the heat transfer coefficient and heat transfer area) were calculated using Eq. 5-3. As can be seen from Figure 5-13, the temperature profile on the solution side in the absorber is non-linear with respect to the absorber capacity. The UA-values were calculated using the ASPEN model “RadFrac” consisting of 4 theoretical stages with the same capacity and the ASPEN model “Heater”, in which the sub-cooling of the rich solution was simulated.

It has to be noted, that as the real temperature profile cannot be analyzed, owing to a lack of measurement data, and the UA-values depend on the combined heat and mass transfer in the absorber, from the simulation results, it is rather impossible to draw any conclusion about the reason for changes in the UA-value.

$$UA_{ABS} = \sum_{i=1}^{n} \frac{\dot{Q}_i}{\Delta T_{i,log}} \qquad 5\text{-}3$$

n=5 … number of the segments in which the absorber is divided;

$\dot{Q}_i$ … capacity of the segment *i* [W];

$\Delta T_{i,log}$ … logarithmic temperature difference of the segment *i*.

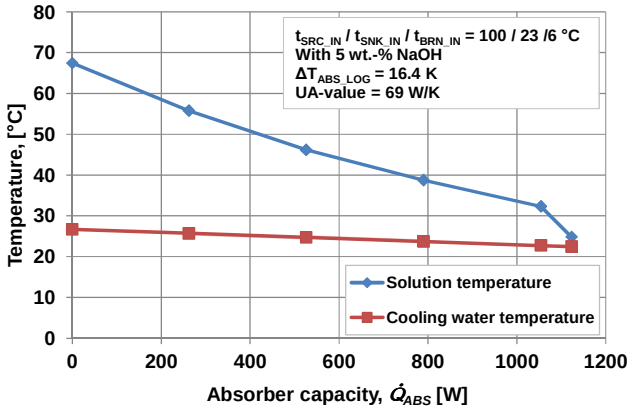

Figure 5-13: Temperature profile in the absorber at t_{SRC_IN} / t_{SNK_IN} / t_{BRN_IN} = 100 / 23 / 6℃ and $\dot{Q}_{GEN}$ = 1300 W

The calculated absorber efficiency, sub-cooling of the rich solution and UA-value of the absorber are discussed for the operation with the bypassed solution heat exchanger and shown in Figure 5-14.

Figure 5-14a shows the absorber efficiency relating to the hot water inlet temperature (t_{SRC_IN}). At cooling water / brine inlet temperatures of 23 / 6℃ it is relatively constant over the range of conditions tested and is approximately 0.94 when operating without *NaOH* decreasing to approximately 0.77 when adding 5 wt.-% *NaOH* to the working mixture. Concerning operation at higher cooling water inlet temperature (32℃), a decrease in the absorber efficiency from approximately 0.95 (without *NaOH*) to 0.82 (with 5 wt.-% *NaOH*) was calculated.

The influence of *NaOH* on the sub-cooling of the rich solution is shown in Figure 5-14b. It is obvious that the sub-cooling for the operation without *NaOH* is relatively constant and varies from 1 K to 2 K. When adding 5 wt.-% *NaOH* the sub-cooling increases roughly linearly with the generator temperature and varies from 4 K to 10 K at a cooling water inlet temperature of 23℃ and from 2 K to 6 K at 32℃.

The calculated UA-values of the absorber are presented in Figure 5-14c. It can be seen, that the UA-value decreases with the increasing generator temperature. Furthermore, the UA-values for the operation without *NaOH* are higher than those for the operation with

5 wt.-% *NaOH*. For instance, at t_{SNK_IN} / t_{BRN_IN} = 23 / 6°C the UA-value decreases from approximately 115 W·K^{-1} to 70 W·K^{-1}.

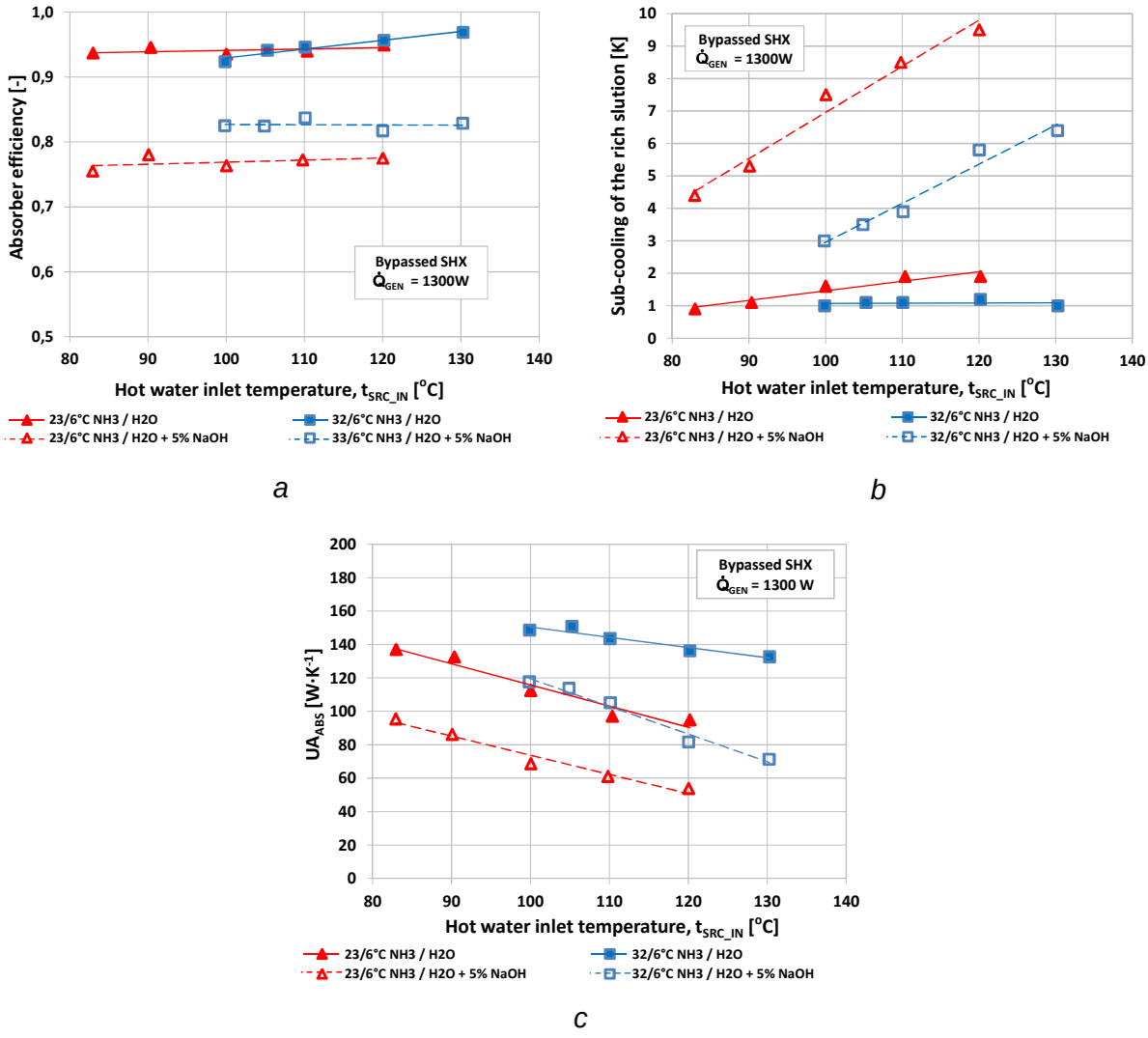

Figure 5-14: Influence of NaOH on the absorber efficiency (a), the sub-cooling of the rich solution (b) and the UA-value of the absorber (c)

In order to analyze the change in the temperature profile in the absorber when adding *NaOH*, Figure 5-15 shows the operation with 0 (a) and 5-wt.% (b) *NaOH*. Apparently, the logarithmic temperature difference in the absorber is higher when operating with 5-wt.% *NaOH* (18.6 K) than without (11.8 K). This means, that the UA-value is lower: 61 W·K^{-1} (with 5-wt.% *NaOH*) and 87 W·K^{-1} (without *NaOH*).

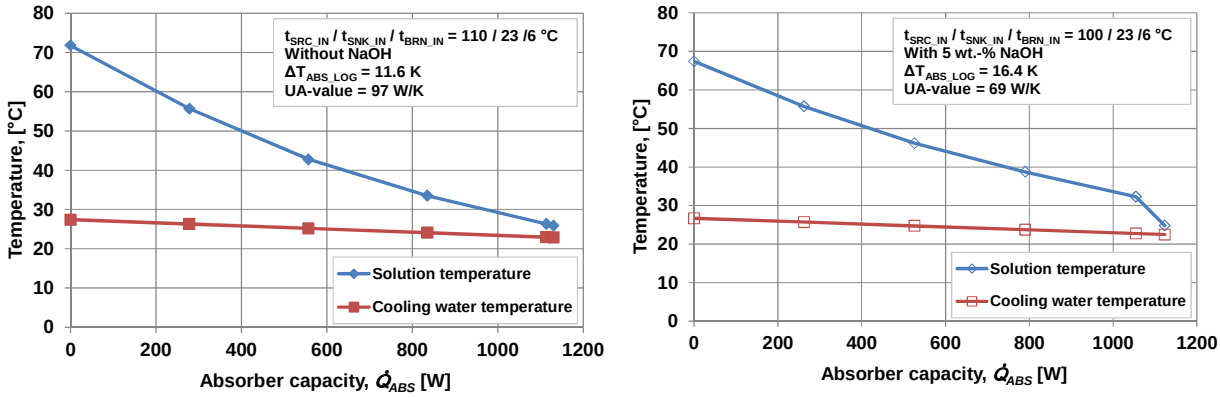

Figure 5-15: Simulated temperature profile in the absorber at t_{SRC_IN} / t_{SNK_IN} / t_{BRN_IN} = 110 / 23 / 6℃ and $\dot{Q}_{GEN}$ = 1300 W: a – without NaOH; b – with 5 wt.-% NaOH

Based on the simulation results, it is possible to conclude, that the use of *NaOH* as an additive to the *NH_3 / H_2O* working mixture affects the absorption of the refrigerant vapor negatively.

The use of *NaOH* leads to a decrease in the *NH_3* mass concentration in the rich and poor solutions. As the *NH_3* mass concentration in the rich solution decreases more than that of the poor solution, the difference between both concentrations ($\Delta\xi_{NH3}$) becomes smaller in comparison to the operation without *NaOH* (see Figure 5-16a). As a consequence, the specific solution flow rate increases when using *NaOH* (see Figure 5-16b).

Generally, this increase in the specific solution flow rate must improve the heat transfer in the absorber and therefore its efficiency. However, in reality it constitutes a penalty to absorption.

The viscosity and surface tension of the *NH_3 / H_2O* working mixture with *NaOH* are higher than those of the *NH_3 / H_2O* mixture without. This means, that a possible reason for the decrease in the absorber efficiency could be the insufficient mass transfer area and poor wettability of the absorber, when operating with *NaOH*.

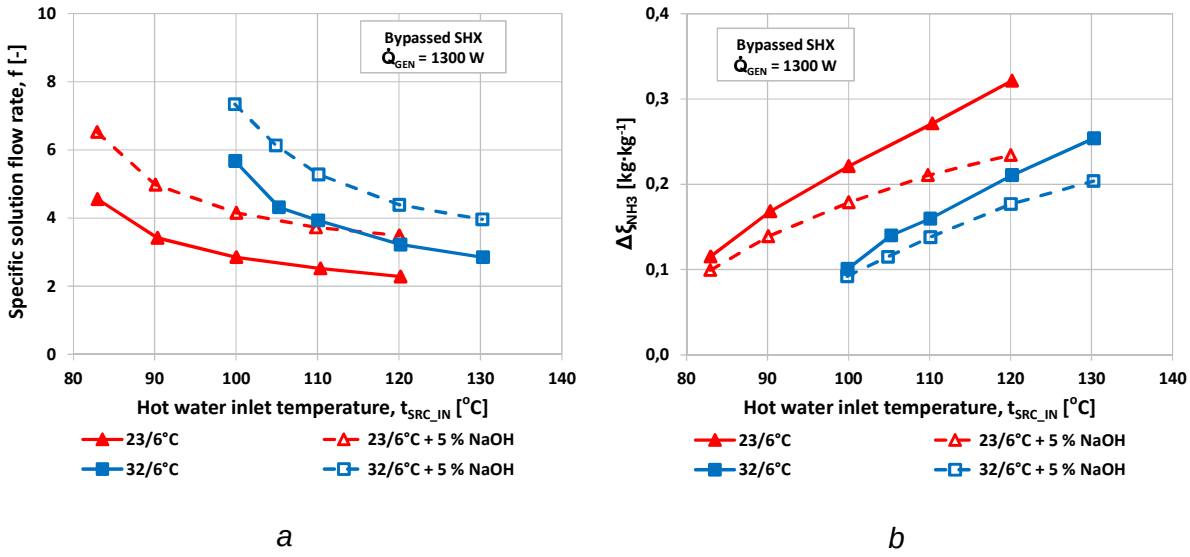

Figure 5-16: Difference between the NH_3 mass concentration in the rich and poor solution (a) and specific solution flow rate (b) depending on the hot water inlet temperature for the operation with and without 5 wt.-% NaOH

5.2.4 Analysis of the influence of NaOH on the operation of the generator

In order to analyze the influence of *NaOH* on the heat exchange in the generator, the UA-values of the generator were calculated using the following equation:

$$UA_{GEN} = \frac{\dot{Q}_{GEN}}{\Delta T_{i,log}} \qquad 5\text{-}4$$

$\dot{Q}_{GEN}$ … calculated generator capacity [W];

$\Delta T_{i,log}$ … logarithmic temperature difference between the hot water side and the solution side.

The calculated UA-values of the generator are shown as they relate to the hot water inlet temperature in Figure 5-17. It is obvious, that for the majority of tests with 5 wt.-% *NaOH* higher UA-values were obtained in comparison to those operations without *NaOH*. It can be also seen that the calculated UA-values decrease with the decreasing generator temperature, due to an increase in the solution flow rate (see Figure 5-16).

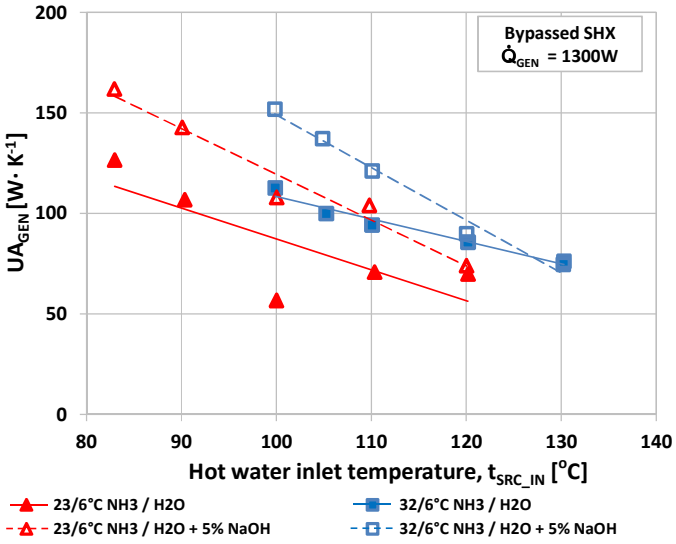

Figure 5-17: Influence of NaOH on the UA-values of the generator

Figure 5-18 compares the calculated temperature profile in the generator of the operation without *NaOH* and with 5 wt.-% *NaOH*. It is visible, that both temperature profiles are roughly linear with respect to the generator capacity. When using *NaOH*, the logarithmic temperature difference in the generator decreases from 11.7 K to 8.8 K. This leads to an enhancement of the heat transfer in the generator: the UA-value is 113 W·K^{-1} for the operation without *NaOH* and 152 W·K^{-1} for the operation with 5 wt.-% *NaOH*.

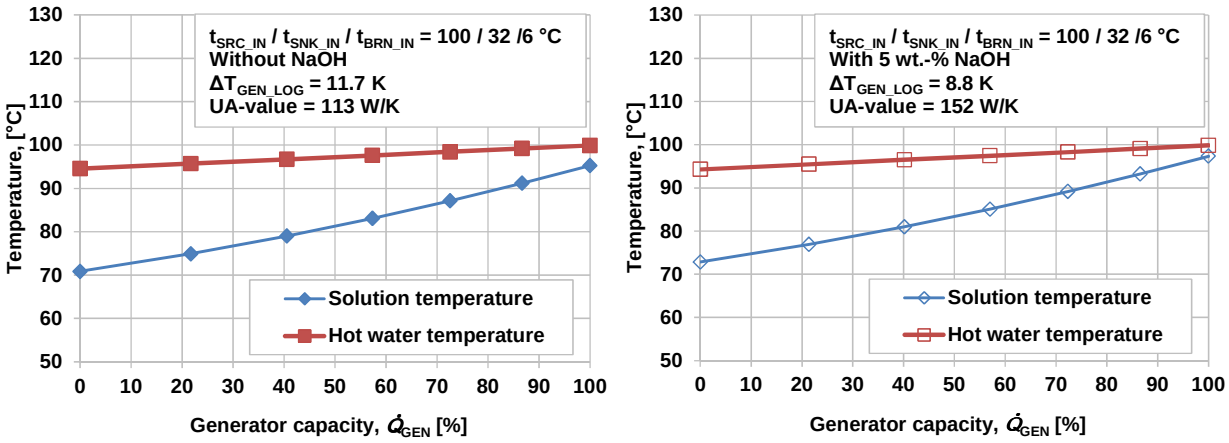

a *b*

Figure 5-18: Simulated temperature profile in the generator at t_{SRC_IN} / t_{SNK_IN} / t_{BRN_IN} = 100 / 32 / 6°C and $\dot{Q}_{GEN}$ = 1300 W: a – without NaOH; b – with 5 wt.-% NaOH

5.2.5 Analysis of the influence of NaOH on the operation of other components

The analysis of the influence of *NaOH* on other components of the AHP test rig such as the evaporator, solution heat exchanger and the rectification column has not shown significant changes in their operation when adding *NaOH*.

The evaluation of the experimental results concerning the NH_3 mass concentration in the generator vapor has shown that they vary from 0.994 to 0.999. The vapor fraction of the refrigerant vapor at the outlet from the evaporator ranges from 0.994 to 1.

For the analysis of the heat exchange in the solution heat exchanger, the UA-values for the operation with the solution heat exchanger at a generator capacity of 1300 W were calculated in ASPEN Plus. From the calculation results shown in Figure 5-19, it can be inferred that there is a slight change in the UA-value of the solution heat exchanger when adding 5 wt.-% *NaOH*. Furthermore, the UA-value decreases with the increasing hot water inlet temperature.

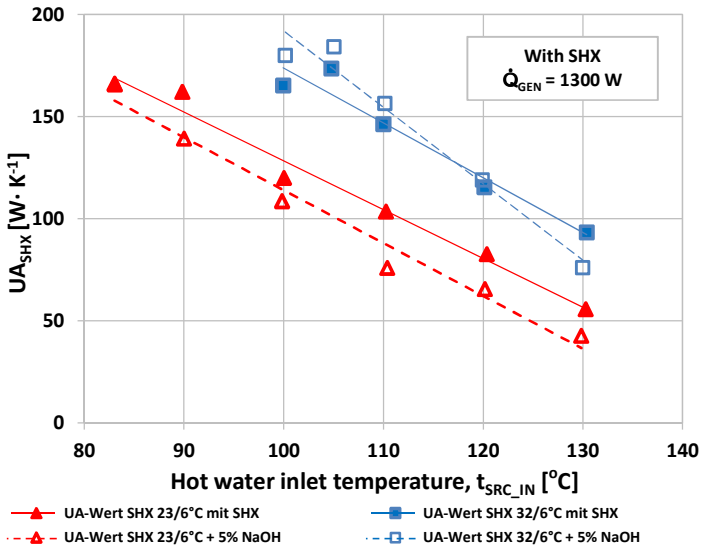

Figure 5-19: Influence of NaOH on the UA-value of the solution heat exchanger at t_{SNK_IN} / t_{BRN_IN} = 23 / 6 and 32 / 6℃ and $\dot{Q}_{GEN}$ = 1300 W

6 SUMMARY AND CONCLUSIONS

The purpose of this work was to analyze innovative absorption heat pumping (AHP) processes found in related literature in order to find an alternative to a conventional ammonia / water (NH_3 / H_2O) AHP that is capable of performing at a higher COP (coefficient of performance) and is potentially competitive with it in cost, operating life and reliability.

From the analysis of the development of the use of renewable energies over the past years, continuous growth of the renewable energy market is to be expected. Apart from conventional applications, new markets, e.g. solar cooling and gas-driven AHP for heating and cooling, will be developed. This makes the use of absorption technologies attractive, first of all in combination with other renewable energy sources, e.g. HVAC-systems consisting of AHP and biomass boilers or solar panels, AHP driven by waste heat, etc. Nowadays, AHP with cooling capacities ranging from 10 kW to 500 kW are available on the market and can be used for different applications.

The majority of produced AHP operate either with the working mixture H_2O / *LiBr or* NH_3 / H_2O. Attempts at bringing new refrigerants onto the market have until now not been successful. The reason for this is that the use of organic refrigerants in AHP, save methanol, is disadvantageous owing to their high specific heat capacity, low heat of evaporation and high solution mass flow rate. The properties of conventional working pairs can be greatly improved either by use of new additives for H_2O / *LiBr or* NH_3 / H_2O or new absorbents instead of *LiBr* and H_2O.

Thermodynamic analysis of innovative AHP-processes

A detailed survey of related literature on the following innovative AHP-processes was presented within this work and they were analyzed by means of thermodynamic simulations using ASPEN Plus:

1. NH_3 / H_2O AHP-process using strong bases as additives;
2. AHT-process using partially miscible working mixtures;
3. AHP-processes using a condensable auxiliary fluid (Rojey cycle and Einstein-Szilard cycle);
4. AHP-processes using ionic liquids as absorbents.

NH_3 / H_2O AHP-process using NaOH as additives: From the simulation results, it can be inferred that the COP_C of a conventional NH_3 / H_2O AHP can be increased and at the same time, the required generator temperature decreased, if *NaOH* is added. For instance, at t_{ABS_OUT} / t_{EVA_OUT} = 45 / 5℃ the COP_C was 0.53 at a generator outlet temperature of 125°C.

When operating with 5 wt.-% *NaOH* in the rich solution the generator outlet temperature could be reduced to 112℃ achieving the same COP_C.

It is necessary to mention, that the temperature difference between the rich solution inlet temperature to the solution heat exchanger and the poor solution outlet temperature from the solution heat exchanger was set equal to 5 K. When using *NaOH,* the specific solution flow rate increases and therefore there is an increase in the ratio of the solution heat exchanger capacity to the generator heat capacity ($\dot{Q}_{SHX}$ / $\dot{Q}_{GEN}$). In real applications it means that the solution heat exchanger with the higher capacity has to be used when using *NaOH* as an additive. Furthermore, an increase in the solution flow rate requires greater heat and mass transfer area in the absorber. The use of the same absorber for both processes with and without *NaOH* might cause a decrease in the absorber efficiency. However, it was set equal to 100% in all simulations.

NH_3 / IL AHP-processes: Thermodynamic simulations of the investigated *NH_3 / IL* AHP-processes showed that their efficiencies at certain boundary conditions are higher than those of a conventional *NH_3 / H_2O* AHP. However, the COP_C of the investigated *NH_3 / IL* AHP-processes decreases more in comparison with a conventional *NH_3 / H_2O* AHP when the temperature lift increases. The reason for this is a low difference between the *NH_3* mass concentration in the rich and poor solution and therefore a high solution flow rate. The best simulation results were obtained for the AHP-process using the working mixture *NH_3 / [bmim][PF_6]*. It is more efficient than a conventional *NH_3 / H_2O* AHP at t_{ABS_OUT} / t_{EVA_OUT} = 25 / 5℃ and 35 / 5℃ if t_{GEN_OUT} is higher than 75℃ and 115℃ respectively.

Concerning the costs of the *NH_3 / IL* AHP-process, no rectification column is necessary, however, to achieve the same cooling capacity in the evaporator, the “larger” components of the sorption cycle, i.e. absorber, generator, solution heat exchanger and solution throttle valve, are necessary.

AHT-process using partially miscible working mixture of water / furfural: Concerning the AHT-process with water / furfural as a working mixture, it can be concluded, that this is currently not competitive compared to a conventional *H_2O / LiBr* AHT. Even if alternative working mixtures are found, which enable the process operation at lower temperature levels with higher efficiency, its application in practice will be rather difficult, owing to the high temperature glide in the condenser and the fact that the temperature lift of this process depends only on the shape of the dew-point curve of the working fluids.

Rojey cycle: The theoretical investigation of the Rojey cycle with 2-stage absorption and the working mixture *NH_3 / H_2O / C_4H_{10}* showed that it is promising for applications at high

generator temperatures and low temperature lifts. For instance, the calculated COP_C of the Rojey cycle at t_{ABS_OUT} / t_{EVA_LOG} = 25 / 1.7°C was higher than that of a conventional NH_3 / H_2O AHP at generator outlet temperatures higher than 70°C. When increasing the absorber outlet temperature to 45°C the Rojey cycle had a similar COP_C to a conventional NH_3 / H_2O AHP but required a generator temperature of 165°C instead of 120°C.

Concerning further research on the Rojey cycle, it must be noted that the NH_3 / C_4H_{10} concentration in the evaporator was set equal to the composition of the azeotropic mixture. When changing the C_4H_{10} concentration in the evaporator, evaporation will occur at gliding temperature. On the one hand, the comparison of the Rojey cycle with a conventional NH_3 / H_2O AHP will be difficult, on the other hand, new application areas for the cycle could be found.

Einstein-Szilard cycle: Within this work the 2-stage absorption for the Einstein-Szilard cycle was suggested. The simulation results showed that the COP_C of this cycle was still much lower than that of a conventional NH_3 / H_2O AHP. For instance, at t_{ABS_OUT} / t_{EVA}=25 / 1.5°C the Einstein-Szilard cycle has a COP_C of 0.19 and a conventional NH_3 / H_2O AHP of 0.75. Thus, to improve the efficiency of the Einstein-Szilard cycle new working mixtures must be investigated.

NH_3 / H_2O / NaOH AHP test rig

The AHP test rig developed within this work for the experimental investigations with the working mixture NH_3 / H_2O using *NaOH* as an additive consists of the following components: the absorber (ABS), condenser (CON), generator (GEN), rectification column with stripping section (STR), rectification section (REC) and dephlegmator (DEP), solution heat exchanger (SHX), rich solution (RSAC), poor solution (SAC) and refrigerant (RAC) accumulators and throttle valves (STH and RTH). Furthermore, there are two bypasses to enable operation with or without SHX. The design of the rectification column also permits the operation use of both the rectification and stripping sections, or only the rectification section.

The absorber and evaporator are designed as vertical falling film components. The predicted absorber capacity is up to about 1400 W and that of the evaporator is up to about 950 W. Optical access to the absorption and evaporation processes is provided by the installation of five sight glasses in each component.

The condenser, generator and solution heat exchanger are plate heat exchangers from the company “Alfa Laval”. For the solution pump, a plunger-membrane pump with a PTFE membrane was used. The installed refrigerant and solution accumulators have a volume of 1.5 l and for temperature measurement thermometer pockets with PT100 were installed.

The electronic expansion valve type AKVA 10-1 (“Danfoss”) with a regulation area ranging from 5% to 100% was installed as the refrigerant throttle valve. An additional manual throttle valve Type SS-1RS6MM (“Swagelok”) was installed in series after the electronic expansion valve. For the solution flow rate regulation the valve type SS-31RS6MM (“Swagelok”) was used.

In order to regulate temperature levels of the high temperature heat source, heat sink and low temperature heat source the hot water, cooling water and brine loops were used. Hot water loop aims to supply heat to the generator at a temperature level from 80℃ to 130℃. The heating medium is distilled water, which was heated by an electric heating element with a heat capacity of 3500 W. To reject heat in the absorber, condenser and the dephlegmator, the cooling water loop of the institute was used. The mobile unit of the institute was used as a low temperature heat source. The brine medium is a mixture of Glysantin and water (43 Vol.-% / 57 Vol.-%).

For the needs of temperature measurements thermocouples and platinum resistance thermometers Pt100 were used, and for the pressure measurement three pressure transmitters “Alphaline” from “Rosemount” were installed. The flow rates in the external loops are measured by means of three flow meters: magnetic inductive flow meters from the company “ABB” for the cooling water and brine and the coriolis mass flow meter from the company “Micro-Motion” for hot water. All measurement devices used in the AHP test rig were calibrated.

The regulation of the AHP test rig occurred by means of the software program “LabView”. The data acquisition was provided by means of 3 IMPs (isolated measurement pod) of the type 35951J from the company “Solartron”. For the regulation of the regulated process values and that of the heating element, an additional IMP of the type 35951D was installed. All gathered data by IMPs were sent to a PC by means of the software program “LabView” and copied to a text-file with the measurement period of 2 sec.

Test results and system analysis using ASPEN Plus

The test results on the NH_3 / H_2O / $NaOH$ AHP test rig were reported and analyzed by means of thermodynamic simulation using ASPEN Plus. The tests were carried out at different cooling water and hot water inlet temperatures and different generator capacities. The test rig operation with and without solution heat exchanger as well as stripping section of the rectification column was analyzed

From the test and simulation results the following can be concluded:

1. Technical feasibility of the NH_3 / H_2O AHP-process using 5 wt.-% *NaOH* as an additive was proven. However, due to the presence of *NaOH* crystals in the evaporator the working mixture had to be regularly changed and the test rig had to be purged with water.
2. Operation at higher *NaOH* concentrations could not be realized. The tests with 10 wt.-% *NaOH* in the working mixture failed, because of the crystallization issues in the lower part of the evaporator and in the pipe between the absorber and evaporator.
3. An increase in the COP_C predicted by the simulations (see Chapter 3.1.4) could not be proven. The evaluation of the test results in ASPEN Plus showed that this was due to decreased absorber efficiency. This penalty to absorption was imposed, on the one hand, by the higher viscosity and surface tension of the working mixture with *NaOH* and, on the other hand, because of the higher solution flow rate when using *NaOH* as an additive.
4. The use of *NaOH* as an additive to the working mixture NH_3 / H_2O leads to a moderate increase in the UA-value coefficient of the generator.
5. From the analysis of the influence of *NaOH* on the evaporator, solution heat exchanger and rectification column, it can be concluded that there are no significant changes between the operation with and without *NaOH*.

Generally, the presented results show that NH_3 / H_2O absorption is hard to best due to the reasons discussed above. Thus, further research and development of the NH_3 / H_2O AHP-process using *NaOH* as additive with regard to the absorber design, which can provide adequate mass transfer areas and thus higher absorber efficiency when operating with *NaOH*, is necessary. Finally, an additional challenge with *NaOH* is that the design of the AHP test rig has to be modified, to prevent the presence of *NaOH* in the refrigerant circuit.

Conclusions and further work required

The following research and development of the NH_3 / H_2O AHP-process using *NaOH* as an additive is needed:

1. The absorber design has to be improved to ensure adequate mass and heat transfer area and, therefore, higher absorber efficiencies when operating with *NaOH*. For instance, the absorber for the operation with *NaOH* could be improved by increasing the diameter of the first internal pipe (falling film) and decreasing the pitch angle of the wire installed on it. The tests must be carried out with two different absorbers: one designed for operation with *NaOH* and another without *NaOH*. Both absorbers must

have the same absorber efficiency during the operation, to allow for the fair comparison of the test results.

2. To ensure the long term operation of the test rig, its construction has to be modified, to prevent *NaOH* entering the refrigerant circuit during the operation. For this, the improvement of the droplet separator construction is necessary. Before installation of the rectification column in the AHP test rig, different types of droplet separators (e.g. a droplet separator with bigger diameter or several droplet separators installed in parallel) have to be experimentally investigated with the working mixture NH_3 / H_2O / *NaOH*.

7 REFERENCES

Alefeld G. and Radermacher R., (1994), “Heat conversion systems”, Boca Raton: CRC Press.

Alonso D., Cachot T., Hornut J.M., (2002), “Performance simulation of an absorption heat transformer operating with partially miscible mixtures”, Appl. Energy 72, 583–597.

Alonso D., Cachot T., Hornut J.M., (2003), “Experimental study of an innovative absorption heat transformer using partially miscible working mixtures”, Int. J. Therm. Sci. 42, 631–638.

Aspen Plus v 7.0, (2009), Aspen Technology, Inc., Cambridge, Massachusetts

Balamuru V. G., Ibrahim O. M., Barnett S. M., (2000), “Simulation of ternary ammonia-water-salt absorption refrigeration cycles” Int. J. Refrigeration 23, 31-42.

Bassols, J., Schneider, R., Veelken, H., Kuckelkom, B. and Ohrt, D., (1994), “1st Operation Results of a Gas-fired 250 kW Absorption Heat Pump with Plate-fin Heat Exchangers”, Intemational Absorption Heat Pump Conference, New Orleans, 73-78.

Biermayr P., Eberl M., Ehrig R., Fechner H., Galosi A., Kristöfel C., Prüggler N., Strasser C., Weiss W., Wörgetter M., (2011), “Innovative Energietechnologien in Österreich Marktentwicklung 2010. Biomasse, Photovoltaik, Solarthermie und Wärmepumpen”, Berichte aus Energie- und Umweltforschung, Nachhaltig wirtschaften 26/2011, BMVIT, Vienna, Austria.

Brass M., Pritzel T., Schulte E., Keller J. U., (2000), “Measurements of Vapor-Liquid Equilibria in the Systems NH3-H2O-NaOH and NH3-H2O-KOH at Temperatures of 303 and 318 K and Pressures 0.1 MPa < p < 1.3 MPa”, Int. J. Thermophys. Vol.21, No. 4.

Bruno J. C., Vidal A., Esteve X., Coronas A., (2005), “Modeling and thermal analysis of ammonia-water-sodium hydroxide absorption refrigeration cycles”, International sorption heat pump conference, Denver, 2005.

Cheron J., Rojey A., (1986), “High performance absorption heat pump with auxiliary fluid”, 2nd international workshop on research activities on advances heat pumps, Graz, 235-254.

Coronas A., Allepus J., Huor M.H., Prevost M., Bugarel R., (1990), “High performance new absorption cycles for refrigeration and air conditioning”. 3rd International Workshop on research activities on advanced heat pumps, Graz, 358-366.

Coronas A. (1995), “Refrigeration Absorption Cycle Using an auxiliary Fluid”, Appl. Energy, Vol. 51, 69-85.

Delano (1998), “Design analysis of the Einstein refrigeration cycle”, PhD Thesis, Georgia Institute of Technology.

EES (2006), “Engineering Equation Solver for Microsoft Windows Operating Systems. Academic Commercial Versions V 8.172-3D”, F-Chart Software. Copyright by S.A. Klein (1992-2006).

Einstein A., Szilard L., (1930), “Refrigeration”, US Patent, No. 1.781.541.

Fenzl T. (2011), “Auswirkung von *NaOH* auf die Effizienz des NH_3 / H_2O Absorptions-Wärmepumpen-Prozesses”, Diploma thesis, Institute of Thermal Engineering, Graz University of Technology, Austria.

Fernandez, A., Garcia, J., Torrecilla, J. S., Oliet, M., Rodriguez, F., (2008), J. Chem. Eng. Data, 53, 1518-1522.

Ficke L. E., Rodriguez H., Brennecke J. F., 2008, J. Chem. Eng. Data, 53, 2112-2119.

Ganster S. (2009), “Simulation eines NH_3/H_2O/NaOH- Absorptions-Wärmepumpenprozesses”, Diploma thesis, Institute of Thermal Engineering, Graz University of Technology, Austria.

Garimella S., Determan M., Meachan M., Lee S., Ernst T. (2011), “Microchannel component technology for system-wide application in ammonia / water absorption heat pumps”, Int. J. Refrigeration, 34, 1184-1196.

Ge, R.; Hardacre, C.; Nancarrow, P.; Rooney, D. W. (2007), J. Chem. Eng. Data 52 , 1819-1823.

Ge, R.; Hardacre, C.; Jacquemin, J.; Nancarrow, P.; Rooney, D. W. (2008), J. Chem. Eng. Data 53 , 2148-2153.

Gilliam R.J., Graydon J.W., Kirk D.W., Thorpe S.J. (2007), “A review of specific conductivities of potassium hydroxide solutions for various concentrations and temperatures”, Int. J. Hydrogen Energy. Vol.32.

Gluesenkamp K., Radermacher R., Hwang Y., (2011), “Trends in absorption machines”, International Sorption Heat Pump Conference (ISHPC11), Padua, Italy, p. 13-22.

Gmehling J., Onken U., Artl W., (1981), “Vapor-Liquid Equilibrium Data Collection. Aqueous-Organic Systems. Supplement 1”, DECHEMA, Frankfurt/Main, Germany.

Gonzalez J., Jabardo J., Stoecker (1992), “Falling Film Ammonia Evaporators”, Review Report, Air Conditioning and Refrigeration Center, University of Illinois.

Grote K.-H., Feldhusen J. (2005), “Dubel, Taschenbuch für den Maschinenbau, Kapitel E Anhang”, Berlin Heidelberg New York, Springer, ISBN 3-540-22142-5.

Holbrey, J. D., Reichert, W. M., Reddy, R. G., Rogers, R. D., (2003), ACS Symposium Series, Vol. 856, 121-133.

Hybrid Energy, (2011), Material of the company "Hybrid Energy" presented online http://sylow.ife.no/hybridenergy/he_files/products, last accessed on 24.07.2011.

Ibrahim O. M., Klein S.A., (1993), "Thermodynamic Properties of Ammonia-Water Mixtures", ASHRAE Trans., Symposia.

Jakob U., Kohlenbach P., (2010), "Recent developments of sorption chillers in Europe", 9th Gustav Lorentzen Conference, Sydney, Australia.

Kang Y., Akisawa A., Kashiwagi T., (2000), "Analytical investigation of two different absorption modes: falling film and bubble types", Int. J. Refrigeration, 23, 430-443.

Kalkgruber J. (2009), "Aufbau und Inbetriebnahme einer Absorptionswärmepumpe zur Untersuchung von Ammoniak-Wasser-Natriumhydroxid Gemischen", Diploma thesis, Institute of Thermal Engineering, Graz University of Technology, Austria.

Kim K.-S., Park S.-Y., Choi, S., Lee H., (2004), J. Chem. Eng. Data, 49, 1550-1553.

Krummen, M., Wasserscheid, P., Gmehling, J., (2002), J. Chem. Eng. Data, 47 , 1411-1417.

Löwer, Bosnjakovic, Grabenhenrich, Knoche, Korsmeier, Malewski, Mühlmann, Seher, Stehmeier, Stephan, Weßing (1987), "Absorptionswärmepumpen", Wärmepumpen Band 6, Müller GmbH, Karlsruhe, Germany.

Luedecke C., Luedecke D. (2000), "Thermodynamik. Physikalisch-chemische Grundlagen der thermischen Verfahrenstechnik", Berlin Heidelberg New York, Springer.

Makita K. (2006), "Development and commercialisation of tripple-effect absorption chiller-heaters", IEA Heat Pump Centre Newsletter, Vol. 24, 20-23.

Marr R. (1997), "Thermische Verfahrenstechnik 1", Lecture script, Graz University of Technology.

Mejbri K., Ben Ezzine N., Guizani Y., Bellagi A. (2006), "Discussion of the feasibility of the Einstein refrigeration cycle", Int. J. Refrigeration, 29, 60-70.

Mills L.E., Kalamazoo M., (1953), "Method of refrigeration using conjugate solutions", US Patent No. 2 638 760.

Mortimer C.E., Müller U., (2007), "Chemie", Stuttgart, Georg Thieme, Germany.

Moser H., (2008), "Ammoniak/Wasser-Absorptionswärmepumpe kleiner Leistung zum Heizen und Kühlen", PhD Thesis, Institute of Thermal Engineering, Graz University of Technology.

Moser H., Rieberer R., (2011), “Analysis of a gas-driven absorption heat pumping system used for heating and domestic hot water preparation“,10th IEA Heat Pump Conference 2011, Tokyo, Japan.

Mostofizadeh C., Kulick C., (1998), “Use of a new type of heat transformer in a food industry”, Appl. Thermal Eng., 18, 857-874.

Niang M., Cachot T., Le Goff P., (1997), “A new trend in heat recovery from wastes by use of partially miscible working fluids”, Energy Convers., 38, 1701-1707.

Niang M., Cachot T., Le Goff P., (1998), “Evaluation of the performance of an absorption-demixtion heat pump for upgrading thermal waste heat”, Appl. Therm. Eng., 18, 1277-1294.

Niebergall W., (1981), “Sorptionskältemaschinen”, Berlin Heidelberg New York, Springer, ISBN 3-540-02404-2.

Niederhauser T., Trepp C., (1994), “Wärme- und Stoffübergang im Wasser/Ammoniak-Rieselfilm an glatten und rauhen Rohroberflächen”, Wärme- und Stoffübertragung. Vol.29.

Phillips B., (1990), “Development of a high-efficiency, gas-fired, absorption heat pump for residential and small-commercial applications”, Final report, Oak Ridge National Laboratory, Tennessee.

Phillips B., Whitlow E., (1998), “Corrosion inhibitor for aqueous ammonia absorption system”, US Patent, No. 5811026.

Quitzsch K, Strittmatter D, Geiseler G., (1969), “Studien zur Thermodynamik binaerer Fluessigkeitgemische mit homologen Formamiden”, Z. Phys. Chem., 240, 107–126.

Rebelo L. P. N., Najdanovic-Visak V., Visak, Z. P., Nunes da Ponte M., Szydlowski J., Cerdeirina C. A., Troncoso J., Romani L., Esperanca J. M. S. S., Guedes H. J. R., de Sousa, H. C., (2004), Green Chem., 6 (8), 369-381.

Rechberger C., (2009), “Wärmerückgewinnung mittels Rauchgaskondensation bei biomassebefeuerten Heizkraftwerken”, Diploma thesis, Institute of Thermal Engineering, Graz University of Technology, Austria.

Reiner R. H., Zaltash A., (1991), “Evaluation of ternary ammonia-water fluids for GAX and regenerative absorption cycles. Report ORNL/CF-91/263”, Oak Ridge National Laboratory, Tennessee.

Reiner R. H., Zaltash A., (1992), “Corrosion screening of potential fluids for ammonia water absorption cycles. Report ORNL/CF-92/41”, Oak Ridge National Laboratory, Tennessee.

Reiner R. H., Zaltash A., (1993), “Densities and viscosities of ternary ammonia water fluids”. ASME winter annual meeting.

Richter L., Safarik M., (2005), “Solar Cooling with Ammonia Water Absorption Chiller”, International Conference Solar Air Conditioning, Bad Staffelstein, Gemany.

Rodriguez, H.; Brennecke, J. F., (2006), J. Chem. Eng. Data, 51 (6), 2145-2155.

Rojey A., (1975), “Verfahren zur Erzeugung von Wärme mittels eines Absorptions-Thermotransformators”, FR No. 2321098, 14.08.1975.

Rojey A., (1979), “Absorption process for heat conversion”, US No. 4167101, 11.09.1979.

Rojey A., Cohen G., (1982),

a. “Process for producing cold and/or heat with use of an absorption cycle”, US No. 4311019, 19.01.1982.
b. “Cold and/or heat production involving an absorption cycle and its use for heating buildings”, US No. 4341084, 27.06.1982.

Rojey A., (1983), “Process for producing cold operated with phase separation”, US 4413479, 08.11.1983.

Rojey A., Larue J., Barreau A., (1983), “Process for producing cold and/or heat by means of an absorption cycle” US No. 4420946, 20.12.1983.

Rojey A., Cheron J., (1984),

a. “Process for producing cold and/or heat by use of an absorption cycle with carbon dioxide as working fluid”, US No. 4433554, 28.02.1984.
b. “Process for cold and/or heat production with use of carbon dioxide and a condensable fluid”, US No. 4448031, 15.05.1984.

Rojey A., Bonifay R., Cariou J. P., (1985), “Process for producing cold and/or heat by means of an absorption cycle comprising at least two absorption steps”, US No. 4532773, 06.08.1985.

Salavera D., Chaudhari S.K., Esteve X., Coronas A., (2005), “Vapor-Liquid equilibrium of ammonia-water-potassium hydroxide and ammonia-water-sodium hydroxide at temperatures from 293.15 to 353.15 K”, J. Chem. Eng. Data, 50, 471-476.

Sanchez, L., Espel, J., Onink, F., Meindersma, G., De Haan, A., (2009), J. Chem. Eng. Data, 54, 2803-2812.

Schaefer L., (2000), “Single pressure absorption heat pump analysis”, PhD Thesis, Georgia Institute of Technology, Atlanta, Georgia.

Seddon, K. R., Stark, A., Torres, M.-J., (2002), ACS Symp. Ser, 819 , 34-49.

Sherwood T. K., Hills W., (1944), “Refrigeration”, US No. 2354884, 01.08.1944.

Solair project, (2009), Project on market implementation of solar air-conditioning systems for small and medium applications in residential and commercial building, http://www.solair-project.eu/148.0.html, last accessed on 12.10.2011.

SolarNext (2012): Technical brochure of the cooling kit ISC11, http://www.solarnext.eu/ger/dow/produktdatenblaetter.shtml; last accessed on 14.05.2012.

Sorensen J. M., Arlt W., (1979), "Liquid-Liquid Equilibrium Data Collection. Binary Systems. Tables, Diagrams and Model Parameters", DECHEMA, Frankfurt/Main, Deutschland.

Speckhardt H., Gugau M., (2005), "Korrosion und Korrosionsschutz von Metallen", Dubbel - Taschenbuch für den Maschinenbau, Berlin Heidelberg, Springer.

Statistik Austria, (2009), "Energiestatistik: Energiebilanzen Österreich 1970 bis 2009, Energetischer Endverbrauch 2009 nach Energieträgern und Nutzenergiekategorien für Österreich", Wien, Austria

Steiu, S., Salavera D., Bruno J.C., Coronas A., (2009), "A basis for the development of new ammonia–water–sodium hydroxide absorption chillers", Int. J. Refrigeration, 32, 577-587.

Tomida, D., Kenmochi, S., Tsukada, T., Qiao, K., Yokoyama, C., 2007, Int. J. Thermophys., 28 (4), 1147-1160.

Valderrama J., Robles P. (2007) "Critical Properties, Normal Boiling Temperatures and Acentric Factors of Fifity Ionic Liquids", Ind. Eng. Chem. Res., 46, 1338 – 1344.

Valderrama J., Robles P. (2007) "Critical Properties, Normal Boiling Temperatures and Acentric Factors of another 200 Ionic Liquids", Ind. Eng. Chem. Res., 47, 1318 – 1330.

Valderrama J., Sanga W. (2008) "Critical Properties and Vapor Pressure of Twenty Imidazolium based Ionic Liquids used in Extraction Bioprocesses", 2nd International Symposium on Biothermodynamcis, Frankfurt, Germany.

Van Valkenburg, M. E., Vaughn, R. L., Williams, M., Wilkes, J. S., 2005, Thermochim. Acta, 425, 181-188.

Verevkin S. (2008) "Predicting Enthalpy of Vaporization of Ionic Liquids: A Simple Rule for a Complex Property", Angew. Chem., 120, 5149 – 5152.

VDI-Wärmeatlas (2006), "Berechnungsblätter für den Wärmeübergang", Berlin Heidelberg New York, Springer, ISBN-10: 3-540-25504-4.

Wilding W.V., Neil F.G., Wilson C.W. (1996), "Phase Equilibrium Measurements on Nine Binary Mixtures", Journal for Chemical and Engineering Data, Vol. 41, No.6 (1996), 1239-1251.

Yokozeki A., Shiflett M. B., 2007:

a. Ammonia solubilities in room-temperature ionic liquids, Ind. Eng. Chem. Res., 46 (5), 1605-1610.
b. Vapor–liquid equilibria of ammonia + ionic liquid mixtures, Appl. Energy, 84, 1258-1273.

Ziegler F., (2002), “State of the art in sorption heat pumping and cooling technologies”, International Journal of Refrigeration, Vol. 25, 450-459.

LIST OF PUBLICATIONS ON THE TOPIC OF THE DOCTORAL THESIS

Publications in Proceedings of Conferences or Scientific Magazines:

Kotenko, O., Moser, H., Rieberer, R., (2011):

a. “Potential und Grenzen von Natriumhydroxid als Zusatz zum Stoffpaar Ammoniak / Wasser in Absorptionswärmepumpen”, Deutsche Kälte-Klima-Tagung, 2011, Aachen, Germany.
b. “Thermodynamic Simulation of Alternative Absorption Heat Pumping Processes Using Natural Refrigerants”, Int. J. Refrigeration (Accepted Manuscript 10.1016/j.ijrefrig.2011.10.005)
c. “Thermodynamic analysis of ammonia / ionic liquid absorption heat pumping processes”. International Sorption Heat Pump Conference 2011, Padua, Italy

Kotenko, O., Moser, H., Rieberer, R., (2010), “Thermodynamic simulation of alternative absorption heat pumping processes using natural refrigerants”, 9th IIR Gustav Lorentzen Conference 2010, Sydney, Australia.

Rieberer, R., Kotenko, O., Moser, H., (2010), “Waste heat recovery - an opportunity for heat pumps”, Application of Heat Pumps for Waste Heat Recovery, 2010, Vienna, Austria.

Kotenko, O., Moser, H., Rieberer, R., (2009):

a. “Feasibility study of alternative absorption heat pump processes”, 3rd International Conference Solar Air-Conditioning 2009, Palermo, Italy.
b. “Untersuchung eines Absorptions-Wärmepumpen-Prozesses mit teilweise mischbaren Arbeitsstoffen”, Deutsche Kälte-Klima-Tagung 2009, Berlin, Germany

Scientific Reports:

Rieberer, R., Kotenko, O., Moser, H., Fenzl T., (2011), “Endbericht: Potential und Grenzen von Natriumhydroxid als Zusatz zum Stoffpaar Ammoniak / Wasser in Absorptions-Wärmepumpen (Hydroxid-AWP) ”, FFG, Vienna, Austria.

Rieberer, R., Kotenko, O., Moser, H., (2011), “Endbericht: Realisierungspotential von Absorptionswärmpumpen mit ionischen Flüssigkeiten (IonA) ”, FFG, Vienna, Austria.

Rieberer, R., Kotenko, O., Moser, H., Heinz, A., Kalkgruber, J., Ganster, S., (2010), “Endbericht: Feasibility Study innovative Absorptions-Wärmepump-Prozesse (InnovAP) ”, FFG, Vienna, Austria.

Rieberer, R., Kotenko, O., Moser, H., Ganster, S., (2009), “Zwischenbericht: Feasibility Study innovative Absorptions-Wärmepump-Prozesse (InnovAP) ”, FFG, Vienna, Austria.

Kotenko, O., Moser, H., Rieberer, R., Malenković, I., (2009), “IEA HPP Annex 34 - Thermally driven heat pumps, Task A: State-of-the-art analysis, Austrian Team Report”.